Investigation on Smoke Movement and Smoke Control for Atrium in Green and Sustainable Buildings

Liu Fang
Peter V. Nielsen
Henrik Brohus

ISSN 1901-726X
DCE Technical Report No. 32

AALBORG UNIVERSITY
Department of Civil Engineering

Aalborg University
Department of Civil Engineering

DCE Technical Report No. 32

Investigation on Smoke Movement and Smoke Control for Atrium in Green and Sustainable Buildings

by

Liu Fang
Peter V. Nielsen
Henrik Brohus

June 2007

Scientific Publications at the Department of Civil Engineering

Technical Reports are published for timely dissemination of research results and scientific work carried out at the Department of Civil Engineering (DCE) at Aalborg University. This medium allows publication of more detailed explanations and results than typically allowed in scientific journals.

Technical Memoranda are produced to enable the preliminary dissemination of scientific work by the personnel of the DCE where such release is deemed to be appropriate. Documents of this kind may be incomplete or temporary versions of papers—or part of continuing work. This should be kept in mind when references are given to publications of this kind.

Contract Reports are produced to report scientific work carried out under contract. Publications of this kind contain confidential matter and are reserved for the sponsors and the DCE. Therefore, Contract Reports are generally not available for public circulation.

Lecture Notes contain material produced by the lecturers at the DCE for educational purposes. This may be scientific notes, lecture books, example problems or manuals for laboratory work, or computer programs developed at the DCE.

Theses are monograms or collections of papers published to report the scientific work carried out at the DCE to obtain a degree as either PhD or Doctor of Technology. The thesis is publicly available after the defence of the degree.

Latest News is published to enable rapid communication of information about scientific work carried out at the DCE. This includes the status of research projects, developments in the laboratories, information about collaborative work and recent research results.

Published 2007 by
Aalborg University
Department of Civil Engineering
Sohngaardsholmsvej 57,
DK-9000 Aalborg, Denmark

Printed in Aalborg at Aalborg University

ISSN 1901-726X
DCE Technical Report No. 32

Investigation on Smoke Movement and Smoke Control for Atrium in Green and Sustainable Buildings

Supported by European Community Asia-link Project

Centre of Sino-European Sustainable Building Design & Construction

(Contract No.: CN/ASIA-LINK/011(91-400))

by

Liu Fang

June 2007

A report submitted in partial fulfillment of the requirements for European Community Asia-link Project

Department of Civil Engineering
Aalborg University
Sohngaardsholmsvej 57
DK-9000 Aalborg, Denmark

Acknowledgements

This research was carried out by the support of European Community Asia-link Project (Contract No.: CN/ASIA-LINK/011(91-400)). The experiments were conducted in the laboratory of civil engineering department of Aalborg University.

I would like to thank the following people and organization who have contributed to this research in various ways:

Thanks to Per Heiselberg, R.M. Yao and B.Z. Li for providing me to work in Aalborg University Denmark and their care during my stay in Aalborg.

Thanks to Per Heiselberg for his instruction on ventilation course. Thanks to P.V. Nielsen for his instruction on similarity theory and the design of the experimental schemes. Their ideas broadened my knowledge and fuelled my enthusiasm to carry out the research.

Thanks to Heidi Stentoft and Torben Christensen for their help with experiment. Thanks to Rasmus Lund Jensen for his help in FDS simulation. Thanks to Henrik Brohus and Carl-Erik Hyldgård for their help.

Thanks to P.V. Nielsen, Bente J. Kjærgaard and Zhigang Li, for their invaluable help with work and life in Aalborg.

Centre of Sino-European Sustainable Building Design & Construction, for providing funding for this research.

Aalborg University, for providing me apartment and office.

Chongqing University, for supporting me.

Abstract

The concepts of green buildings and sustainable buildings are promoted actively in the developed countries. Targets are on protecting the environment, using less energy through natural ventilation provisions and daylight utilization, developing better waste management and taking resource conservation into account. Architectural and building design, electrical and mechanical systems, and building management have to be upgraded. However, there are problems in dealing with fire safety, especially in complying with the existing prescriptive fire codes. A hot argument is that smoke control system design in the green or sustainable buildings with an atrium.

Since the physics of air entrainment is not yet clearly understood, most of the fire plume expressions reported in the literature was derived empirically. Experiments and CFD simulation were used to study the different types of thermal plumes such as axisymmetric plume, wall plume, corner plume and balcony spill plume in this report.

As many large space buildings such as cinema, sports arenas containing the sloping floor are designed to meet the function and aesthetic requirement. The smoke movement in atrium with sloping floor is also discussed in this report.

Computational Fluid Dynamics and scale model experiments are two possible methods for the determination of mass transport, contaminant transport, smoke movement and energy transport in large building. The scale model experiments and FDS (Fire Dynamic Simulation) are used in this report.

Three axisymmetric plume equations and two balcony spill plume models are assessed by comparing with the CFD and experiment results. Investigations in this report are useful for fire engineers in designing smoke control systems.

This thesis also describes many significant atrium smoke movement and smoke management research, related efforts and future research, the major topics are as follows: types and configurations of atrium buildings; approach to atrium smoke management design calculation in NFPA92B and comparison of two methods of calculating smoke layer interface heights; smoke exhaust system modes and smoke

exhaust effectiveness; atrium smoke filling process and its time constant; pre-stratification and detection ; airflow for smoke control between the atrium and communicating space; sprinkler effect, etc.

This report was written as a work report of my stay at the department of civil engineering of Aalborg University from January 2007 to June 2007. As the time limitation the further analysis of the result is needed when I go back to Chongqing University.

Key Words

Sustainable building/ atrium/ smoke movement/ smoke control/ CFD/ scale model

Table of Contents

1 Introduction

1.1 Background

Over the last few decades, large undivided volume buildings such as atrium buildings, covered shopping malls, airport terminals and sports arenas have become increasingly popular. These buildings typically contain large spaces or voids which can occupy many storey in height. The term ‘atrium’ can be applied to the large spaces within these types of buildings.

The concept of an atrium dates back to Roman times, when used as an entrance hall in a typical house. An atrium within a building is a large open space created by an opening or series of opening in floor assemblies, thus connecting two or more stories of a building that is closed at top. The sides of an atrium may be open to all floors, to some of the floors or closed to all or some of the floors by unrated or rated fire-resistant construction. As well, there may be two or more atria with in a single building, all interconnected at the ground floor or on a number of floors.

Developments in architectural techniques now allow an atrium to be an integral part of large buildings (e.g. covered shopping malls). Modern atria are designed with the intention to provide a visually and spatially external environment in doors [1] [2].

In terms of fire protection, floors, ceilings and partitions are traditionally used to provide space to limit the spread of fire and smoke within a building. However, atrium buildings violate this fundamental approach in terms of horizontal space and vertical separation. With a fire on the floor of an atrium or in any space open to it, smoke can fill the atrium and connected floor spaces. The fire risks of atrium building are different from those of traditional buildings, and the associated problems related to smoke should be dealt with carefully.

‘Green buildings’ are of great interest to the developed countries towards the end of the last century. Now, this is extended further to ‘sustainable buildings’ similar actions are taken in big cities of China and Denmark. Although the concepts behind the two are different, the assessment procedure is roughly the same. A ‘relative scale’ to a typical building in a region will be applied for a green building. Sustainable building is more

‘absolute’ on controlling energy and mass flows internationally. Indoor environment, environmental protection, energy-saving through better provisions of natural ventilation and utilization of daylight, water consumption and waste management are the common approaches to satisfy the assessment criteria for those green or sustainable buildings.

Normally, three items will be covered:
1) Architectural features including building construction element.
2) Electrical and mechanical systems to give a comfortable environment, but the system would use energy directly or indirectly.
3) Management including energy management, environmental management and fire safety management.

However, some architectural features of those buildings might not be satisfied with the fire safety codes. There are problems in dealing with fire safety, especially in the green or sustainable buildings with an atrium. Smoke spreading would give problems and smoke control was identified to be a key issue. Providing enough evacuation time, smoke filling or no smoke exhaust system is good method to be designed to keep the smoke layer above the safety height. An alternative solution is to install a smoke control system, a mechanical ventilation system or natural vents have to be designed.
Therefore smoke movement and smoke control in an atrium is very important and investigation smoke movement and smoke control in atrium buildings becomes the objective of this thesis.

1.2 Types and Configurations

Atrium buildings can be classified into five types in terms of theirs configurations closed atrium; open-sided atrium; linear atrium; multi-lateral atria; partial atrium as shown in Fig. 1.1 [3] [4].

According to their fire protection designs, atrium buildings can be divided courtyard atrium (with fire resistant glass), closed atrium and unrestricted atrium [5].

In order for a suitable smoke control design to be identified, Morgan et al [6] categorized atria into the following groups depending upon the type of enclosure:

Sterile tube atrium; closed atrium; partially open atrium, and fully open atrium.

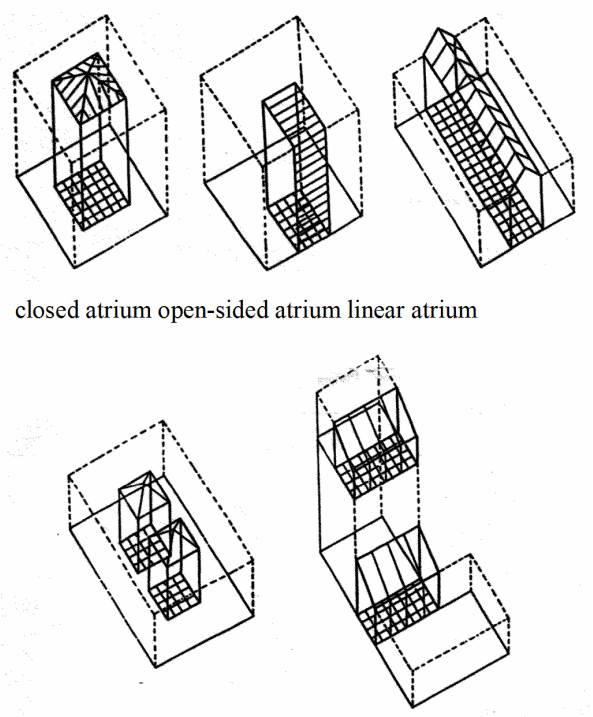

Fig. 1.1 Atrium Classification from structure relations

The sterile tube atrium is where the atrium space is separated from the remainder of the building by a façade which is both fire and smoke resisting. This façade will act as a barrier to fire and smoke spread between the atrium and the adjacent spaces. The ideal sterile tube atrium would contain no flammable material on the atrium floor. The atrium space would generally have no functional use apart from as a circulation area for the occupants of the building.

A closed atrium in which, the atrium is separated from the remainder of the building by a non fire resisting façade. This façade may not necessarily be smoke resisting. The atrium space may possibly have a functional use.

A partially open atrium is when there are communicating spaces between the atrium space and the adjacent areas on some of the lower storey. A non fire resisting façade provides separation between the atrium and adjacent areas on the upper storey.
A fully open atrium is when large openings exist between the atrium and adjacent areas on all stores.

From the results of a survey geometrical shapes of the atrium spaces in Hong Kong, three main types of atria are classified for the purpose of analyzing the fire environment inside to produce a general picture of potential fire risk[7] [8]. Such a classification is discussed in this thesis. Fire simulations in those three types of atria are also discussed. The three types of atria are described below.

1.2.1 Atrium Type 1 Cubic

The atrium space is of cubic shape and the design is commonly found in Hong Kong. About 60% of the atrium spaces can be classified as this type. They are smaller in scale (i.e., usually of length less than 20 m) and most of them are integrated into the shopping center. They can be characterized as having dimensions (length * width * height) of L*L*L, as shown in Fig. 1.1.

1.2.2 Atrium Type 2 Flat

The atrium has large transverse dimension in comparison with its height, and this type is often found in large multi-level shopping malls. About 25% of the Hong Kong atria can be classified as the flat type. They are characterized by having dimensions of 2L*L*L, as shown in Fig. 1.2.

1.2.3 Atrium Type 3 High

This is the kind of atrium with a height-to-width (or length) ratio of more than two. They are usually found in prestigious office buildings and luxurious hotels. About 15% of local atria are this type. Their characteristic dimensions are L*L*3L, as shown in Fig. 1.2.

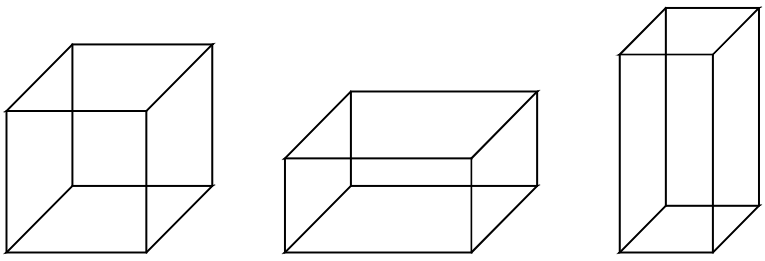

cubic flat high

Fig. 1.2 Configuration of the atria

1.2.4 Atrium Fire Environment Simulation

Simulations that are on the fire environment in the three different types of atria using the zone models have been presented by Chow and Wong. The simulations show that the potential fire risks in atrium buildings are quite high with smoke being the major cause of hazard. The predicted hot gas temperature profile indicates that flashover is unlikely to occur if 600℃ is the criterion for flashover. Also, the smoke will not be hot enough to activate sprinklers installed at the top of the atrium unless it is a very big fire. It is shown that different atrium geometrical configuration (same volume) will give different fire behavior. The smoke development rate of the flat type atrium is the slowest, but the one for a high atrium will be very high. It is illustrated that specifying only the volume of the atrium space is not good enough to determine whether a smoke extraction system has to be installed. The geometrical configuration is recommended to be specified in the code as well. In addition, simulations on the effect of smoke extraction indicate that installing a smoke extraction system will reduce the smoke layer thickness and the hot gas temperature.

1.2.5 Atrium Types in Mainland China

Obviously, the height of atrium is one of the most important parameters, which affect smoke movement. With the same cross-sectional area, the smoke in the high atrium flows more difficultly than the one in the low atrium. In the lower atrium, smoke flows through then window in the ceiling, while in the higher atrium, smoke is pulled out mechanically, and its efficiency decreases with the height increasing. The height of atrium cannot be only one factor which effects on smoke movement.

Both height and cross section area can affect smoke movement. Atrium geometry aspect factor is defined as the ratio of the atrium cross-sectional area and the square of the atrium height is given by:

$$\xi = A/H^2 \qquad \text{(A is atrium area, } m^2\text{; H is atrium height, m.)}$$

This geometry aspect factor reflects the degree of confined plume. With the same atrium height, if atrium shape factor is large, that means atrium cross-sectional area is large and the degree of confined plume is small; On the contrary, if atrium shape factor is small, atrium cross-sectional area is small and the degree of confined plume is large. Therefore atrium shape factor, which shows the degree of confined plume and

classifying the types of atrium according to their shape factor for studying the different atrium fire, is reasonable and scientific.

A survey of the geometrical shapes of the atrium spaces in China mainland was made. Thirty buildings with atrium in China mainland were studied. Statistic Figures show that the geometrical shape of the atrium spaces have rectangle, ladder-shaped, circle and irregular shape and so on. For the geometrical shapes, there are twenty-five rectangle atriums that are the 83 percent of the total and irregular shape atrium such as circle and pentagon are less. The scale of the statistic atrium area is between 9.4 and 1000 m^2. There are twenty-one atriums whose areas are between 100 and 1000 ㎡, that is 70 percent of the total. Atrium geometry aspect factor H^2/A is between 0.002 and 11.2. There are 40% atrium, whose factor is between 0.4 and 2; there are about 36% atrium, whose factor is smaller than 0.4; and there are 23% atrium whose factor is larger than two.

Fig. 1.3 shows the types of atrium aspect factor, they can be classified into three types: atrium whose shape factor is smaller than 0.4, is thin and high type, the atrium whose shape factor is between 0.4 and 2, is cubic type, and the atrium whose shape factor cubic atrium is commonplace in China mainland and it is 40 percent of the total； thin and high atrium is 36 percent and this type is also commonplace； While flat and even atrium is less than the other two types and it is 23 percent.

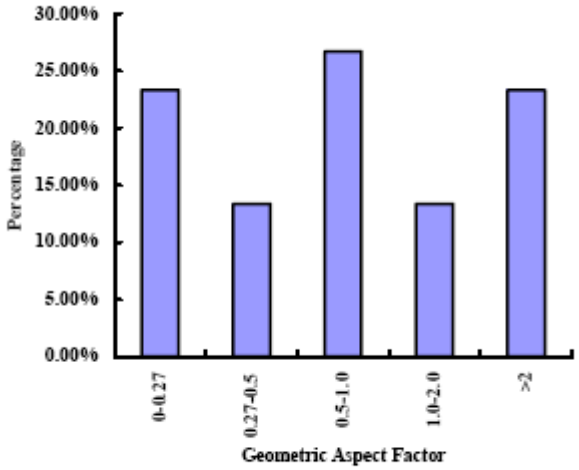

Fig. 1.3 Geometric Aspect Factors of Atria in Mainland China

1.3 Smoke Control

Knowledge on fire environment with in a building is a vital element of architectural design. Research results show that smoke is the first and the most rapidly developed threat to life in fire on a atrium, smoke will bring many problems, and controlling smoke is essential to providing safety in the atrium spaces[9] [10].

1.3.1 Objectives for Smoke Control

Some form of smoke control (known as smoke management in the USA) is often required in atrium buildings primarily for life safety purposes. Milke [11] gives five design objectives for smoke control systems in atrium buildings:

1) Maintain a tenable environment in the means of egress in the atrium during the time required for evacuation.
2) Confine the smoke in the atrium to a limited region in that space.
3) Limit the migration of smoke into adjacent spaces from the atrium.
4) Provide conditions in the atrium that will assist emergency response personnel in conducting search-and-rescue operations and locating and controlling the fire.
5) Contribute to the overall protection of life and reduction in property loss.

Milke states that a design may be to achieve either one, or a combination of, these objectives. Milke also lists a number of ‘hazard parameters’ in which the design objectives can be evaluated in measurable terms, such as: smoke layer depth; visibility through the smoke layer; carbon monoxide concentration; temperature rise in the smoke layer.

1.3.2 Smoke Control Systems

Smoke control systems are defined as engineering systems that includes all the methods that can be used singly or in combination to reduce smoke production or to modify smoke movement (ASHRAE and NFPA). The objectives of a smoke control system are reduce deaths and injures from smoke, reduce properly loss.

Methods to reduce smoke production in atria include the installation of automatic sprinklers and limitation on the quantity of combustible materials used in the construction of the building and located on the floor of the atrium Sprinklers are

effective in suppressing fires in floor spaces with limited ceiling heights, but, because of delayed response, sprinklers may not be effective in suppressing fires in space with ceiling heights greater than 11 to 15 m or in controlling fires in atria exceeding 20 m in height. Sprinkler effect is discussed in section 1.9.

Passive methods to modify smoke movement include the use of smoke barriers or draft curtains to limit smoke incursion into communicating spaces and egress routes. Another passive method is to allow the smoke to fill the upper portion of the atrium space while the occupants evacuate the atrium. The latter approach applies only to large-volume spaces where the smoke-filling time is sufficient for both occupant response and evacuation.

For those cases in which passive smoke management methods produce insufficient time for occupant response and evacuation, upper layer mechanical exhaust systems are frequently used to maintain the smoke level above the occupants until they are able to evacuate. This system decreases the rate at which the smoke layer descends in the atrium. A common approach for the design of an upper mechanical exhaust system for atrium smoke management is to design a system that will maintain the smoke at a steady clear height assuming a steady-state design fire. Such a system can be designed using a calculation method based on plume equations in NFPA 92B. This method is included in the BOCA (1996) and ICBO (1994) building codes. It is the method that discussed in section 1.4.

There are a number of different smoke control strategies available for atrium buildings.

1) Smoke filling

This approach can be applied to atria which have large volumes, such that smoke ventilation may not be necessary. This strategy becomes viable when smoke can be contained in a roof void for the duration of the required safe egress time for the occupants of the building. In this case, the height of the smoke layer may not reach an unacceptable value before the fire consumes the available fuel. This approach assumes that the fire grows at a predictable rate. Fig. 1.4 shows a smoke filling.

Klote and Milke [12] [13] provide empirical relationships to determine the smoke layer height above the fire with respect to time for both steady and growing fires.

Calculations of smoke layer height are discussed further in section 1.4.

This strategy should only be used if the smoke control designer can demonstrate by calculation that smoke ventilation is not necessary.

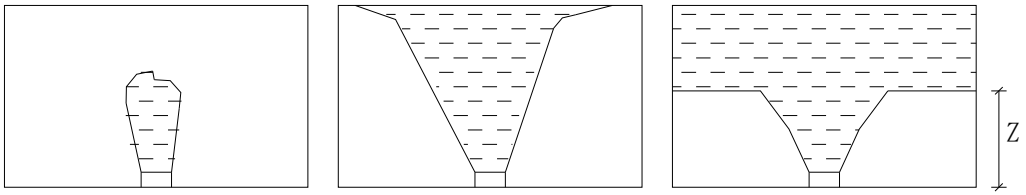

Fig. 1.4 Smoke filling of atrium space

2) Smoke clearance

This approach provides sufficient ventilation to remove smoke from the atrium after the fire has been suppressed.

3) Smoke and heat exhaust ventilation from the atrium

This strategy uses the buoyancy of the smoky gases from the fire to form a layer above the occupants of the building, providing a safe means of escape. This form of smoke control is the main work of this research and is described in detail in the following section1.3.3.

4) Temperature control ventilation from the atrium

This strategy is used when the height of the smoke layer above the floor is not a critical design parameter. In this case, smoke exhaust can be used to achieve a maximum value of the temperature of the layer of smoky gases. This approach allows the use of materials which would otherwise be damaged by hot gases (e.g. atrium façade materials which are not fire-resisting).

5) Smoke and heat exhaust from each storey separately

In some cases it may be impractical to provide smoke exhaust ventilation from the atrium space if the height of rise of the smoke layer from the floor is too large. It may be beneficial to prevent smoke from entering the atrium altogether (particularly for fully open atria). This can be achieved by the use of strategically placed smoke curtains around the atrium space at each storey, and providing smoke exhaust ventilation from each storey separately.

6) Atrium depressurization

Where the boundary between the atrium space and the adjacent areas is linked by small openings (e.g. doors gaps, leaky facade), it is possible to prevent smoke from traveling through these openings by reducing the pressure of the gases in the smoke layer. This approach is known as depressurization. The purpose of this technique is to prevent smoke from traveling into the adjacent spaces and does not provide protection to the atrium space. This technique is similar to that employed for natural environmental ventilation in atrium buildings.

7) Combination of above strategies (hybrid smoke control)

Various combinations of the above strategies can also be applied, such as atrium depressurization with smoke and heat exhaust ventilation.

1.3.3 Smoke and Heat Exhaust Ventilation Systems (Smoke Exhaust System)

Smoke and Heat Exhaust Ventilation Systems for atrium buildings provides smoke and heat exhaust from the upper regions of a building to create a clear layer beneath a buoyant stratified smoke layer, thus providing conditions for safe means of escape. For this approach to be effective, it is necessary for the temperature of the gas layer to be high enough to remain buoyant when at the design height. Smoke Exhaust System may be naturally driven or mechanically driven (mechanical exhaust fans).

For the smoke exhaust to be effective, it is necessary to provide an adequate amount of inlet air to replace the hot gases being removed.

Smoke control design in codes and guides is based on the zone fire model concept. In the zone model, smoke forms an upward-flowing fire plume reaches the ceiling and is considered to form a perfectly mixed layer under the ceiling of the room of fire origin. Smoke production depends on the heat release rate of the fire and the height of the fire plume. Fig. 1.4 depicts the development of the fire plume, the formation of the smoke layer interface, and the descent of smoke layer as a result of a heat source located in a position where the fire plume does not meet the wall of the enclose. Klote explains the physical concepts of the steady fire, unsteady fire, zone fire model, and the fire plume that are the basis of atrium smoke control. Information about those is not described further in this report.

In order to properly design smoke exhaust system for a large space, one needs to know the heat release rate of the expected fire in order to determine the fire size. From that, one can estimate the amount of smoke. It is then possible to calculate the time needed for smoke to reach a point that could endanger the occupants and to compare that time to the egress time. If the smoke layer time is less than the egress time, a smoke management system should be provided to exhaust smoke at a minimum of the rate at which the smoke is produced. This is approach used by BOCA (Building Officials and Code Administrators) National Building Code. It establishes a design criterion that the smoke management system keeps the smoke layer interface at or above the six-foot (1,828mm) level for not less than 20 minutes (1200 s). BOCA contains a calculation method base on NFPA 92B to evaluate compliance with criterion.

1.4 Steady Smoke Layer Interface

In fact, there are two calculation methods to predict the location of the smoke layer interface in NFPA 92B [14]. One is based on a predictive correlation that generated a smoke layer interface position at any given time, the other is based on a mass flow-based calculation correlation to predict the position of a smoke layer interface. The (BOCA) Building Code codified the NFPA 92B approach. The 1996 BOCA National Building Code presents two calculation methods for determining the position of smoke layer interface. They are referred to as “regular” ceiling method to be utilized for flat-ceiling spaces, and the “irregular” ceiling method, indicating the method to be utilized for spaces with varying horizontal cross-sectional areas. Two methods are briefly described as follows:

1.4.1 Regular Ceiling Method

The position of the smoke layer interface, Z, is predicted at any time using the following equation:

$$Z = 1.11H - 0.28H \ln\left[\frac{tQ^{1/3}H^{2/3}}{A}\right] \tag{1.1}$$

Where:

Z--height from the floor to the smoke interface, m;

t--time, s;

H--ceiling height above the fire, m;

Q--steady-state heat release rate, kW;
A--cross-sectional area of the atrium, m^2.

Equation 1.1 is derived from the steady smoke-filling equation in NFPA 92B. Equation 1.1 is based on plume that has no contact with the walls and for a constant cross-sectional area with respect to height. This equation is appreciated for A/H2 from 0.9 to 14 and for values of Z greater than or equal to 20% of H.

It is straight using Equation 1.1 to determine a given point (Z) in a defined time period. The regular ceiling method is presented as a single-point “test” to determine if the smoke layer interface has reached the critical height (design objective level) in a given period.

1.4.2 Irregular Ceiling Method

The volume of smoke produced at any height Z is predicted by the following equation (BOCA):

$$Ve = 0.059 Q_c^{1/3} Z^{3/5} + 0.0015 Q_c \quad (1.2)$$

Where
V_e--volumetric rate of smoke production, m^3/s;
Q_c--convective portion o the heat release rate, kW. (Q_c=0.7Q)

For a particular height, V_e defines a volume of smoke produced per unit of time. Smoke is assumed to be deposited on the ceiling in uniform thickness across the entire surface. No transit time from the fire to the ceiling, or radically from the center of plume contact to the perimeter walls, is incorporated into the equation.
Equation 1.2 is derived from NFPA 92B’s mass flow equation:

$$m = 0.071 Q_c^{1/3} Z^{3/5} + 0.0018 Q_c \quad (1.3)$$

Where
m--mass flow rate in plume at height Z, kg/s.
Mass flow is converted to volume flow using the following relationship:

$$Ve = m / \rho \quad (1.4)$$

Where
ρ--density of smoke, kg/m^3.

By making assumption of the density of smoke to be 1.2 kg/m^3 corresponding to 21℃, the mass flow equation from NFPA 92B (Equation 3) can be converted to volume flow equation. Equation 1.2 would represent the “slowest” filling time for an atrium (no increase in layer temperature above ambient).any increase in layer temperature will result in faster filling rates than would be predicted by Equation 1.2.

Calculating the layer position by Equation 1.2 is not as straightforward as was the case for the regular ceiling method. The first iteration uses H as the value for Z. This method, intended for use in spaces where the horizontal cross-sectional area varies with height, is to be used in an iterative manner, as opposed to the single-point test described for the use of the regular ceiling method.

Use of Equation 1.2 is limited to values of Z that are above the limiting elevation. For information about this, the reader can be referred to Brooks (1997) [15].

1.4.3 Comparison of Methods

Comparison of the two calculation methods for a range of atrium areas and aspect ratios has been presented by Brooks (1997) [14]. Assuming that:
(1) Atrium A/H^2 aspect ratios are between 0.9 and 14;
(2) Fire size are limited to 2110 kW and 4640kW;
(3) The ceiling of the space is flat;
(4) The space has a constant horizontal cross-section area.

Two different building areas were selected and for each cases both calculation methods were used to predict the position of the smoke layer interface as a function of time for two different atrium aspect ratios. The results illustrate that the two methods are not equivalent and will not produce comparable results. There are foreseeable conditions where the use of the regular ceiling method will require a smoke management system and the use of the irregular ceiling method will not. The irregular ceiling method is likely to predict a slower than observed smoke layer interface descent, while the regular ceiling method is likely to predict a faster than observed descent. Further analysis was then conducted to reconcile the two methods and develop an approach that will permit designers to produce comparable hazard analyses regardless of the method used. A suggested series of adjustments is provided to align the regular ceiling

and irregular ceiling calculation method results over a broad range of interface heights.

For “irregular” calculation method, use of a plume centerline temperature correlation to adjust the maximum expected layer temperature is suggested as a reconciliation technique. Equation 1.2 produces the slowest filling since the density correlation inherent to the coefficient on the right side of the equations is for air at 21 ℃. Equation1.2 must be adjusted to reflect layer temperatures higher than 21℃ (ambient temperature). Brooks recommends that the average temperature of smoke layer is the temperature of the smoker plume centerline temperature, measured at the critical height. A density correlation based on 74℃ smoke layer temperature (approximation of automatic sprinkler activation temperature) is suggested.

For “regular” calculation method, it is necessary to reevaluate the fundamental correlation used as the basis for the regular ceiling calculation method, in order to bring it into agreement with the mass flow used in the irregular ceiling calculation methods. Brooks argues that six sets of test data are summarized as forming the basis for the development of the regular calculation method and only two of the test was conducted in rooms large enough to be considered atria with heat release rates comparable to expected design fires. Equation 1.1 is predicting smoke layer interface descent based on a much higher temperature than 74℃. If Equation 1.1 is to be continued in use, it will have to be modified to reflect the lower layer temperature in current atrium design.

1.5 Smoke Exhaust Rate

1.5.1 Equation

Smoke extraction systems are designed to keep the smoke layer high enough to give a greater clear height. For a steady fire, it is to exhaust smoke from the top of the atrium in order to achieve a steady clear height. Consider that the only flow into the smoke layer is from the plume, and the only flow from the smoke layer is the smoke exhaust. From the principle of conservation of mass for a steady process, the exhaust flow must equal the flow from the plume. The mass flow equation (NFPA 92B 1995) listed above can be used to calculate the exhaust flow rate. The adiabatic exhaust temperature is

$$T_p = T_a + \frac{Q_c}{mC_p} \tag{1.5}$$

Where

T_p--adiabatic exhaust temperature, ℃;

T_a--ambient temperature, ℃;

m--mass flow of exhaust air, kg/s;

C_p--specific heat of plume gases, kJ/(kg·℃).

Using the calculated adiabatic temperature and the ideal gas law, the volumetric flow rate of smoke can be estimated by Equation 1.4. BOCA uses the following equation to determine the minimum exhaust rate:

$$Ve = Q_c^{1/3} Z^{3/5} + 0.0015 Q_c \qquad (1.6)$$

Where

V_e-- volumetric rate of exhaust air, m^3/s.

BOCA uses 74℃ as the temperature of the smoke being exhausted. Alternatively one can use ambient temperature as an approximation. The exhaust rate is then to be adjusted in accordance with a table to allow for increase in time for the smoke layer interface to reach the critical height. The volumetric flow rate defined by Equation 1.6 is used to determine the capacity of the mechanical exhaust system.

1.5.2 Discussion

The basic calculation methods in this section are not application when the design exceeds the range of applicability of the equations presented.

The calculation method above is only for an ax symmetric plume (a fire located in the atrium). For a fire located in the communication space, a balcony spill plume or a window plume is formed. The information about these other plumes, they are discussed in NFPA 92B (1995) and Chow and Lau.

The design fire has a major impact on the atrium smoke management system. The fire size is expressed in terms of the rate of heat release. Designs may be based on either steady or unsteady fires. It is the nature of fires to be unsteady, but the steady fire is a useful idealization. A steady fire has a constant heat release rate. An unsteady fire is one that varies with respect to time. Fire protection engineers often use a “t-squared” approximation for an unsteady fire. A ‘t-squared’ fire is one in which the burning rate

varies proportionally with the square of time , ‘t-squared’ fires are classed (by speed of growth) as ultra-fast, fast, medium, and slow, based on the time to reach a heat release rate of 1,055 kW. A ‘t-squared’ fire can be described as follow:

$$Q = \alpha t^2 \tag{1.7}$$

Where

α--growth coefficient. Four types of t-square fire are shown as in Fig. 1.5.

In many applications, use of a steady design fire leads to straightforward and conservative design. Klote [12] recommends three typical steady design fires of 2,000 kW, 5,000 kW, and 25,000 kW for atria as list in Table 1.1.

Table 1.1 Steady design fire size

Fire scene	Heat release Q/kW
minimum fire of combustible is limited in the atria	2000
minimum fire of combustible is not limited in the atria	5000
maximum fire of combustible is not limited in the atria	25000

For a t-squared fire, the location of the smoke layer interface can be estimated by the unsteady filling equation from NFPA 92B. The most convenient method of analysis for the unsteady design approach is by a computer zone fire model, and it is not discussed further in this research report.

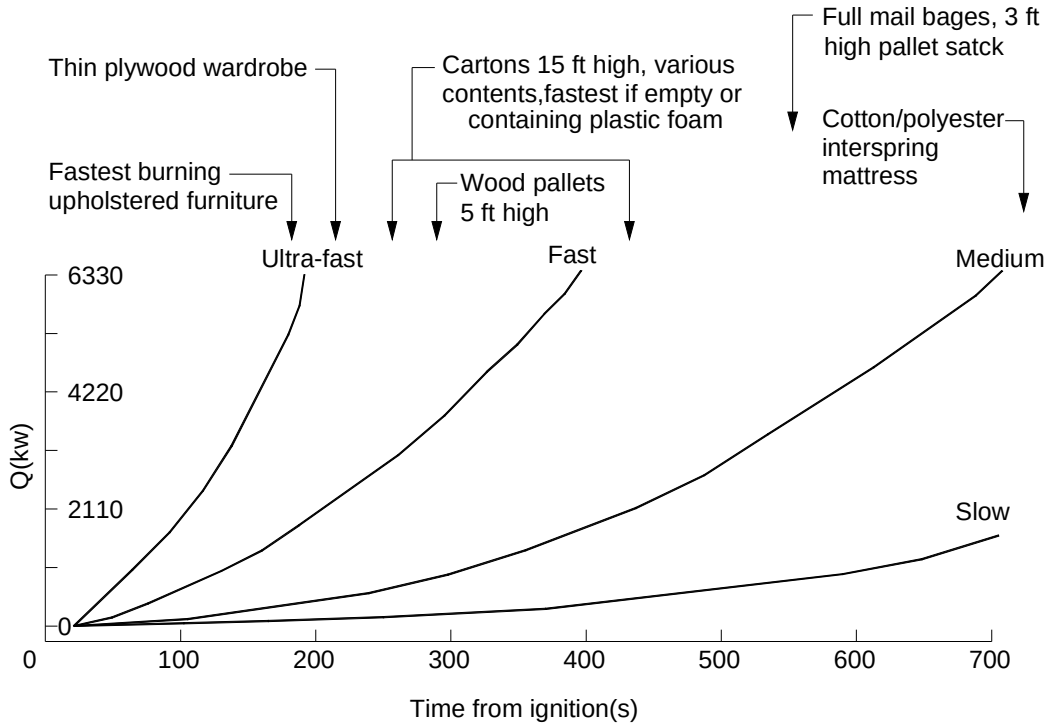

Fig. 1.5 t-square fire

Smoke control system design for atria is more complicated because of the number of factors that affect air and smoke movement. Atrium smoke management systems have been mandated by building codes since early 1980s. Early requirements were based on the air change rate methods, whereby the total volume of the enclosed space was used to determine airflow rates. Formerly smoke control specifications only use the volume of atrium space as a criterion for designing smoke extraction system. Obviously it is not reasonable. Fire size and the risks posed by the position of a smoke layer interface are not documented in these earlier editions.

The National Fire Protection Association (NFPA) established the Technical Committee on Smoke Management Systems in 1985. Its first committee project became NFPA 92A, Recommended Practice for Smoke Control Systems, which was published in 1988. The second project was the development of NFPA 92B, Guide for Smoke Management Systems in Malls, Atria, and Large Areas, first published in 1991.

1.6 Smoke Extraction System Modes and Smoke Exhaust Effectiveness

To protect atrium and all communicating space from smoke, mechanical extraction

system is common installed. There are two possible methods known as ‘smoke extraction through atrium’ and ‘smoke extraction away from atrium’ [3].

The method of ‘smoke extraction through atrium’ is a conventional method that provides vents located at the top of the atrium, smoke can be extracted by natural or mechanical means. The method of ‘smoke extraction away from atrium’ is a method that provides extraction system located within individual shops and arcade area at each floor.

Two methods have been compared by Xiong [16]. The results show that advantages of the method of ‘smoke extraction through atrium’ are its reliable performance, easy control and convenient commissioning. But its effectiveness is not good, when a fire locates in the shopping mall adjacent to the atrium and the fire size is very large. For extracting smoke from the shopping mall adjacent to the atrium, the method of “smoke extraction away from atrium” is effective. But this is not a effective mean for extracting smoke provided by a fire in the atrium or migrated into the atrium when a fire occurs in the compartment connected to an atrium. Yin [17] suggests that the combination of the two methods is a better method.

There are a number of situations that may detrimentally impact the effectiveness of the smoke management system. These include obstructions in the smoke plume or the formation of a pre-stratification layer in the atrium. Under some conditions, another phenomenon may impact the effectiveness of a smoke control system: air from the lower (cold) layer can mix with the smoke in the upper layer as it is being exhausted by the smoke management system. This phenomenon reduces the effectiveness of the smoke management. As a result, the clear height in the atrium is reduced and people in some spaces may be exposed to smoke and toxic gases. To study the effects of this phenomenon on a mechanical exhaust system used for atrium smoke management, a project was initialed by ASHRAE and the National Research Council of Canada in 1995. The project applied both physical and numerical modeling techniques to atrium smoke exhaust systems to investigate the effectiveness of such systems [18]. The experimental facility is a large compartment with dimensions of 9 m by 6 m by 5.5 m. The design of exhaust system in that study is based on the correlation in NFPA 92B. The research results demonstrate that, when the exhaust systems operate near or just below their design capacity, they are effective in extracting gases from the hot layer

without drawing in air from the lower layer. As expected, when the systems operate well above the required flow rates, fresh air from the lower layer enters the system. This, however, does not make system ineffective, as the lever of the smoke layer remains at an acceptable height.

There is concern about exhaust effectiveness for relatively thin smoke layers. There is possibility of pulling some air from below the smoke layer into the exhaust, and such reduced effectiveness would result in a smoke layer interface going below the design value and could expose occupants to smoke. Therefore the project outlined above also studied the depth of the smoke layer required to prevent atrium exhaust from pulling air from the lower layer. If the exhaust inlets were located well above the clear height, the location of the exhaust inlets did not impact the effectiveness of the mechanical exhaust system. If the exhaust inlets were located at or below the height for which the mechanical system had sufficient capacity to maintain a clear height, the relatively thin smoke layer formed below the exhaust inlets. The exhaust gases will include both entrained air from the lower cold layer and the smoke produced by the fire. Further research will be needed to determine the parameters that affect the depth of the smoke layer below the exhaust inlets and scaling of this depth to full scale.

1.7 Smoke Filling Processes and Time Constant

The smoke filling processes in an atrium, simulated by using four zone models, have been reported by Chow [19]. Zone modes FIRST, CFAST and CCFM.VENTS, developed at Building and Fire Research Laboratory at NIST, U.S.A., and the NBTC one-room and two-room hot layer models of the FIRECALC, developed at the CSIRO, Australia, were used to simulate the smoke filling process. Experimental results on full scale atrium smoke–filling processes available in the literature were used for comparing the results on the transient variation of smoke temperature and the development of the smoke layer predicted by the four zone models. That study illustrated that a smoke layer would be formed at the ceiling of atrium space and zone models could be applied to simulate the smoke filling process in an atrium building.
As described above, a survey on the geometrical shapes of atrium spaces in Hong Kong showed that they can be classified into three main types: cubic, flat, and high. Simulations of smoke filling processes in those three types of atria using the zone model FIRST have been reported [20] and the smoke filling times in different types of

atria with the same volume would be very different. It was recommended that a time constant is to be used for specifying the development of smoke and the smoke filling time in the atrium space. A time constant, τ_1, describing how fast the atrium will be filled up with smoke was defined by Chow using the empirical air entertainment rate equation for an atrium space of volume V, floor area A_f, height H, perimeter of fire p and smoke density ρ:

$$\tau_1 = \left(\frac{2\rho}{0.188p}\right)\left(\frac{\sqrt{V}}{\xi}\right) \tag{1.8}$$

The geometrical aspect factor, ξ, of the atrium space is given by:

$$\xi = \sqrt{\frac{H^2}{A_f}} \tag{1.9}$$

Note that there are two parts in the expression for the time constant. The first is related to the properties of a fire and the second part to the geometry of the atrium space.
A correlation of constant time with the time, t_r, required to fill 80% of an atrium with smoke was found. Comparison with experimental data on full-size atria available in the literature was made and fairly good correlation was obtained:

$$t_r = a\tau_1 \qquad (\alpha=1.04\pm 0.2) \tag{1.10}$$

It is common in design to assume the time of escape to be 2.5 minutes (150 seconds), and the time required to fill 80% of the atrium with smoke is suggested to be longer than this value. Therefore, whether a smoke extraction system has to be installed can be determined by the value of the time constant, rather than by the volume only.

Chow (1997) argued that the time constant, τ_1, was defined through the use of the empirical equation expressing the mass entrainment rate to the 3/2 power of the clear height. The equation holds only when the flame tip touches the smoke layer, and the flame temperature was taken to be 1100 K (827℃). Another time constant using the plume equation proposed by Zukoski was defined by Chow:

$$\tau_2 = \left(\frac{3\rho}{2K_2}\right)\left(\frac{A_f}{H^{2/3}}\right) \tag{1.11}$$

Where

$$K_2 = \frac{6\pi}{5}\rho_\infty \alpha_p K_1 C_r$$

And

$$K_1 = C_v \left(\frac{g}{C_p \rho_\infty T_\infty} \right)^{1/3} Q^{1/3}$$

The entrainment coefficient, α_p, of the plume lies between 0.0980 and 0.1878, Q is the heat release rate in kW. Putting in expressions K_1 and K_1 with the numerical Figures of ρ_∞ (1.2111kg/m^3), g(9.81m/s^2), C_p (1,015J/(kg·K)), T_∞ (290K), T_0 (1500K), and C_v (1.11) would give:

$$\tau_2 = \frac{6.245}{\alpha_p Q^{1/3}} \left(\frac{A_f}{H^{2/3}} \right) \tag{1.12}$$

The second time constant was further evaluated by Chow using three other zone models—CFAST and CCFM.VENTS developed in U.S. and BRI2 developed in Japan. Results of the zone modeling simulation supported the fact that the time required to fill 80% of the atrium space with smoke is related to its time constant. A correlation of t_r with the time constant predicted using the zone model FIRST is given by:

$$t_r = 0.798\tau_2 \tag{1.13}$$

The correlation relation is supported by the simulation results of three other zone models–CFAST, CCFM.VENTS, and BRI2. Experimental data on the smoke filling process available in the literature were used to evaluate this time constant. The value of time constant was recommended to specify the smoke filling time for an atrium space for design purposes. Whether a smoke extraction system has to be installed can be determined by checking whether the atrium with a certain time constant will give a time required to fill 80% of the atrium with smoke that is less than 2.5 minutes (150s) using Equation (1.13).

1.8 Airflow for Smoke Control between Atrium and Communicating Spaces

Airflow can be used to prevent smoke flowing from a fire in a communicating space to atrium and also can be used to prevent smoke flowing from the atrium to the communicating space. If it is desired to use airflow to prevent smoke producing in the communicating space from flowing into the atrium, the air needs to be exhausted from the communicating space. The exhaust flow rate needs to be sufficient to result in an average air velocity in the opening between the communicating space and the atrium to prevent smoke flow. NFPA 92B (1995) recommends the following equation for the limiting velocity to prevent smoke backflow:

$$V = 0.64\sqrt{\frac{gH\left(T_f - T_0\right)}{T_f}} \tag{1.14}$$

Where

V--average air velocity, m/s;

g--acceleration of gravity, m/s^2;

H--height of opening, m;

T_f--temperature of heated smoke, K;

T_0--temperature of ambient air, K.

Air can be supplied to a communicating space to achieve a specific average velocity at the opening to the atrium. This velocity should be such that smoke flow to the communicating space is prevented. For opening locations below the smoke layer and 3 m above the base of the fire, the equation (NFPA 92B) for this velocity is

$$V = 0.057\left(\frac{Q}{Z}\right)^{1/3} \tag{1.15}$$

Where

V--average air velocity, m/s;

Q--heat release rate of the fire, kW;

Z--distance above the base of the fire to the bottom of the opening, m.

If the velocity calculated from the above equation is greater than 1 m/s, then a velocity of 1 m/s should be use. This limitation was made out of concern that greater velocities could disrupt the plume flow and have an adverse effect on atrium smoke management. For openings above the smoke layer interface, Equation 15 should be used to calculate

the velocity.

Klote (1997) addressed that research should be needed concerning use of airflow for smoke control between the atrium and communicating spaces. There is insufficient information to evaluate whether these systems provide any significant level of protection to life or if their sole benefit is property protection. The issue of evaluation of the potential benefit of these systems is further complicated by the concern about airflow supplying combustion air for a fire and information is needed to evaluate the potential benefits of these airflow systems. If the benefits support use of these systems, research is needed to develop new approaches for sprinkled fires.

1.9 Sprinkler Effect

Automatic sprinkler systems are installed in many buildings including atria to control fire. Chow [3] indicates that there are three key points to be considered in assessing the performance of an atrium sprinkler: the possibility of actuating the sprinkler in a pre-flashover fire; the thermal response of the sprinkler head and the interaction between the water spray and smoke layer.

Theoretical analysis is as follow. The gas temperature rise at the ceiling can be roughly estimated by the expression:

$$\Delta T_g = \frac{0.22Q^{2/3}}{H^{5/3}} \tag{1.16}$$

Where

ΔT_g --gas temperature rise at ceiling, K;

Q--rate of heat release from the fire plume, kW;

H--height of atrium, m.

Normally, the sprinkler heads would have a temperature rating between 57℃ and 68 ℃. If the ambient air temperature is 20℃ and the heat release rate is 5 MW, then the sprinklers will only be actuated if the atrium height is less than 20m. A normal sprinkler head installed by a fire is of less than 5 MW. For an atrium of 30m height, the value of Q actuating a sprinkler head would be 17MW or more.

The time required for actuating a sprinkler head up to an excess temperature of 50℃ is:

$$t_a = 188 \ln\left(\frac{\Delta T_g}{\Delta T_g - 50}\right) \tag{1.17}$$

Where

t_a--actuation time, s;

τ--time constant, $m^{3/2}s^{3/2}$. (for the normal sprinkler head, τ=188)

For an atrium of height 15m with a 5 MW fire, the time required for actuation (normal head) is about 6 minutes. Therefore, normal sprinkler head is not suitable for the purpose. A fast response sprinkler head seems to be more appropriate as the time constant, τ, in the Equation 1.18 will drop to a value about 50 $m^{3/2}s^{3/2}$, the actuation time becomes much shorter. Similar ceiling height of 15 m requires only 1 minute for actuation.

Even when the sprinkler head is actuated, the smoke is cooled by the discharged water spray and loses its buoyancy. This together with the reaction force due to the air drag experienced by the water droplets would pull the smoke layer downward and give adverse effects on the occupants still staying inside the atrium space. If a smoke extraction system is installed, the effectiveness of it might be reduced due to this strong downward force acting on the smoke layer. Therefore the provision of a mechanical smoke extraction system seems essential. It is doubtful whether sprinkler should be installed in a high headroom atrium.

Chow and Chau (1994) also indicate that automatic sprinklers installed at the atrium ceiling might not be good in controlling an atrium fire. Mawhinney (1994) suggests that a review of current, strategies and assumptions about the behavior of cold smoke in atria in sprinkled building should be conducted. The scenario of smoke from a shielded, sprinkled fire in a floor area adjacent to an atrium could be considered. ASHRAE has a research project to study the hazard to life resulting from sprinkled fires in a communication space.

1.10 Research Objective

Currently, there are a number of calculation methods available to designers for smoke

control of atrium buildings. And there are also many researches on smoke movement in atrium building. Different geometrical arrangements of fire inside a building could lead to different entrainment, and hence different plume expressions.

The amount of air entrained into the plume will depend on the configuration of the plume produced. Milke identified five configurations of smoke plume which may exist within atrium buildings, these are:

1) Axisymmetric plume

An axisymmetric plume is generally expected from a fire located near the centre of an atrium floor. This type of plume is typically remote from any walls and air is entrained around all sides of the plume. Entrainment of air will occur over the full height of the plume until it reaches the interface with a smoke layer which may have formed above. A classical analysis of axisymmetric plumes has been carried out by Morton, Taylor and Turner [21].

2) Wall plume

A plume which is generated from a fire against a wall is known as a wall plume. Zukoski[22] developed a wall plume entrainment correlation based on “mirror symmetry”. Work by Poreh and Garrad has highlighted that further research on wall plume entrainment is desirable.

3) Corner plume

A plume which is generated from a fire located in the corner of a room, where the walls form a 90^{o} angle, is known as a corner plume. Zukoski [23] treated the corner plumes in a similar manner to a wall plume with the use of “mirror symmetry” for plume entrainment. Again, work by Poreh and Garrad has demonstrated that further research is desirable for corner plume entrainment.

4) Spill plume

A spill plume is a vertically rising plume resulting from an initially horizontally moving smoke layer which then subsequently rises at a spill edge (e.g. at an opening onto an atrium space). This type of plume is the major focus of this work as is described in detail in the following section 6.

5) Window plume (door plume)

A window plume is a plume which flows from a window (or doorway) into an atrium space. Typically, window plumes are generated from post-flashover fires. An entrainment correlation was developed by Heskestad, by comparing the air entrainment for a window plume with that of an axisymmetric plume. The window plume entrainment correlation is given by Klote and Milke [24].

Full-scale burning tests were performed to derive the plume expressions empirically. However, widespread use of this approach is not economically feasible and experimental data are limited. With the rapid development of computational fluid dynamics (CFD), it is now possible to assess the plume equations, and CFD might be regarded as a useful tool in solving some plume flows in buildings. There had been earlier works on assessing the temperature and mass flux formulae for some expressions on axisymmetric plumes and balcony spill plumes with CFD packages.

However, there is less research on the effect of fire location on plume entrainment, balcony plume entrainment and smoke movement in large space with the sloping floor. There are three specific objectives which this report aims to address, these objectives are described below:

1) Plume entrainment in a large space with different fire location
2) Balcony plume in a large space building with communicating compartment
3) Smoke movement in a large space with sloping floor

Computational Fluid Dynamics and scale model experiments are two possible methods for the determination of smoke movement in the large building.

2 Governing Equations and Large Eddy Simulation

Smoke and fire movement in a building is usually a turbulent flow with significant density variation due to large temperature gradients. In the field of fire protection engineering, zone models are frequently used for study of fire hazards or design of protections systems. In recent years, however, computational fluid dynamics (CFD) has shown great value as a tool to study smoke and fire movement. In the CFD approach a limited number of assumptions are made and a high-speed digital computer are used to solve the resulting governing fluid dynamic and heat transfer equations.
CFD is divided into three types:
(1) Direct numerical simulation (DNS);
(2) Reynolds averaged Navier-Stokes equation (RANS);
(3) Large eddy simulation (LES).

DNS requires the grid resolution to be as fine as a viscously determined scale. Using DNS with simple geometry and a low Reynolds (Re) number flow provides very valuable information for verifying or improving turbulence models. However, the number of DNS grid points required for the resolution of all scales increases approximately as Re. This creates difficulty in handling high Re numbers with strong buoyant flows, such as fire and smoke movement problems in realistic conditions.
Large-eddy-simulation (LES) for solving the fluid dynamic equations of 3D elliptic, reacting flow.

LES is considered somewhere between DNS and k-e turbulence model computations.
The basic idea behind the LES technique is that eddies that account for most of the mixing is large enough to be calculated with reasonable accuracy from the equations of fluid dynamics. The small-scale eddy motion can be crudely accounted for. The LES approach systematically captures more and more of the dynamic range contained in the Navier-Stokes equations as the spatial and temporal resolution is improved. This approach to the field modeling of fire phenomena emphasizes high enough spatial and temporal resolution with an efficient flow solving technique.

In a LES calculation where the grid is not fine enough to resolve the diffusion of fuel and oxygen, an adjusted mixture fraction-based combustion model is used. The

large-scale transport of combustion products can be simulated directly, but combustion processes occurring at small length and time scales are represented in an approximate manner.

2.1 Governing Equation

Smoke movement is a compressible physics phenomenon and it should be satisfied by the following compressible flow equations:

$$\frac{\partial \rho}{\partial t}+\frac{\partial}{\partial x_i}(\rho u_i)=0 \tag{2.1}$$

$$\frac{\partial}{\partial t}(\rho u_i)+\frac{\partial}{\partial x_j}(\rho u_i u_j)=\frac{\partial p}{\partial x_i}+\frac{\partial}{\partial x_j}\left[\mu\left(\frac{\partial u_i}{\partial x_j}+\frac{\partial u_i}{\partial x_i}\right)\right]-\frac{2}{3}\frac{\partial}{\partial x_i}\left(\mu\frac{\partial u_j}{\partial x_j}\right)+\rho g_i \tag{2.2}$$

$$\frac{\partial}{\partial t}(\rho c_p T)+\frac{\partial}{\partial x_j}(\rho u_j c_p T)=\frac{\partial}{\partial x_j}\left(\lambda\frac{\partial T}{\partial x_j}\right)+q \tag{2.3}$$

$$\frac{p}{\rho}=RT \tag{2.4}$$

Here, all symbols have their usual fluid dynamical meaning: is the density, u the velocity vector, p the pressure, g the gravity vector, cp the constant pressure specific heat, T is the temperature, λ is the thermal conductivity, t is the time, q is the prescribed volumetric heat release, R is the gas constant equal to the difference of the specific heats $R=C_p-C_v$.

2.2 Turbulence Model

LES solves the large eddy motion by a set of filtered equations governing the three-dimensional, time-dependent movements. The small eddies are modeled independently from the flow geometry.

The filtering operation decomposes a full field, $\phi(x,t)$, into a resolved component $\bar{\phi}(x,t)$ and a sub-grid scale component $\phi'(x,t)$ [25]. The resolvable-scale component, $\phi(x,t)$, is obtained from its full field, $\phi(x,t)$, by employing a filter $G(x,\Delta)$ of specified width Δ:

$$\bar{\phi}(x,t)=\int_{\Omega} G(x-x',\Delta)\phi(x',t)\,dx' \tag{2.5}$$

Where, Ω is the interested domain. The unresolved field, component, $\phi(x,t)$ is given by:

$$\phi'(x,t)=\phi(x,t)-\bar{\phi}(x,t) \tag{2.6}$$

With the finite volume method used in the LES formulation, it seems natural to define the filter width as an average over a grid volume ($\Delta_i=(\Delta x\Delta y\Delta z)^{1/3}$).

In most LES involving compressible flows, the variables are Favre-filtered (i.e. density weighted) by $\tilde{f}=\overline{\rho f}/\bar{\rho}$ (f is a variable, and ρ is the density) in order to consider density fluctuations.

Applying the filtering operation to each term in the conservation equations of mass, momentum, energy and species, and decomposing the dependent variables (u; v; w; p; etc.) into resolved and subgrid components results in the filtered governing equations, shown below:

$$\frac{\partial\overline{\rho_l}}{\partial t}+\frac{\partial\overline{\rho_l}\overline{u_i}}{\partial x_i}=0 \tag{2.7}$$

$$\frac{\partial\overline{\rho_l}\overline{u_j}}{\partial t}+\frac{\partial}{\partial x_i}\left(\overline{\rho_l u_j u_i}-\overline{p}-\bar{\sigma}_{ij}\right)=-\frac{\partial\overline{\tau_{ij}^{*}}}{\partial x_i} \tag{2.8}$$

$$\frac{\partial\left(\overline{\rho}\,\overline{h}\right)}{\partial t}+\frac{\partial\left(\overline{\rho\,u_i}\overline{h}\right)}{\partial x_i}+\frac{\partial\overline{q_i}}{\partial x_i}-\frac{\partial\overline{p}}{\partial t}-\overline{u_j}\frac{\partial\overline{p}}{\partial x_i}-\bar{\sigma}_{ij}=\bar{Q}_{HR}-C_V\frac{\partial Q_i}{\partial x_i}-\Pi_d+\Sigma_v \tag{2.9}$$

Where $\bar{u}_i$ is the filtered velocity, $\bar{\rho}$ is the filtered density, $\bar{p}$ is the filtered pressure, $\bar{h}$ is the filtered enthalpy per mass, CV the constant volume specific heat, and $\bar{Q}_{HR}$ the filtered volumetric heat release rate that is represented the following section. Here, the diffusive fluxes are given by:

$$\overline{\sigma_{ij}}=2\bar{\mu}\bar{S}_{ij}-\frac{2}{3}\bar{\mu}\delta_{ij}\bar{S}_{kk} \tag{2.10}$$

$$\overline{q_i} = -k\frac{\partial T}{\partial x_i} \tag{2.11}$$

Where $\bar{\mu}$ is the molecular viscosity, and k is the thermal conductivity corresponding to the filtered temperature T. The effect of the SGS terms appears through the SGS stresses S_{ij}, the SGS heat flux Q_i, the SGS pressure dilatation Π_d, and the SGS contribution to the viscous dissipation Π_d. These quantities are defined as,

$$\tau_{ij} = \bar{\rho}\left(u_i u_j - \bar{u}_i \bar{u}_j\right) \tag{2.12a}$$

$$Q_i = \bar{\rho}\left(u_i T - \bar{u}_i T\right), \quad \Pi_d = \overline{pS_{kk}} - \bar{p}\bar{S}_{kk}$$

$$\Sigma_v = \overline{\sigma_{ij} S_{ij}} - \sigma_{ij} S_{ij} \tag{2.12b}$$

2.3 Sub Grid Scale Models

The sub grid scale (SGS) models for the unresolved terms in the momentum and energy equations must be carefully treated. Among the various SGS turbulence models, such as the mixed model and the two parameter mixed model for compressible turbulence offered the best trade off between accuracy and cost. In the thesis, the modeling of the SGS stresses has received comparatively more attention than the other unclosed terms (2.2b) for compressible flows. The anisotropic part of the SGS stresses is treated using the Smagorinsk model, while the Skkis modeled with a formulation developed by Yoshizawa],

$$\tau_{ij} - \frac{\delta_{ij}}{3}\tau_{kk} = -C_R 2\bar{\Delta}^2 \left|S\right|\left(S_{ij} - \frac{\delta_{ij}}{3}S_{kk}\right) = C_R a_{ij} \tag{2.13a}$$

$$\tau_{kk} = C_I 2\bar{\rho}\bar{\Delta}^2 \left|S\right| S^2 = C_I \beta \tag{2.13b}$$

$$a_{ij} = -2\bar{\Delta}^2 \bar{\rho}\left|S\right|\left(S_{ij} - \frac{\delta_{ij}}{3}S_{kk}\right), \quad \beta = 2\bar{\Delta}^2 \bar{\rho}\left|S\right|^2 \tag{2.13c}$$

Where C_R and C_I are model constants

Yoshizawa proposed an eddy -viscosity model for weakly compressible turbulent flows using a multi-scale, direct-interaction approximation method and suggested that C_R=0.0256 and C_I=0 based on theoretical arguments.

The SGS heat flux (2.12b) needs to be closed. A simple approach is to use an eddy diffusivity model of form

$$Q_i = -\frac{\bar{\rho}\nu_T}{\mathrm{Pr}_T}\frac{\partial T}{\partial x_j} = -C_R\frac{\bar{\Delta}^2\rho|S|}{\mathrm{Pr}_T}\frac{\partial T}{\partial x_j} \tag{2.14}$$

The turbulent Prandtl number $\mathrm{Pr_T}$ can be fixed (e.g $\mathrm{Pr_T}$=0.7, $\mathrm{Pr_T}$=0.4)

2.4 FDS Introduction

The CFD model used in this study was Fire Dynamics Simulator (FDS) which has been developed by McGrattan et al of the National Institute of Standards and Technology.

This model numerically solves a form of the Navier-Stokes equations appropriate for low-speed, thermally driven flows typically generated by smoke and heat transport from fires. The fundamental equations and the numerical algorithm within the model are given by McGrattan et al and are discussed in section 2.2 and 2.3. In this study, FDS was set to treat turbulence by means of the Smagorinsky form of Large Eddy Simulation (LES).

A complete description of the FDS model is given in references [26].Inputs required by FDS include the geometry of the structure, the computational cell size, the location of the ignition source, the energy release rate of the ignition source, thermal properties of walls, ceilings, floors, furnishings, and the size, location, and timing of door and window openings to the outside which critically influence fire growth and spread.

The results of the model have been visualized using the post processing tool called Smokeview (version 3.1) developed by Forney and McGrattan. Smokeview is a 3-dimensional imaging software tool which can show isosurfaces (e.g. temperature, mixture fraction) and 3D data files (e.g. temperature, velocity and pressure).

Smokeview is a scientific visualization program that was developed to display the results of an FDS model computation Smokeview allows the viewing of FDS results in three dimensional snapshots or animations. Smokeview can display contours of temperature, velocity and gas concentration in planar slices. It can also display properties with isosurfaces that are three-dimensional profiles of a constant value of

the property. Iso-surfaces are most commonly used to provide a three-dimensional approximation of the flame surface where fuel and oxygen are present such that flames may exist.

From the predicted airflow pattern and temperature fields, the smoke layer interface or thermal stratified layer, height is obtained by inspecting the positions where there are sharp changes of temperature in the vertical direction. The hot layer temperature is taken to be the average value over all at the control cells in the smoke layer.

3 Similar Theory and Dimensionless Numbers

Scale model experiments are based on the similarity principle. Similarity criterion numbers can be found from the governing equations of smoke flow.

3.1 Similar Theory

The governing equations for mass flow, energy flow and contaminant flow in a room will be the continuity equation, Navier-Stokes equations, the energy equation and the mass transport equation, respectively.

The continuity equation for an incompressible flow is given by the following expression:

$$\frac{\partial u}{\partial x}+\frac{\partial v}{\partial y}+\frac{\partial w}{\partial z}=0 \tag{3.1}$$

u, v, and w are the instantaneous velocities in the three coordinate directions x, y, z. It means velocity is the sum of a mean value and a turbulent fluctuation, such as u is the sum of a mean value $\bar{u}$ and turbulent fluctuation u' ($u=\bar{u}+u'$).

The Navier-Stokes equation in the direction of gravity(y-direction) is given by the expression:

$$\rho(\frac{\partial v}{\partial t}+u\frac{\partial v}{\partial x}+v\frac{\partial v}{\partial y}+w\frac{\partial v}{\partial z})=-\frac{\partial p}{\partial y}+\mu\left(\frac{\partial^2 v}{\partial x^2}+\frac{\partial v}{\partial y^2}+\frac{\partial v}{\partial z^2}\right)-\rho g\beta\left(T-T_0\right) \tag{3.2}$$

p, T, t are temperature and time, respectively, and T_0 is a reference temperature (supply temperature). And ρ, β, μ and g is density, volume expansion coefficient, viscosity and gravitational acceleration, respectively. The density and the viscosity are in principle functions of the instantaneous temperature T, but except for the gravitational term the effect is ignored due to the level of temperature differences that occur in practice. The term $\left(T-T_0\right)$ expresses the influence of the temperature in the gravitational term in a formulation called Boussinesq approximation.

The energy equation is given by the expression:

$$\rho c_p\left(\frac{\partial T}{\partial t}+u\frac{\partial T}{\partial x}+v\frac{\partial T}{\partial y}+w\frac{\partial T}{\partial z}\right)=\lambda\left(\frac{\partial^2 T}{\partial x^2}+\frac{\partial^2 T}{\partial y^2}+\frac{\partial^2 T}{\partial z^2}\right)+q \tag{3.3}$$

c_p, λ, and q are specific heat, thermal conductivity and heat release rate of heat source. Where, in the fire location there is a heat source and its power is q, otherwise in the other areas q is equal to zero.

The equations (3.1) to (3.3) describe the velocity u, v, w, the temperature distribution T and pressure distribution p. The variables can also be used for calculation for air volume flow, convective air movement.

It should be noted that radiant heat transfer, which can be an important part of the heat flow in a building, has not been considered.

According to the similarity principles, the governing equations in a no dimensional form can be developed. The defining dimensionless, independent variables as:

$$x^* = x/h_0 \quad y^* = y/h_0 \quad z^* = z/h_0 \tag{3.4}$$

Where, h_0 is a characteristic length of interest in the problem. A typical characteristic length in ventilation problems is the height of supply slot h_0 or the square root of the supply area. The height of a hot or a cold surface can also be used as characteristic length in situations where free convection is the most important problem as for example in the case of cold downdraught in an atrium at low outdoor temperatures. In fire smoke movement, a typical characteristic length h0 is the height of the model.
The velocities:

$$u^* = u/u_0 \; v^* = v/u_0 \quad w^* = w/u_0 \tag{3.5}$$

Where u_0 is a characteristic velocity, normalized by the supply velocity u0 found from:

$$u_0 = Ve_0 / A_0 \tag{3.6}$$

Where V_{e0} is the volume flow rate to the inlet and A_0 is the supply opening area of inlet.

$$T^* = \frac{T - T_0}{T_R - T_0} \tag{3.7}$$

Where, T_0, T_R is supplement temperature, exhaust temperature respectively.

Pressure p, heat source Q and the independent variable time t are normalized by the following expressions:

$$p^* = p / \rho u_0^2 \tag{3.8}$$

$$Q^* = \frac{Q}{Q_0} \tag{3.9}$$

$$t^* = t u_0 / h \tag{3.10}$$

Where, Q_0 is a characteristic heat release of the fire source.

Equations (3.5), (3.6), (3.7), (3.8), (3.9) and (3.10) are substituted into equations (3.1) to (3.4) and the following dimensionless governing equations are obtained

$$\frac{\partial u^*}{\partial x^*} + \frac{\partial v^*}{\partial y^*} + \frac{\partial w^*}{\partial z^*} = 0 \tag{3.11}$$

$$\frac{\partial v^*}{\partial t^*} + u^* \frac{\partial v^*}{\partial x^*} + v^* \frac{\partial v^*}{\partial y^*} + w^* \frac{\partial v^*}{\partial z^*} = -\frac{\partial p^*}{\partial y^*} + \frac{\mu}{\rho h_0 u_0}\left(\frac{\partial^2 v^*}{\partial x^{*2}} + \frac{\partial v^*}{\partial y^{*2}} + \frac{\partial v^*}{\partial z^{*2}}\right) - \frac{\beta g h_0}{u_0^2}\left(T_R - T_0\right) T^* \tag{3.12}$$

$$\frac{\partial T^*}{\partial t^*} + u^* \frac{\partial T^*}{\partial x^*} + v^* \frac{\partial T^*}{\partial y^*} + w^* \frac{\partial T^*}{\partial z^*}) = \frac{\lambda}{c_p \rho_0 h_0 u_0}\left(\frac{\partial^2 T^*}{\partial x^{*2}} + \frac{\partial^2 T^*}{\partial y^{*2}} + \frac{\partial^2 T^*}{\partial z^{*2}}\right) + \frac{Q_0}{\rho_0 c_p u_0 T_0 h_0^{\ 2}} Q^* \tag{3.13}$$

It is obvious that the following dimensionless numbers appear in the equations:

$$Ar = \frac{\beta g h_0 \left(T_R - T_0\right)}{u_0^2} \tag{3.14}$$

$$\mathrm{Re} = \frac{\rho h_0 u_0}{\mu} \tag{3.15}$$

$$\mathrm{Pr} = \frac{\mu c_p}{\lambda} \tag{3.16}$$

$$D_{II} = \frac{Q_0}{\rho_0 c_p u_0 T_0 h_0^{\ 2}} = \frac{Q_0}{\rho_0 c_p g^{1/2} T_0 L^{5/2}} \tag{3.17}$$

A_r, Re and Pr DII are called Archimedes number, Reynolds number, Prandtl number and Damlohler's ratio respectively.

The Archimedes number may be considered as a ratio of thermal buoyancy force to inertial force, while the Reynolds number may be looked upon as a ratio of inertial

force to viscous force. The Reynolds number can also be considered as a ratio of turbulent diffusion to laminar diffusion. The Prandtl number is the ratio of momentum diffusivity to thermal diffusivity. Damlohler's ratio is the ratio of heat release rate by burning to convection.

3.2 Similarity Principles and Conditions for Model Experiments

The general conditions for scale model experiments with flow in a room are:
1) Identical dimensionless sets of boundary conditions, including geometry, in room and in model.
2) Identical dimensionless numbers, equations (3.10) to (3.12), in the governing equations for the flow in the room and in the model.
3) The constants ρ, β, μ in the governing equations (equation (3.1) to (3.5)) should only have a small variation with in the applied temperature and velocity levels.

The requirements of identical dimensionless boundary conditions are met when the model is geometrically similar to full scale in the details that are important for the volume flow and the energy flow.

In smoke movement experiments the problem can be deal with the Reynolds number is high and the flow pattern is governed mainly by a fully developed turbulence. The Archimedes number or Froude number is the only important dimensionless number and they can both be fulfilled by an appropriate combination of velocity and temperature difference.

In the fire small scale model experiment design, Reynolds number is large enough that the movement is turbulent flow with fully developed flow. The experiments are characterized by the Archimedes number and Damlohler's ratio:

$$Ar = \frac{\beta g h_0 \left(T_R - T_0\right)}{u_0^2} = idem \tag{3.18}$$

$$D_{II} = \frac{Q_0}{\rho_0 c_p u_0 T_0 h_0^{\,2}} = idem \tag{3.19}$$

The reduced scale model is geometric similarity to the full scale model. The geometric

scale λ is as follow

$$\frac{L_m}{L_f} = \lambda_L = const. \tag{3.20}$$

$$x_m = x_F \left(L_m / L_f \right) \tag{3.21}$$

Where

L--length;

x--location;

Subscripts;

F--full-scale;

m--reduced-scale model.

The temperature is the same in the corresponding location between the reduced scale model and full scale model.

$$T_m = T_f \tag{3.22}$$

According to the equation (3.16), velocity and volumetric rate scaling relationship is as follow:

$$v_m = v_f \left(\frac{L_m}{L_f} \right)^{1/2} = v_f \lambda_L^{1/2} \tag{3.23}$$

$$Ve_m = Ve_f \left(\frac{L_m}{L_f} \right)^{5/2} = Ve_f \lambda_L^{5/2} \tag{3.24}$$

Where

v--velocity, m/s;

V_e--volumetric inlet air supply rate or smoke exhaust rate, m^3/s.

According to the equation (3.17) and (3.20), the fire heat release rate scaling relationship is as follow:

$$Q_{c,m} = Q_{c,F} \left(L_m / L_F \right)^{5/2} \tag{3.25}$$

Where

Q_c--convective heat release rate, KW.

Scaling relationships for the physical modeling are shown as in Table 3.1.

Table 3.1 Scaling relationships for the physical modeling

location	$x_m = x_f \left(L_m / L_f \right)$
temperature	$T_m = T_f$
velocity	$v_m = v_f \left(L_m / L_f \right)^{1/2}$
heat release rate	$Q_{c,m} = Q_{c,f} \left(L_m / L_f \right)^{5/2}$
volumetric rate	$Ve_m = Ve_f \left(L_f / L_m \right)^{5/2} = Ve_f \lambda_L^{5/2}$

Where

x--position;

L--length, m;

T--temperature, K;

v--velocity, m/s;

V_e--volumetric exhaust rate, KW;

Q_c--convective heat release rate, KW.

Subscripts

F--full-scale;

m--reduced-scale model.

4 Scale Model Experiment: Apparatus and Methodology

4.1 Physical Scale Model

The experimental facility used for this study is shown in Fig. 4.1. The physical model is designed to be a 1/15 scale model of a theatre, which has a length, width and height 20*20*30 m .The facility is a compartment with interior dimensions of 1.335 m length by 1.335 m width by 2.055 m height with an exhaust opening on the center of the ceiling. The exhaust opening has a diameter of 0.10 m, which is connected with an exhaust duct. The ceiling, floor and one of walls were made of wood. Three walls were made of Perspex (glass). The two inlets were designed on the bottom of every side wall as shown in Fig. 4.1. These inlets connected with air supply duct, had a width 300-mm and height 200 mm, which had holes on, with 40 percentage areas available for air supply. To allow for visual observation within the compartment, one glass observation was remained, and the two were shielded by shades. The inlet duct and smoke exhaust duct were connected with an orifice flow meter and a fan respectively as shown in Fig. 4.1.

The physical scale model is shown in Fig. 4.2.

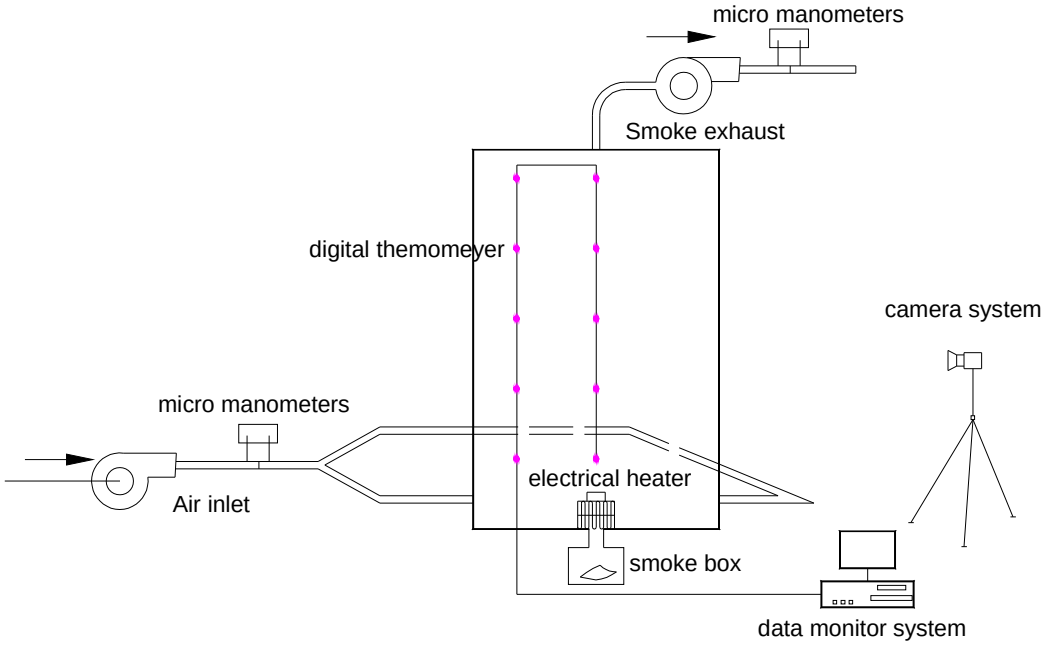

Fig. 4.1 Sketch of the model

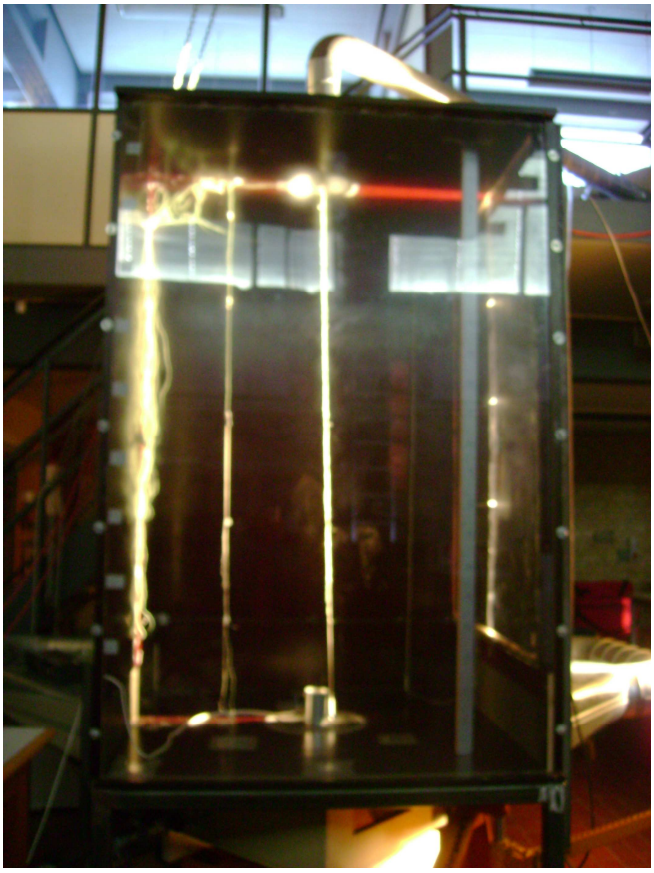

Fig. 4.2 The physical scale model

4.2 Instrumentation

In the test compartment there were thermocouple trees to test the smoke temperature. The electrical heater was used as the fire source. The smoke was produced by smoke box using fuming liquid.

Frequency conversion method was used to change the fans rotation speed. The two transducers were used for the air supplement fan and smoke exhaust fan respectively. And then the designed inlet air volume rate and exhaust rate could be obtained by changing the electric frequency.

The volume flow rate was measured using the throttle aperture mounted in the each air supply duct and smoke exhaust duct. Firstly the throttle aperture ducts were standardized. The rate of the smoke exhaustion and inlet air were deduced from the static pressure difference measured by the micro manometers and the temperature measured by the thermocouple. There is a ruler put in the model to measure the smoke

layer height.

The two sets of throttle duct were used in the experiment. One is large and the other is small. Their equations for calculating the volumetric rate are as follow:

For the small duct set, the relationship between the pressure difference and volumetric rate are as follow:

$$\Delta p = 0.00998 \cdot Ve^{2.04977} \tag{4.1}$$

$$Ve = 9.465 \cdot \Delta p^{0.4879} \tag{4.2}$$

Where,

Δp --mmH_2O;

Ve --m^3/h.

For the large duct set, the pressure difference and volumetric rate are as follow:

$$\Delta p = 0.005957 \cdot q_v^{2.03975} \tag{4.3}$$

$$Ve = 12.325 \cdot \Delta p^{0.490256} \tag{4.4}$$

$$Ve_m = Ve \cdot \sqrt{\frac{1.2}{\rho}} \tag{4.5}$$

Δp --Pa

q_v --m^3/h;

Ve --m^3/h;

Ve_m --the practical volumetric rate in the test.

The volume rate can be calculated by the pressure difference tested in the experiment. Inlet air velocity may be calculated by the volumetric rate and actual inlet areas.

$$V_{in} = \frac{V_e}{A} \tag{4.6}$$

4.3 Test Methods

Before the test, the exhaust and inlet fans were opened. The transducers were adjusted to ensure the designed air supply rate and smoke exhaust rate according to the experimental cases. The smoke producer and electrical heater were turned on for several minutes. When the air flow in the model began to the steady, then carefully made the smoke filled the smoke box, and the air pump was switched on at a fixed voltage to obtain a uniform outlet velocity.

In the experiment beginning the smoke entered into the compartment, the smoke plume rose quickly up to the ceiling, then the plume spread horizontally and down, eventually formed steady smoke depth and then stopped at a certain height in several minutes. The smoke layer height, smoke temperature and inlet air temperature were measured during the test.

The smoke layer height was deduced from the temperature profile collected by thermocouple and the smoke image observed or caught by video. Temperature data were recorded every ten seconds during the test times on a multi-channel data acquisition system. The conditions in the test space were observed by a video camera.

5 Experiment and FDS Simulation on Plume Entrainment for the Different Fire Location

The volume of smoky gases generated from a fire within an atrium is highly governed by the mount of air entrained into the rising smoke plume. The volume of smoke must be calculated in order to determine the required fan capacity or vent area for a smoke ventilation system. The amount of air entrained into the plume will depend on the configuration of the plume produced. Milke identified five configurations of smoke plume which may exist within atrium buildings.

The axisymmetric plumes were discussed in this section. The series of experiments and FDS simulations with the steady-state fire were conducted to study the effect of the fire location on smoke movement or entrainment rates of air from the surroundings.

The fire source was placed in the four different locations on the floor, shown as in Fig. 5.1 and Table 5.1. The inlet air supply rate and smoke exhaust conditions in each fire location experiments were shown in Table 5.1.

Table 5.1 Different fire location and designed fire power in experiment

Scheme	A(center)	B(beside the wall)	C(corner)	D(Between a and C)
Heat release rate(W)	300/500	300	300/500	300
X position(m)	668	668	85	376
Y position(m)	668	85	85	376

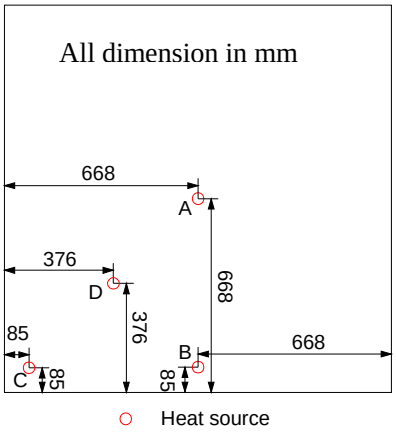

Fig. 5.1 Location of heat source on the floor

Three trees of the thermocouple were collocated in the diagonal of the model shown as Fig. 5.2. A set of 6 thermocouples with 380mm intervals was vertically placed at the center of the compartment over the fire source. A second set of 6 thermocouples with 38-mm intervals was also vertically placed at the corner of the compartment, and a third set of 3 thermocouples with 380mm, 155mm intervals was also vertically placed at the other corner of the compartment, as shown in Fig. 5.2.

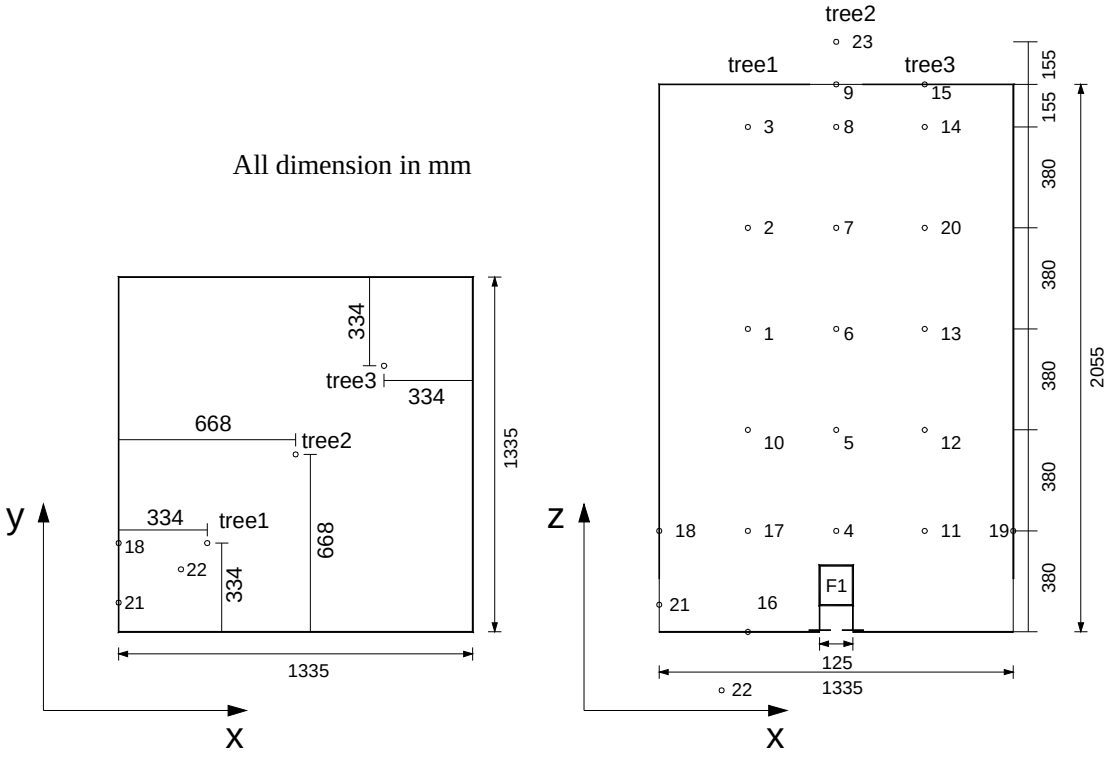

Fig. 5.2 The arrangement of thermocouples

5.1 Experimental Conditions

The series of experiments with the steady-state fire on filling (no ventilation) and ventilation condition were conducted. The smoke exhaust rate and inlet air supply rate were designed in order to get a steady smoke layer height.

The inlet air supply rate and smoke exhaust conditions were summarized in Table 5.2.

5.2 Smoke Filling

Smoke filling experiments has been conducted that the steady-state fire located in the four different location on the floor with heat release 300W and 500W.

Table 5.2 Inlet air supply rate and smoke exhaust rate in the experiment

case	Inlet air supply rate (m^3/s)	Inlet air velocity (m/s)	Smoke exhaust rate (m^3/h)	Smoke exhaust velocity (m/s)
1	0.006	0.031	22.9	0.811
2	0.009	0.044	32.6	1.154
3	0.012	0.060	44.2	1.564
4	0.016	0.079	57.8	2.046
5	0.020	0.097	71.2	2.517
6	0.025	0.122	89.8	3.178
7	0.030	0.147	108.2	3.828
8	0.044	0.215	157.9	5.585
9	0.058	0.283	207.6	7.342
10	0.071	0.350	257.3	9.099
11	0.085	0.418	307.0	10.856
12	0.099	0.486	356.6	12.614

To obtain more information about the smoke movements in large space building, CFD simulations were finished by adopting large eddy simulation (LES) technique. In the simulations, the smoke movement was simulated by a steady fire, and the combustion stoichiometry is similar to polyurethane. The initial temperature was set according to the temperature measurements in the experiments.

Fig. 5.3 shows the measured results of vertical temperature distribution of the thermocouple tree 1 located in the southwest corner as a function of the time for the 300W fire located in the center (Fire 1).

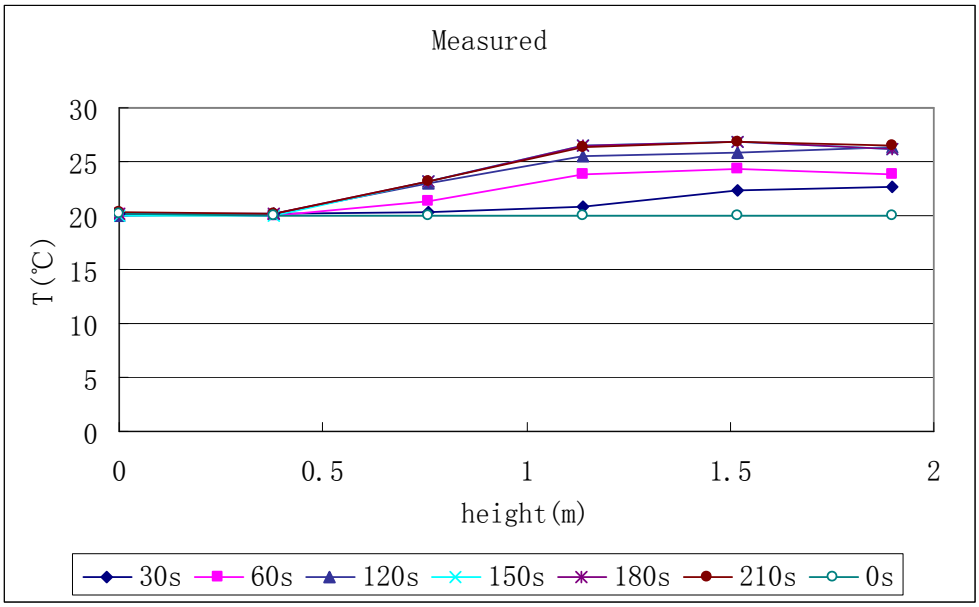

Fig. 5.3 Test vertical temperature distribution (tree 1) versus time in smoke filling (Center fire)

It is obvious that at the beginning of the ignition, the temperatures are almost constant from the bottom to the top of the thermocouple tree. It should be noted that the experimental data taken from the measurements during 1-3.5 minutes show that the temperatures close to the ceiling increase markedly and then all the temperatures increase uniformly. The descent of the smoke layer is very quick at the first period but slows down later. This is attributed to the fact that the rate of air entrainment from the lower layer decreases as the smoke layer descends further. The vertical temperature distribution with smoke tends to be non-uniform with a temperature gradient from the floor to the ceiling. Temperature continuously increased with height up to the region near the ceiling. Stratification effect can be discerned from the temperature changes along the vertical direction at given times. The temperature distribution indicates a distinct interface between the hot upper layer and the relatively cool lower layer, being thick transition zone. The hot gas temperature is not too high. It also indicates that it takes about a litter less than 3 minutes for smoke to descend the floor in the model.

The photographs of smoke filling prediction captured by a digital camera for the fire located in the center and corner are shown in Fig. 1 in Appendix A.

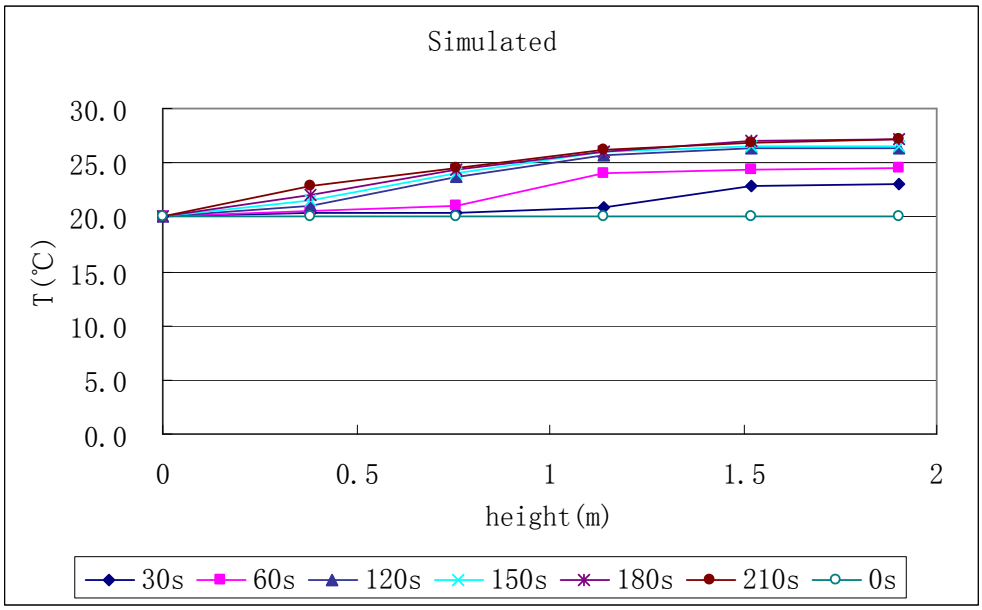

Fig. 5.4 Simulated vertical temperature distribution (tree 1) versus time in smoke filling (Center fire)

Fig. 5.4 shows the temperature profile of the thermocouple on tree 1 simulated by FDS in smoke filling process. It shows the same trends of the smoke filling with the experiment. However the temperature distribution does not indicates a distinct interface between the hot upper layer and the relatively cool lower layer.

Fig. 5.5 shows a comparison of smoke temperature at point 1 and 3 on the tree 1 between experiment and FDS simulation. According to the results of experiments and simulation, the following conclusions can be made from Fig. 5.3. The smoke temperature tested in experiment is little higher than that FDS simulation. But it shows relatively good coincidence in FDS result and experiment.

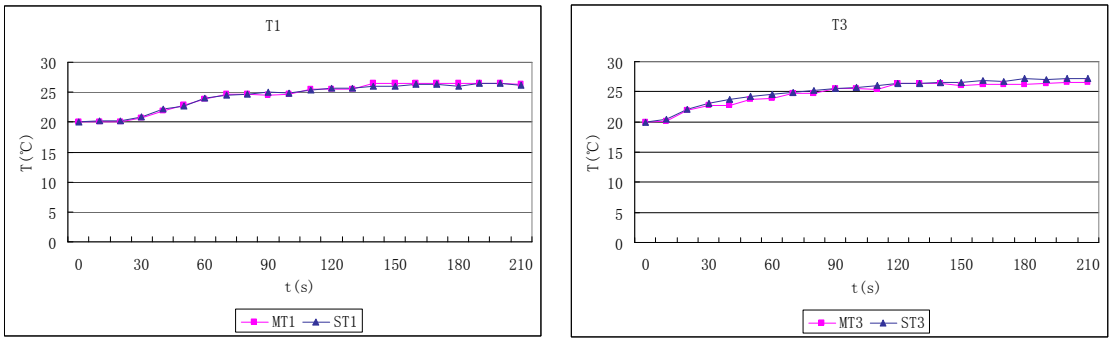

Fig. 5.5 Comparison of temperature between experimental dada and FDS predictions in smoke filling (Center fire)

The photographs of smoke filling prediction simulated by FDS for the fire located in the four locations are shown in Fig. 2 in Appendix A.

Table 5.3 Smoke filling time and its entertainment coefficient

	Fire A		Fire B		Fire C		Fire D	
Heat power (W)	300	500	300	500	300	500	300	500
Filling time (s)	120	90	180	150	210	180	150	120
entertainment coefficient α_p	0.0727		0.0459		0.0388		0.0562	

The filling times simulated by FDS are shown in Table 5.3. According to filling time constant equation (1.12) and (1.13), the entrainment coefficient α_p, of the plume lies between 0.0388 and 0.0727. For the center fire, its entertainment coefficient, 0.0727, is the maximal one. And the entertainment of fire in the corner is the minimal one. Results are accord with the plume theory. Just as the fire was put near the corner, its coefficient is not quarter of the fire in the center.

5.3 Center Fire (Fire A)

1) Experimental result

Fire placed on the different position in the test, the volume rate of the air supplement and smoke exhaust are chosen in Table 5.2. This section discusses the center fire results.

For the center fire with heat release 300W and 500W, the smoke layer height, inlet air temperature, exhaust smoke temperature, and Archimedes number calculated are shown in Table 5.4 and Table 5.5 respectively.

Table 5.4 The experiment result for the fire placed in the center (300W)

Case	Layer height/m	T_{in}/℃	T_{out}/℃	Dimensionless height Z/H	Archimedes number
A1	0.350	20.9	33.3	0.170	837.203
A2	0.400	20.9	32.5	0.195	383.763

A3	0.500	20.7	29.3	0.243	154.379
A4	0.600	21.3	28.7	0.292	77.461
A5	0.700	21.4	28.6	0.341	49.715
A6	0.800	21.6	28.1	0.389	28.116
A7	0.900	21	27.9	0.438	20.545
A8	1.100	20.8	27.4	0.535	9.219
A9	1.300	20.9	26.3	0.633	4.362
A10	1.500	21.1	25.7	0.730	2.418
A11	1.700	21	25.3	0.827	1.587
A12	1.850	21.4	24.5	0.900	0.848

Table 5.5 The experiment result for the fire placed in the center (500W)

Case	Layer height/m	T_{in}/℃	T_{out}/℃	Dimensionless height Z/H	Archimedes number
A1	0.300	20.4	34.5	0.146	951.981
A2	0.400	20	33	0.195	430.079
A3	0.450	21	32.4	0.219	204.642
A4	0.550	20.6	31.8	0.268	117.238
A5	0.600	20.9	31.1	0.292	70.430
A6	0.700	21.4	30.6	0.341	39.795
A7	0.800	21.1	29.5	0.389	25.011
A8	1.000	20.8	29.6	0.487	12.292
A9	1.200	21.2	28.6	0.584	5.977
A10	1.350	21.1	27.8	0.657	3.522
A11	1.500	21.1	27.2	0.730	2.252
A12	1.650	21.1	26.5	0.803	1.476

The relationship between the dimensionless smoke layer height and Archimedes number from the heat release rate 300W experiment is shown in Fig. 5.6. A trend line is added on the Figure which expressing the relationship between dimensionless smoke layer height and Archimedes number. In order to verify the equation 5.1, the test result from the 500W fire is also put in Fig. 5.6. It is obvious that the experiment points from 500W fire are distributed around the trend line.

The relationship between Archimedes number and dimensionless smoke layer height can be described as a formula as follow:

$$\frac{z}{H} = 0.9104 Ar^{-0.2543} \quad (5.1)$$

Which Z is the smoke layer height; H is the height of the room.

Correlation coefficient is 0.99 ($R^2 = 0.9969$)

With the believable level 99%, so the confidence level of the relationship between Archimedes number and dimensionless smoke layer height is very high.

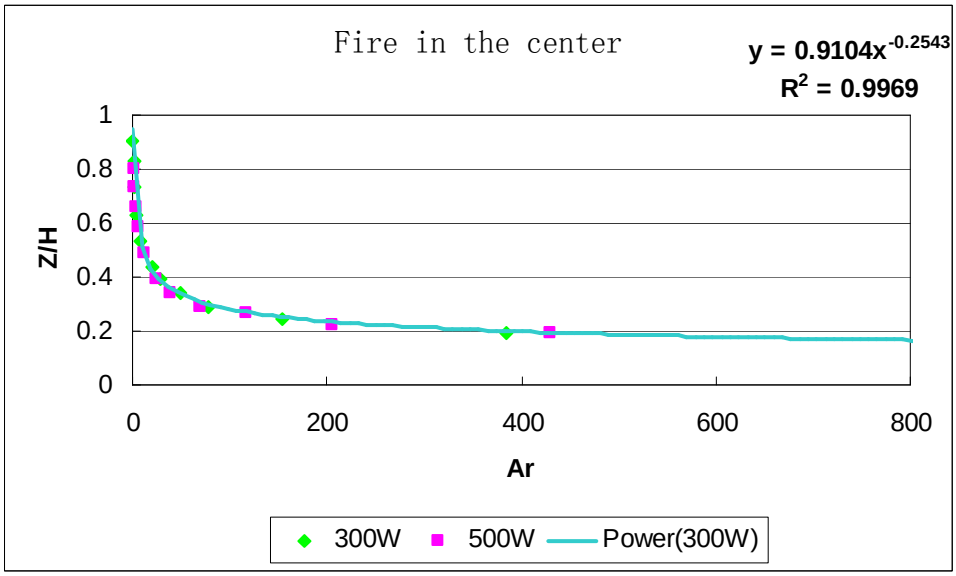

Fig. 5.6 Dimensionless smoke layer height vs. Archimedes number, the fire located in the center of the floor

2) FDS Simulation

To obtain more information about the smoke layer on the smoke exhaust condition, CFD simulations were finished by adopting large eddy simulation (LES) program. In the simulations, the smoke movement was simulated by a steady fire, the initial temperature and air inlet volume and smoke exhaust rate were set according to the measurements in the experiments.

Fig. 5.7 shows a comparison of smoke temperature profile at the corner of the model (tree 1) between experimental and numerical temperature simulated by FDS. The CFD simulation seems to over predict the temperature near the ceiling and shows a temperature gradient within hot layer, while the experimental data indicate that the temperature in the hot layer is uniform. Despite the difference in the temperature

values between the simulation and experimental data, there is a good agreement between the experimental and numerical hot layer height in the compartment.

Comparison of experimental data with CFD model predictions indicate that, while a one to one comparison of temperature does not give very good results, the CFD model was able to predict the level of the hot layer as well as the average temperature in this layer.

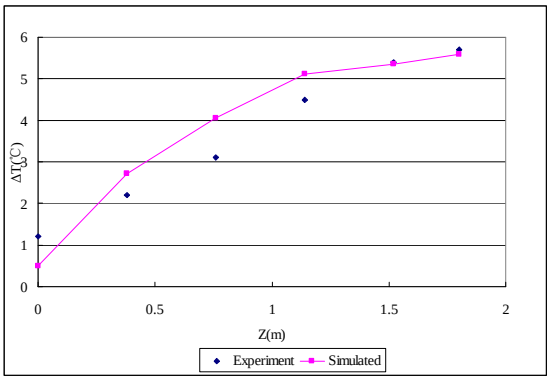

Air supply rate 0.006 m^3/s

Smoke exhaust rate 22.9 m^3/h

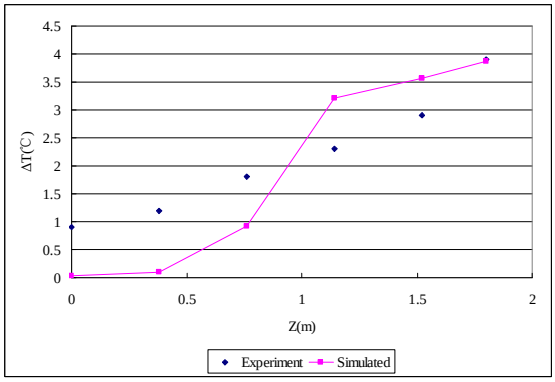

Air supply rate 0.03 m^3/s

Smoke exhaust rate 108.2 m^3/h

Fig. 5.7 Comparison of temperature rise between experimental dada and FDS predictions (300W center fire)

The smoke layer interface height photo obtained by video and FDS are shown in Fig. 3 and Fig. 4 in Appendix A.

5.4 Wall Fire (Fire B)

1) Experimental result

For the fire near the wall with heat release rate 300W, the smoke layer height, inlet air temperature, exhaust smoke temperature, and Archimedes number calculated are shown in Table 5.6.

Table 5.6 The experiment result for the fire placed beside the wall (300W)

Case	Layer height/m	T_{in}/℃	T_{out}/℃	Z/H	Archimedes number
B1	0.450	21.2	29.7	0.219	573.889
B2	0.600	21.7	29.1	0.292	244.814

B3	0.700	21.4	28.4	0.341	125.657
B4	0.800	21.7	27.9	0.389	64.900
B5	0.900	21.8	27.1	0.438	36.596
B6	1.100	21.6	26.4	0.535	20.763
B7	1.200	21.5	26.1	0.584	13.696
B8	1.500	21.9	25.6	0.730	5.168
B9	1.750	21.6	25.3	0.852	2.988
B10	1.950	21.1	25.1	0.949	2.103
B11	2.000	21.7	24.8	0.973	1.144
B12	-	-	-	1	-

The relationship between the dimensionless smoke layer height and Archimedes number from the heat release rate 300W experiment is shown on Fig. 5.8. A trend line is added on the Figure which expressing the relationship between dimensionless smoke layer height and Archimedes number.

The relationship between Archimedes number and dimensionless smoke layer height can be described as a formula as follow:

$$\frac{z}{H} = 1.0894 Ar^{-0.2448} \tag{5.2}$$

2) FDS Simulation

For the fire near the wall in scale model with heat release rate 500W, the smoke layer height on the different smoke exhaust was simulated by FDS. Inlet air temperature, exhaust smoke temperature, and Archimedes number calculated are shown in Table 5.7.

In order to verify the equation 5.2, the FDS simulation result of the 500W fire is also put on the Fig. 5.8. It is obvious that the experiment points from 500W fire are distributed around the trend line.

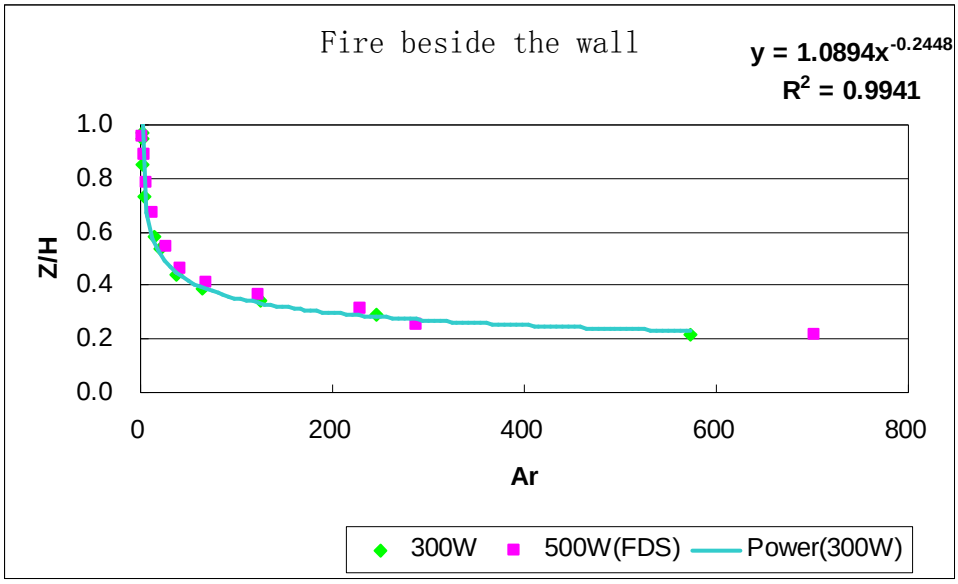

Fig. 5.8 Dimensionless smoke layer height vs. Archimedes number, the fire located beside the wall

Table 5.7 FDS result for the fire placed beside the wall in the scale model (500W)

Case	Layer height/m	T_{in}/℃	T_{out}/℃	Dimensionless height Z/H	Archimedes number
B1	0.450	20	30.4	0.195	702.170
B2	0.520	20	29.7	0.253	287.822
B3	0.650	20	28	0.316	143.608
B4	0.750	20	27.7	0.365	80.601
B5	0.850	20	27.4	0.414	51.096
B6	0.950	20	26	0.462	25.953
B7	1.100	20	24.5	0.545	13.399
B8	1.320	20	25.1	0.672	7.124
B9	1.610	20	24.5	0.783	3.635
B10	1.820	20	24.1	0.886	2.155
B11	1.960	20	23.5	0.954	1.292
B12	-	-	-	-	-

5.5 Corner Fire (Fire C)

1) Experimental result

For the corner fire with heat release 300W and 500W, the smoke layer height, inlet air temperature, exhaust smoke temperature, and Archimedes number calculated are

shown in Table 5.8 and Table 5.9 respectively.

Table 5.8 The experiment result for the fire put in the corner (300W)

Case	Layer height/m	T_{in}/℃	T_{out}/℃	Dimensionless height Z/H	Archimedes number
C1	0.500	20.9	30.3	0.243	634.65
C2	0.600	20.9	29.5	0.292	284.51
C3	0.750	20.7	29.2	0.365	152.58
C4	0.900	21.3	28.8	0.438	78.51
C5	1.000	21.4	27.6	0.487	42.81
C6	1.150	21.6	27.1	0.560	23.79
C7	1.300	21	26.9	0.633	17.57
C8	1.650	20.8	25.4	0.803	6.43
C9	1.900	20.9	24.3	0.925	2.75
C10	2.000	21.1	23.5	0.973	1.26
C11	-	-	-	-	-
C12	-	-	-	-	-

Table 5.9 The experiment result for the fire placed in the corner (500W)

Case	Layer height/m	T_{in}/℃	T_{out}/℃	Dimensionless height Z/H	Archimedes number
C1	0.450	21.2	33.7	0.219	843.95
C2	0.550	20.6	32.7	0.268	400.30
C3	0.700	21.1	31.9	0.341	193.87
C4	0.800	20.9	30.6	0.389	101.54
C5	0.900	21	29.3	0.438	57.31
C6	1.000	21.3	28.8	0.487	32.44
C7	1.150	20.8	27.9	0.560	21.14
C8	1.500	20.6	26.2	0.730	7.82
C9	1.750	20.8	25.8	0.852	4.04
C10	2.000	20.8	24.8	0.973	2.10
C11	-	-	-	-	-
C12	-	-	-	-	-

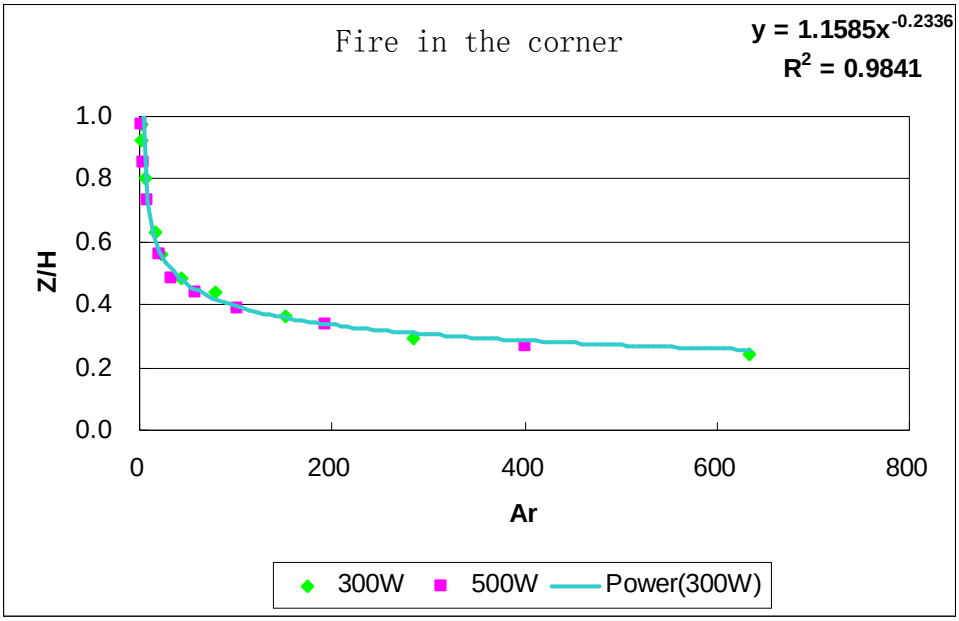

Fig. 5.9 Dimensionless smoke layer height vs. Archimedes number, the fire located in the corner of the floor

The relationship between the dimensionless smoke layer height and Archimedes number from the heat release rate 300W experiment is shown on Fig. 5.9. A trend line is added on the Figure which expressing the relationship between dimensionless smoke layer height and Archimedes number.

The relationship between Archimedes number and dimensionless smoke layer height can be described as a formula as follow:

$$\frac{z}{H} = 1.1585 Ar^{-0.2336} \tag{5.3}$$

In order to verify the equation 5.3, the test result of the 500W fire is also put on the Fig. 5.9. It is obvious that the experiment points from 500W fire are distributed around the trend line.

Fig. 5.10 shows a comparison of smoke temperature profile at the corner of the model (tree 1) between experimental and numerical temperature simulated by FDS. The CFD simulation seems to over predict the temperature near the ceiling and shows a temperature gradient within hot layer, while the experimental data indicate that the temperature in the hot layer is uniform. There is a good agreement between the

experimental and numerical hot layer height in the compartment. The CFD model was able to predict the level of the hot layer as well as the average temperature in this layer.

The smoke layer interface height obtained by video and FDS are shown in Fig. 5 and Fig. 6 in Appendix A.

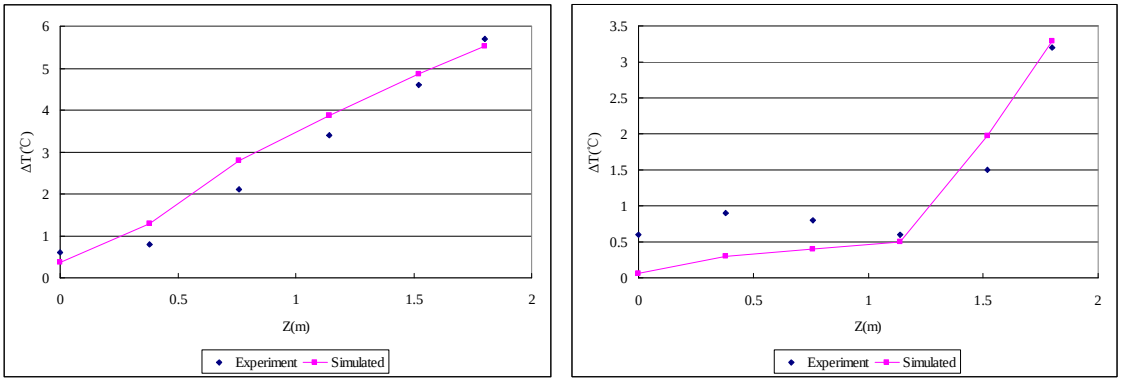

Air supply rate 0.006 m^3/s Air supply rate 0.03 m^3/s

Smoke exhaust rate 22.9 m^3/h Smoke exhaust rate 108.2 m^3/h

Fig. 5.10 Comparison of temperature rise between experimental dada and FDS predictions (300W corner fire)

5.6 Comparison

The Table 5.10 and Fig. 5.11 show the smoke layer height of the three fire location schemes on the same ventilation condition. It is obvious that the smoke layer height with the fire located on the position C that is on the corner, is higher than the others, on the same air volumetric and smoke exhaust rate conditions.

If the fire located in the center a symmetry plume or free plume is formed and the ambient air is entrained through the plume boundary. The decrease in temperature with height is accompanied by broadening of the plume and a reduction in the upward flow velocity.

With the unconfined plume, there are no physical barriers to limit vertical movement or restrict air entrainment across the plume boundary. If the fire (source) is located close to the wall, or in the corner formed by the intersection of two walls, the entrainment will be reduced compared to the entrainment in a free plume and the resulting

restriction on free air entrainment will have a significant effect. In a buoyant plume, temperature will decrease less rapidly with height as the rate of mixing with cold ambient air will be significantly less than for the unbounded case.

The dimensionless smoke layer height vs. Archimedes number for the three fire location is shown on Fig. 5.6.

Table 5.10 Comparison of smoke layer height on the same ventilation condition (300W)

Layer height/m	A	B	C
1	0.350	0.450	0.500
2	0.400	0.600	0.600
3	0.500	0.700	0.750
4	0.600	0.800	0.900
5	0.700	0.900	1.000
6	0.800	1.100	1.150
7	0.900	1.200	1.300
8	1.100	1.500	1.650
9	1.300	1.750	1.900
10	1.500	1.950	2.000
11	1.700	2.000	
12	1.850		

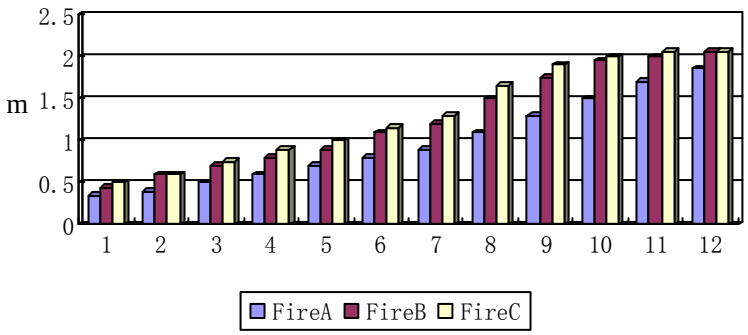

Fig. 5.11 Smoke layer height

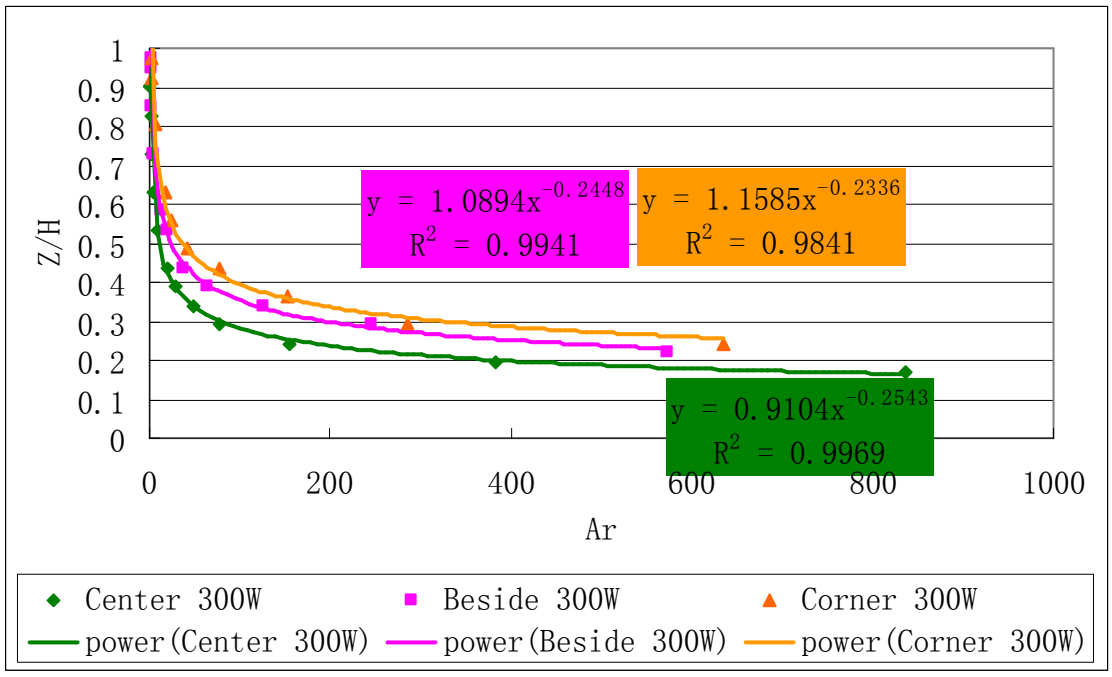

Fig. 5.12 Comparison of three fire location

The order to analyze the smoke layer interface position and air entrainment coefficient of the three fire location cases, the test results are compared with the algebraic equations of plume entrainment.

As reported in the literature [28] [29] [30] [31], a fire plume can be divided into three distinct regions. Those are the ‘continuous’ and ‘intermittent’ flame regions close to the source, and a ‘conventional buoyant plume’ region above the flame tip. Experiments indicate that entrainment rates of air into the plume would be different for those three regions. Therefore, different models and correlation parameters are required for these regions. The flame region is very complex with buoyancy-induced turbulence, chemical reactions, and thermal radiation. The entrainment processes are not as well-understood as the other regions. Even the factors affecting the plume behavior are not clearly identified.

Experiments have been carried out to get some empirical correlation, but very different results were obtained by different researchers. Simple empirical equations on mass flow for a ‘large fire’ based on roof venting experiments were reported by Thomas et al. The mass flow rate was found to be independent of the heat output, but proportional to the perimeter of the fire source and clear layer height to the power of 3/2. Although

there is little theoretical justification for the 'large fire' equation, it was validated to be consistent with existing experimental data by Hinkley [32]. This equation has the same form as that by Zukoski et al. on the mass flow rate in the continuous flame region.

Only the thermal plume behavior is considered in this thesis. This is taken as a natural convective problem. Four axisymmetric plume equations are commonly used to calculate the mass flow rate m (in kg/s) at height Z (in meters) above a fire of convective heat release rate Qc(in kW):

NFPA-92B equation [13]:

$$m = 0.071 Q_c^{1/3} Z^{5/3} + 0.0018 Q_c \tag{5.4}$$

for $z>z_f$, where z_f is the luminous flame height.

Equation by Zukoski :

$$m = C_m \left(\frac{\rho_a g}{C_p T_a} \right)^{1/3} Q_c^{1/3} Z^{5/3} \tag{5.5}$$

for $z>z_f$, where z_f depends on Q_D and the diameter of the pool fire D, and

$C_m = 0.21$

Equation by McCaffrey [33] [34]:

$$m = 0.124 Q_c \left(\frac{Z}{Q_c^{2/5}} \right)^{1.895} \tag{5.6}$$

for $\frac{Z}{Q_c^{2/5}} > 0.2$

Equation by Thomas et al. and Hinkley :

'Small fire' equation

$$m = 0.153 \rho_a \left[\frac{Q_c g}{\rho_a C_p T_a} \right]^{1/3} \left(Z + 1.5 A_f^{1/2} \right)^{5/3} \tag{5.7a}$$

for $Z_f^{1/2}$ and $Z_f \le H$, $Z \le H + A_f^{1/2} - d$

'Large fire' equation:

$$m = 0.188 P Z^{3/2} \tag{5.7b}$$

for $A_f^{1/2} > (H -)/2$, $Z_f > (H - d)$ and $Z \le (H - d)$

where ρ_a, C_p, and Ta are the density, specific heat, and temperature of the ambient air, H is the ceiling height, P is the perimeter of the fire, d is the depth of the layer of hot gas beneath the ceiling, and A_f is the areas of the fire.

The equilibrium smoke layer interface position can be estimated for a particular heat release rate and exhaust rate using the test data in experiment.

The basic principle of such an estimate is based on a statement of conservation of mass applied to the upper smoke layer:

$$m = m_{out} \tag{5.8}$$

Volumetric smoke exhaust from the upper layer is:

$$m_{out} = \rho_s Ve \tag{5.9}$$

Where

V_e--volumetric flow rate of exhaust gases (m^3/s);

ρ_s--density of smoke exhaust (kg/m^3), determined based on the ideal gas law as:

$$\rho_s = \frac{353}{T_s} \tag{5.10}$$

Where

T_s--temperature of exhaust smoke(℃)

The temperature of the exhaust smoke was tested in the experiment.

The experimental results on a mass flow rate of the center fire case are shown in Fig. 5.13. The results predicted by the existing three axisymmetric plume equations are also shown in the Figures.

It is observed that experiment predicted results on the mass flow rate agreed well with the equations listed in NFPA-92B, the equation reported by Zukoski. The results deviated from the equation due to McCaffrey. Note that this equation described the induced behavior of the strong plume near the flame tip with turbulent effects. Higher entrainment rates resulted due to turbulences.

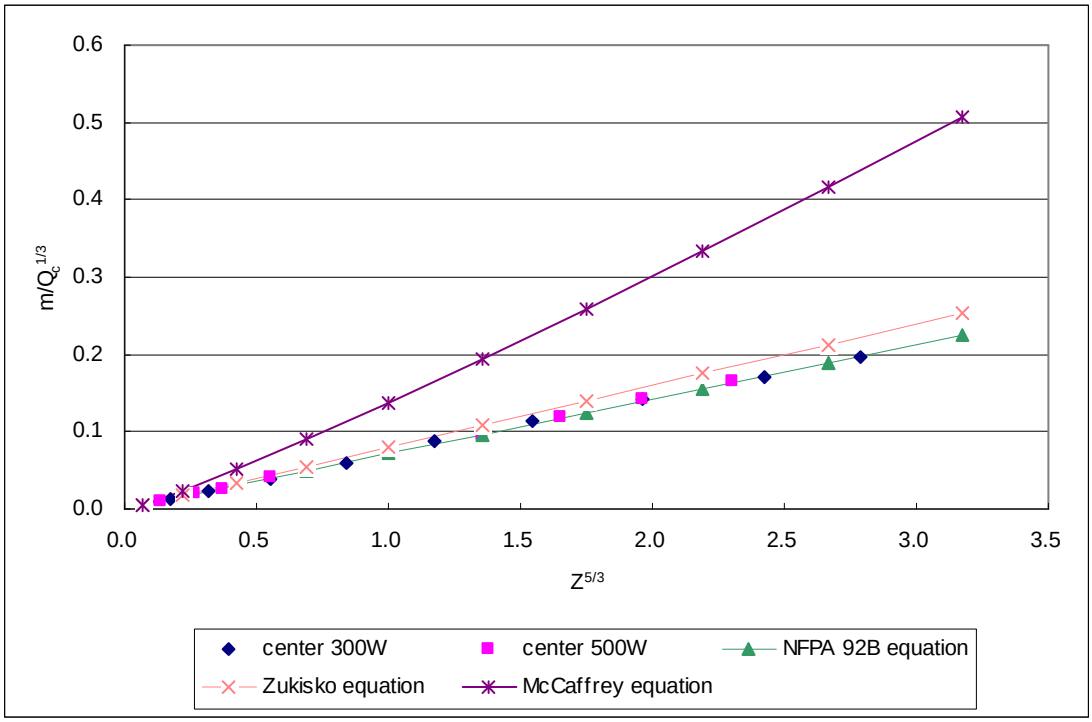

Fig. 5.13 Variation of mass flow rate with height

The experimental results on a mass flow rate of the three different fire location cases are shown in Fig. 5.14.

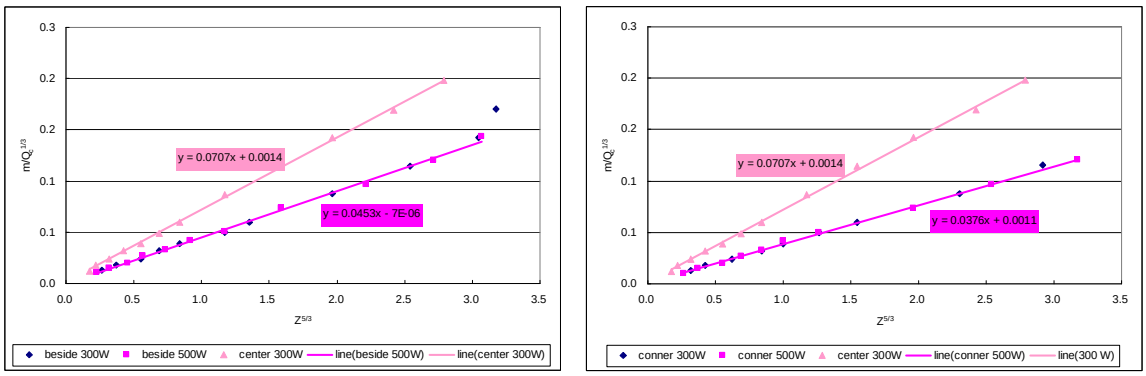

Fire located near to the wall Fire located near to the corner

Fig. 5.14 Comparison of Entrainment Coefficients

It is obvious that the plume entrainment coefficients are about 0.0707, 0.0478, and 0.0376 for the fire located in the center, near to the wall and near to the corner respectively. It shows that the flow rate is 64% of the flow in a free central plume if the fire is located near to the wall, and the flow rate is 48% of the flow in a free central plume if the fire is located near to the corner.

6 Experiment and FDS Simulation on Balcony Plume

In order to study the smoke flowing from a fire in a communicating space to atrium and smoke flowing from a fire in the atrium to the communicating space, the one half of the test compartment was used as communicating and divided into four parts in vertical direction by three clapboard as shown Fig. 6.1.

Fig. 6.1 Test compartment with communicating compartment

The communicating space dimension and thermocouples were shown as Fig. 6.2. There are four trees of thermocouple.

A set of experiments that fire put on the floor were done. Fire location on the floor was shown as Fig. 6.3 and Table 6.1.

Table 6.1 Fire location

case	X(mm)	Y(mm)
AA	668	668
AB	85	85
AC	668	85
AD	668	1001
AE	668	1250
AF	85	1250

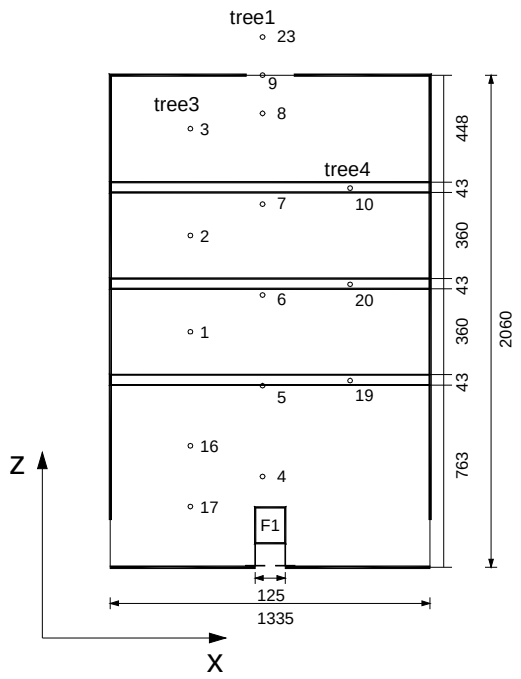

(a)

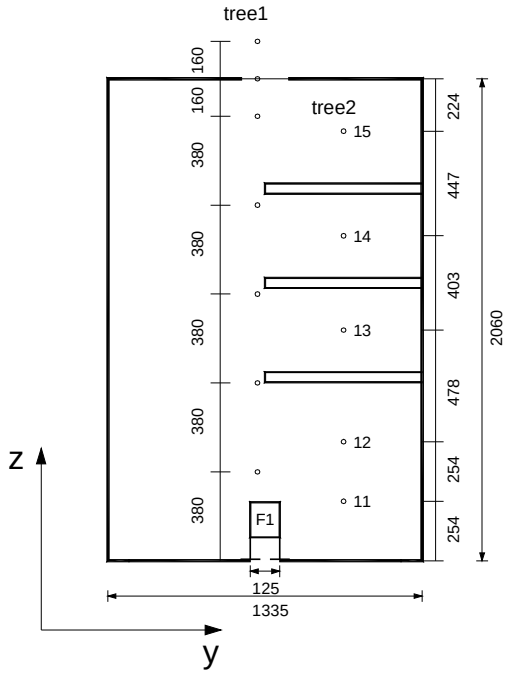

(b)

All dimension in mm

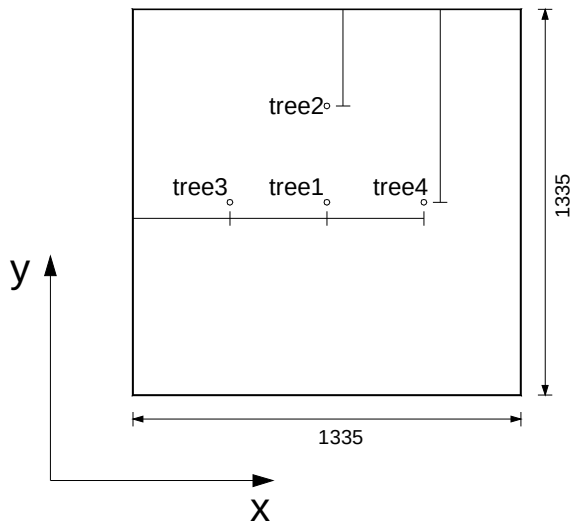

(c)

Fig. 6.2 Model dimension and thermocouple

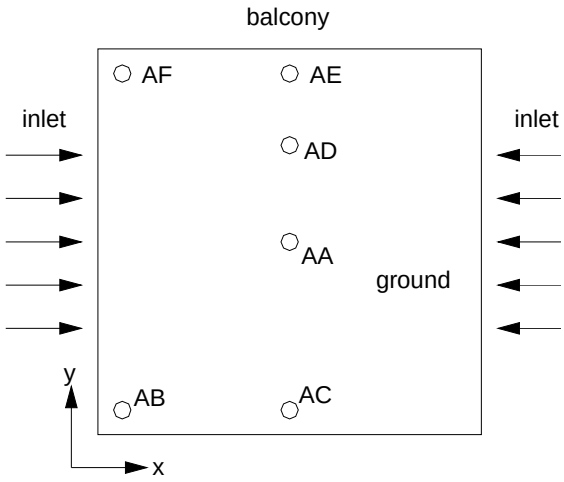

Fig. 6.3 Fire location on the floor

6.1 Smoke Movement from Atrium to Communicating Space

Smoke experiments with heat release rate 300W were done that fire put on the three different location of the atrium floor as shown in Fig. 6.3.

The smoke exhaust rate and inlet air supply rate were designed in order to get a steady smoke layer height. The inlet air supply rate and smoke exhaust conditions were summarized in Table 6.2.

Table 6.2 Inlet air supply rate and smoke exhaust rate in the experiment

case	Inlet air supply rate(m^3/s)	Inlet air velocity (m/s)	Smoke exhaust rate (m^3/h)	Smoke exhaust velocity (m/s)
1	0.006	0.031	22.9	0.811
2	0.009	0.044	32.6	1.154
3	0.012	0.060	44.2	1.564
4	0.016	0.079	57.8	2.046
5	0.020	0.097	71.2	2.517
6	0.025	0.122	89.8	3.178
7	0.030	0.147	108.2	3.828
8	0.044	0.215	157.9	5.585
9	0.058	0.283	207.6	7.342
10	0.071	0.350	257.3	9.099
11	0.085	0.418	307.0	10.856
12	0.099	0.486	356.6	12.614

The fire placed in the center of floor that is case AA, fire near to the communicating space, case AB fire in the corner of atrium, case AC fire beside the wall in the atrium. At the test beginning the inlet and exhaust fans and the smoke box were opened.

Case AA

Case AB

Case AC

Air supply rate 0.03 m^3/s
Smoke exhaust rate 108.2 m^3/h.

Fig. 6.4 Experimental smoke layer height recorded by video

For the case AA, at the test beginning the smoke plume quickly rose up to the ceiling and the plume spread horizontally and down, and meanwhile some of them spread into the second and third communicating space in the smoke move up process. Eventually formed steady smoke depth in atrium and then stopped at a certain height in several minutes. Meantime some smoke spread in the communicating space. Even if smoke exhaust rate was very larger and smoke layer height in atrium was also high, but there was smoke spread into the second communicating space as shown in Fig. 6.4. That is the fire close to the communicating space so smoke is easy to spread into the communicating space in the process of smoke move up.

For the fire located in the corner or near the wall of the atrium that is case AB and AC, smoke move up to the ceiling and down, and spread into the communicating space. But steady smoke layer height both in the atrium and the communicating space is the same as shown in Fig. 6.4.

During the test, the inlet air temperature, smoke exhaust temperature and smoke layer height in atrium were measured.

The tested inlet air temperature, smoke temperature, smoke layer height, and Archimedes number for the case AA, AB and AC are shown in Table 6.3, Table 6.4 and Table 6.5 respectively. The smoke layer height in the tables is the smoke height in the atrium of the model.

The dimensionless smoker layer height vs. Archimedes number and inlet air volumetric

flow rate are shown in Fig. 6.5 and Fig. 6.6. The test result of the case FA, that is fire located in the center of the compartment without communicating space, is also shown in the Figures.

Table 6.3 Inlet air and exhaust smoke temperature, smoke layer height, and Archimedes number for the case AA

AA300W					
q_{in} [m^3/s]	T_{in} [°C]	T_{out} [°C]	Measured smoke layer height Z [m]	Calculated dimensionless height Z/H [-]	Archimedes number [-]
0.006	20.5	33.3	0.500	0.243	863.66
0.009	20	32.6	0.700	0.341	416.85
0.012	20.1	32.2	0.800	0.389	217.21
0.013	20.2	31.6	0.900	0.438	176.64
0.020	20.8	29.9	1.100	0.535	60.96
0.030	19.9	29.1	1.250	0.608	27.27
0.044	19.5	26.5	1.400	0.681	9.75
0.058	19.7	25.1	1.500	0.730	4.35
0.071	19.8	24.9	1.600	0.779	2.68
0.085	19.7	24.3	1.800	0.876	1.70
0.099	19.7	24.1	1.900	0.925	1.20

Table 6.4 Inlet air and exhaust smoke temperature, smoke layer height, and Archimedes number for the case AB

AB300W					
q_{in} [m3/s]	T_{in} [°C]	T_{out} [°C]	Measured smoke layer height Z [m]	Calculated dimensionless height Z/H [-]	Archimedes number [-]
0.006	19.2	30.4	0.700	0.341	756.18
0.009	19.8	30.1	0.800	0.389	307.67
0.012	20.0	29.4	0.950	0.462	168.74
0.016	20.2	28.6	1.100	0.535	98.40
0.020	20.7	27.3	1.300	0.633	59.38
0.025	18.7	26.2	1.500	0.730	22.33
0.030	19.5	25.8	1.650	0.803	8.80
0.044	19.4	25.8	1.750	0.852	5.17
0.058	19.7	25.2	1.850	0.900	2.89
0.071	21.3	24.9	1.900	0.925	2.81

0.085	-	-	2.000	0.973	-
0.099	-	-	-	-	-

Table 6.5 Inlet air and exhaust smoke temperature, smoke layer height, and Archimedes number for the case AC

AC300W					
q_{in} [m3/s]	T_{in} [°C]	T_{out} [°C]	Measured smoke layer height Z [m]	Calculated dimensionless height Z/H [-]	Archimedes number [-]
0.006	20.3	31.3	0.600	0.292	607.65
0.009	20.4	30.5	0.750	0.365	301.06
0.012	20.4	29.4	0.850	0.414	161.56
0.016	20.8	29.2	1.000	0.560	87.93
0.020	20.4	29.0	1.150	0.657	59.38
0.025	20.7	28.7	1.350	0.730	34.60
0.030	19.5	28.0	1.500	0.779	25.31
0.044	19.8	26.5	1.600	0.827	9.36
0.058	20.1	26.1	1.700	0.876	4.85
0.071	19.8	25.7	1.800	0.925	3.10
0.085	20.7	26.3	1.900	0.925	2.07
0.099	-	-	-	-	-

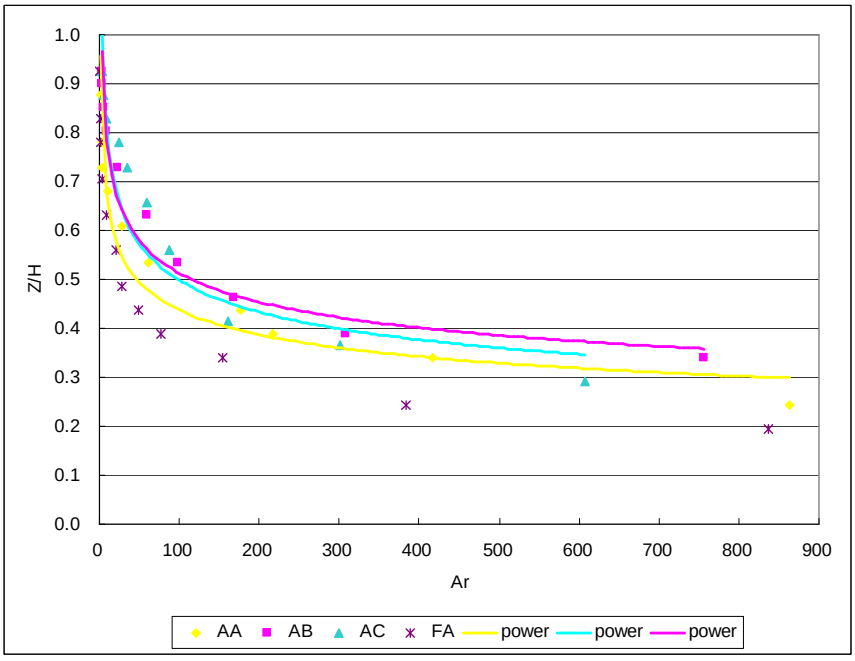

Fig. 6.5 Dimensionless smoke layer height vs. Archimedes number

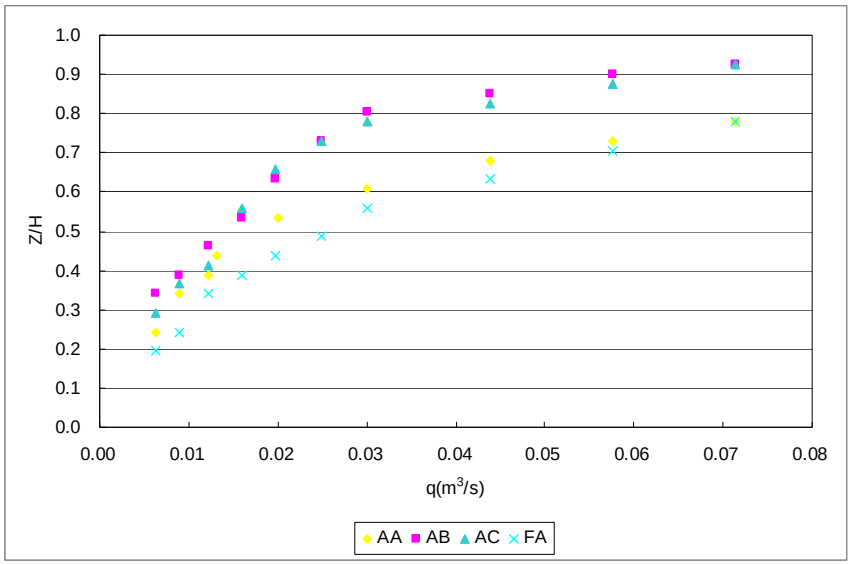

Fig. 6.6 Dimensionless smoke layer height vs. air inlet supply rate

It is obvious that the smoke layer height for the case AA is lower than the case AB and case AC on the same air volumetric and smoke exhaust rate conditions. That is fire in the center of the compartment, the plume entrain the ambient air. If the fire (source) is located close to the wall, or in the corner formed by the intersection of two walls, the entrainment will be reduced compared to the entrainment in a center plume and the resulting restriction on the air entrainment will have a significant effect.

Compare to the case FA that is the fire located in the center of the compartment, the smoke layer height is higher in the case AA. That is some of the smoke spread into the half of compartment with the balcony in the case AA.

6.2 Smoke Movement from Communicating Space to Atrium

6.2.1 Experiment Result

In order to study the balcony plume entrainment and the effect of fire location on entrainment coefficient, smoke experiments with heat release rate 300W were done that fire put on the three different location of the recessed ground level room as shown in Fig. 6.3. The fire placed in the center of the recessed ground level room is case AD, which is the fire located in the center of the communicating space. The case AE is the fire in the corner of the ground level communicating space, case AF is that the fire beside the wall in the ground level communicating space. At the test beginning the inlet and exhaust fans and the smoke box were opened.

The smoke exhaust rate and inlet air supply rate were designed in order to get a steady smoke layer height. The inlet air supply rate and smoke exhaust conditions were summarized in Table 6.2.

During the test, the inlet air temperature, smoke exhaust temperature and smoke layer height in the atrium were measured.

The tested inlet air temperature, smoke temperature, smoke layer height, and Archimedes number for the case AD, AE and AF are shown in Table 6.6, Table 6.7 and Table 6.8 respectively. The smoke layer height Z_p and Z_b in the tables are the smoke height in the atrium of the model and the level space respectively as shown in Fig. 6.7.

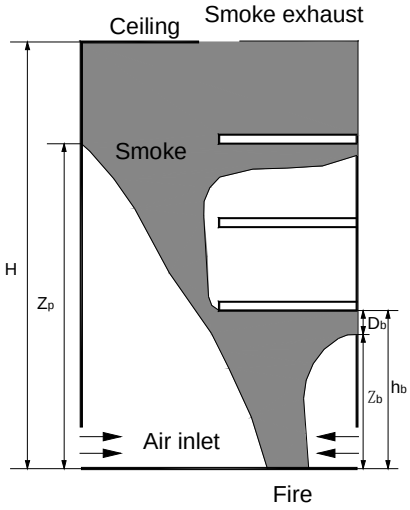

Fig. 6.7 Typical balcony plume

Table 6.6 Inlet air and exhaust smoke temperature, smoke layer height, and Archimedes number for the case AD

AD300W								
q_{in} [m^3/s]	v_{in}[m/s]	T_{in} [°C]	T_{out} [°C]	Smoke layer height Z_p[m]	dimensionless height Z_p/H	Z_b [m]	Z_b/h_b	Archimedes number
0.006	0.031	21.0	29.4	0.400	0.195	0.400	0.524	567.14
0.009	0.044	21.2	29.6	0.500	0.243	0.450	0.590	277.90
0.012	0.060	21.4	29.4	0.550	0.268	0.460	0.603	143.61
0.016	0.079	21.3	29.2	0.600	0.292	0.460	0.603	82.69
0.020	0.097	21.3	29.0	0.650	0.316	0.470	0.616	53.17
0.025	0.122	21.8	28.7	0.750	0.365	0.480	0.629	29.85
0.030	0.147	20.6	25.7	0.800	0.389	0.500	0.655	15.19
0.044	0.215	20.7	25.7	0.850	0.414	0.500	0.655	6.98
0.058	0.283	20.9	25.5	0.900	0.438	0.500	0.655	3.72
0.071	0.350	21.1	25.3	0.950	0.462	0.500	0.655	2.21
0.085	0.418	21.2	25.2	1.000	0.487	0.500	0.655	1.48
0.099	0.486	21.3	24.9	1.050	0.511	0.500	0.655	0.98

Table 6.7 Inlet air and exhaust smoke temperature, smoke layer height, and Archimedes number for the case AE

AE300W								
q_{in} [m^3/s]	v_{in}[m/s]	T_{in} [°C]	T_{out} [°C]	Smoke layer height Z_p[m]	dimensionless height Z_p/H	Z_b [m]	Z_b/h_b	Archimedes number
0.006	0.031	20.8	27.2	0.500	0.243	0.500	0.655	432.10
0.009	0.044	20.7	27.5	0.600	0.292	0.550	0.721	224.96
0.012	0.060	21.1	27.8	0.650	0.316	0.580	0.760	120.27
0.016	0.079	21.2	27.9	0.700	0.341	0.600	0.786	70.13
0.020	0.097	21.6	27.8	0.750	0.365	0.600	0.786	42.81
0.025	0.122	21.9	27.6	0.800	0.389	0.600	0.786	24.66
0.030	0.147	22.2	28.2	0.850	0.414	0.600	0.786	17.86
0.044	0.215	21.9	27.9	0.900	0.438	0.600	0.786	8.38
0.058	0.283	21.9	27.0	0.950	0.462	0.600	0.786	4.12
0.071	0.350	22.1	26.4	1.000	0.487	0.600	0.786	2.26
0.085	0.418	22.3	25.7	1.050	0.511	0.600	0.786	1.26
0.099	0.486	22.0	25.0	1.100	0.535	0.600	0.786	0.82

Table 6.8 Inlet air and exhaust smoke temperature, smoke layer height, and Archimedes number for the case AF

AF300W								
q_{in} [m^3/s]	v_{in}[m/s]	T_{in} [°C]	T_{out} [°C]	Smoke layer height Z_p[m]	dimensionless height Z_p/H	Z_b [m]	Z_b/h_b	Archimedes number
0.006	0.031	20.8	27.6	0.550	0.268	0.550	0.721	459.11
0.009	0.044	21.2	27.6	0.650	0.316	0.580	0.760	211.73
0.012	0.060	21.0	28.2	0.700	0.341	0.580	0.760	129.25
0.016	0.079	21.4	28.0	0.750	0.365	0.600	0.786	69.09
0.020	0.097	21.3	29.2	0.800	0.389	0.600	0.786	54.55
0.025	0.122	21.6	28.2	0.850	0.414	0.600	0.786	28.55
0.030	0.147	20.9	27.1	0.900	0.438	0.600	0.786	18.46
0.044	0.215	21.4	26.8	0.950	0.462	0.600	0.786	7.54
0.058	0.283	21.3	26.5	1.000	0.487	0.600	0.786	4.20
0.071	0.350	21.5	26.2	1.050	0.511	0.620	0.813	2.47
0.085	0.418	21.4	25.9	1.100	0.535	0.650	0.852	1.66
0.099	0.486	21.7	26.0	1.150	0.560	0.650	0.852	1.18

The dimensionless smoker layer height vs. Archimedes number and inlet air volumetric

flow rate are shown in Fig. 6.8 and Fig. 6.9 for the case AD AE and AF.

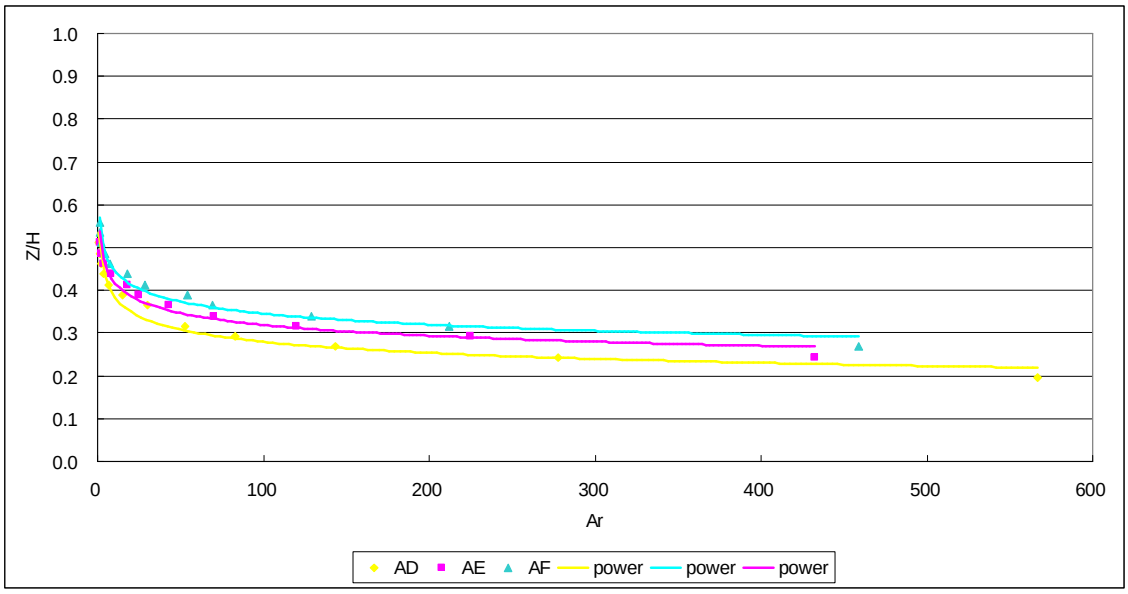

Fig. 6.8 Dimensionless smoke layer height vs. Archimedes number

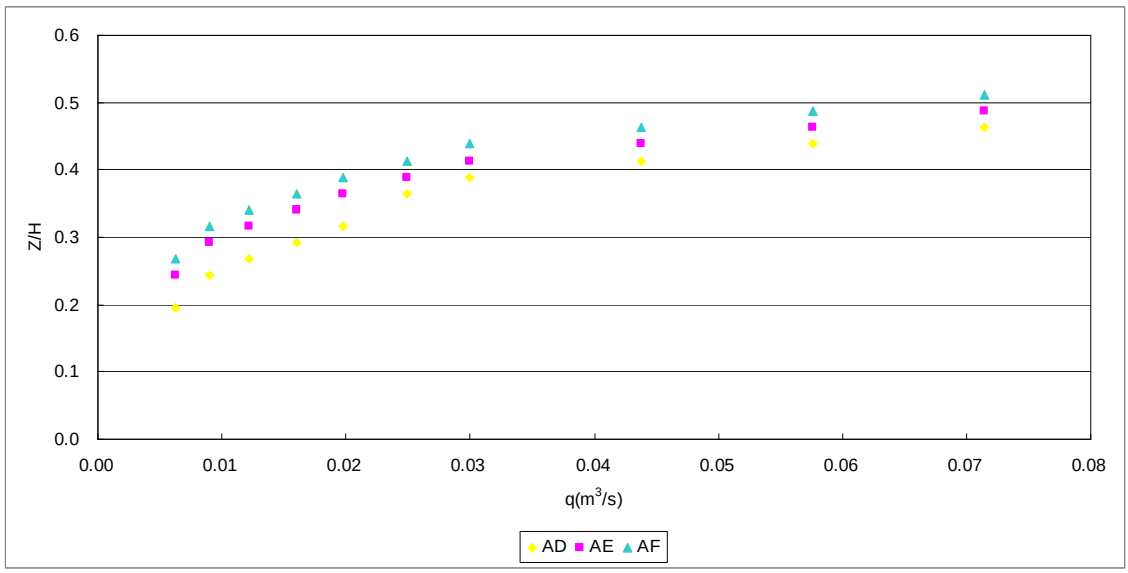

Fig. 6.9 Dimensionless smoke layer height vs. air inlet supply rate

It is obvious that at the same Archimedes number and air supply rate the smoke layer height is the lowest for the case AD. It is that the fire at the center of the communicating space it is an axisymmetric plume and air is entrained around all sides of the plume. In case AE and AF the fire placed near a wall or the corner of the wall and their entrainment are restricted.

6.2.2 FDS Simulation

To obtain more information about the smoke layer on the smoke exhaust condition,

CFD simulations were finished by adopting large eddy simulation (LES) program. In the simulations, the smoke movement was simulated by a steady fire, the initial temperature and air inlet volume and smoke exhaust rate were set according to the measurements in the experiments.

Table 6.9, Table 6.10 and Table 6.11 show the result for the 300W fire simulated by FDS.

Table 6.9 Inlet air and exhaust smoke temperature, smoke layer height, and Archimedes number for the case AD by FDS

AD300W								
q_{in} [m^3/s]	v_{in}[m/s]	T_{in} [°C]	T_{out} [°C]	Smoke layer height Z_p[m]	dimensionless height Z_p/H	Z_b [m]	Z_b/h_b	Archimedes number
0.012	0.060	20.0	23.5	0.584	0.284	0.414	0.543	62.83
0.016	0.079	20.0	23.4	0.613	0.298	0.450	0.590	35.59
0.020	0.097	20.0	23.1	0.664	0.323	0.461	0.604	21.41
0.025	0.122	20.0	23.1	0.698	0.340	0.461	0.604	13.41
0.030	0.147	20.0	23.0	0.720	0.350	0.468	0.613	8.93
0.044	0.215	20.0	22.5	0.734	0.357	0.482	0.632	3.49
0.058	0.283	20.0	22.1	0.765	0.372	0.500	0.655	1.70
0.071	0.350	20.0	21.8	0.802	0.390	0.501	0.657	0.95
0.085	0.418	20.0	21.6	0.822	0.400	0.504	0.661	0.59
0.099	0.486	20.0	21.3	0.884	0.430	0.509	0.667	0.36
0.012	0.060	20.0	21.3	0.925	0.450	0.510	0.668	0.33
0.016	0.079	20.0	21.3	1.020	0.496	0.512	0.671	0.26

Table 6.10 Inlet air and exhaust smoke temperature, smoke layer height, and Archimedes number for the case AE by FDS

AE300W								
q_{in} [m^3/s]	v_{in}[m/s]	T_{in} [°C]	T_{out} [°C]	Smoke layer height Z_p[m]	dimensionless height Z_p/H	Z_b [m]	Z_b/h_b	Archimedes number
0.012	0.060	20.0	24.5	0.597	0.291	0.503	0.659	80.78
0.016	0.079	20.0	24.4	0.638	0.310	0.578	0.758	46.06
0.020	0.097	20.0	24.3	0.661	0.322	0.623	0.817	29.69
0.025	0.122	20.0	24.2	0.706	0.344	0.635	0.832	18.17
0.030	0.147	20.0	23.8	0.725	0.353	0.583	0.764	11.31
0.044	0.215	20.0	23.7	0.769	0.374	0.567	0.743	5.17
0.058	0.283	20.0	23.6	0.777	0.378	0.597	0.782	2.91

0.071	0.350	20.0	23.5	0.803	0.391	0.594	0.779	1.84
0.085	0.418	20.0	23.5	0.916	0.446	0.560	0.734	1.29
0.099	0.486	20.0	23.3	0.975	0.474	0.509	0.667	0.90
0.102	0.500	20.0	23.1	1.030	0.501	0.568	0.744	0.80
0.116	0.569	20.0	22.9	1.100	0.535	0.568	0.744	0.58

Table 6.11 Inlet air and exhaust smoke temperature, smoke layer height, and Archimedes number for the case AF by FDS

AF300W								
q_{in} [m^3/s]	v_{in}[m/s]	T_{in} [°C]	T_{out} [°C]	Smoke layer height Z_p[m]	dimensionless height Z_p/H	Z_b [m]	Z_b/h_b	Archimedes number
0.012	0.060	20.0	23.2	0.627	0.305	0.565	0.740	57.44
0.016	0.079	20.0	23.0	0.653	0.318	0.632	0.828	30.36
0.020	0.097	20.0	22.9	0.685	0.333	0.637	0.835	20.02
0.025	0.122	20.0	22.9	0.715	0.348	0.653	0.856	12.11
0.030	0.147	20.0	22.8	0.755	0.367	0.617	0.809	8.04
0.044	0.215	20.0	22.7	0.760	0.370	0.627	0.822	2.65
0.058	0.283	20.0	21.9	0.821	0.400	0.652	0.855	1.53
0.071	0.350	20.0	21.9	0.886	0.431	0.653	0.856	0.79
0.085	0.418	20.0	21.5	0.933	0.454	0.657	0.861	0.55
0.099	0.486	20.0	21.5	1.060	0.516	0.597	0.782	0.41
0.102	0.500	20.0	21.3	1.100	0.535	0.607	0.796	0.33
0.116	0.569	20.0	21.2	1.180	0.574	0.615	0.806	0.24

Fig. 6.10 shows a comparison of smoke temperature profile at the center of the model (tree 1) between experimental and numerical temperature simulated by FDS for the case AD. The CFD simulation seems to over predict the temperature near the ceiling and shows a temperature gradient within hot layer, while the experimental data indicate that the temperature in the hot layer is uniform. Despite the difference in the temperature values between the simulation and experimental data, there is a good agreement between the experimental and numerical hot layer height in the compartment.

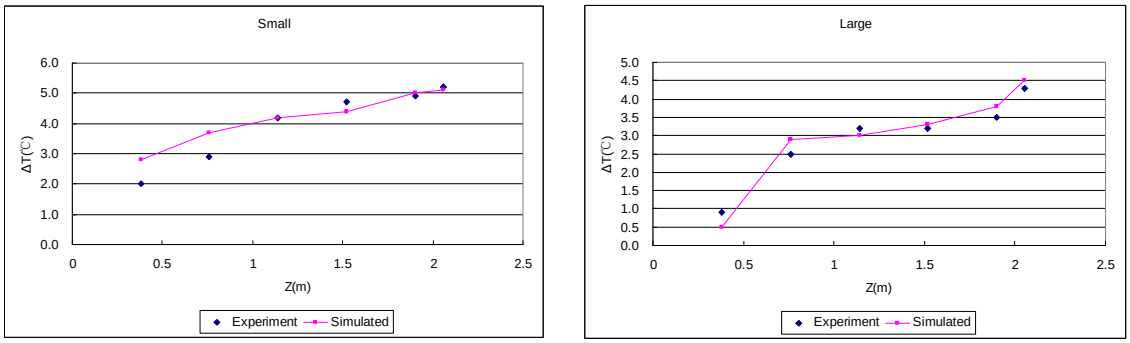

Air supply rate 0.006 m^3/s Air supply rate 0.03 m^3/s

Smoke exhaust rate 22.9 m^3/h Smoke exhaust rate 108.5 m^3/h

Fig. 6.10 Comparison of experimental and Simulation, Fire located in the center of communication space, (case FD)

Fig. 6.11 shows a smoke layer height for the case FD captured by video.

Air supply rate 0.006 m^3/s Air supply rate 0.03 m^3/s

Smoke exhaust rate 22.9 m^3/h Smoke exhaust rate 108.5 $m^{3/}h$

Fig. 6.11 Experiment photos for the case FD

Fig. 6.12 shows the temperature and smoke layer result simulated by FDS for the case FD in the condition of air supply rate 0.006 m^3/s and smoke exhaust rate 22.9 m^3/h.

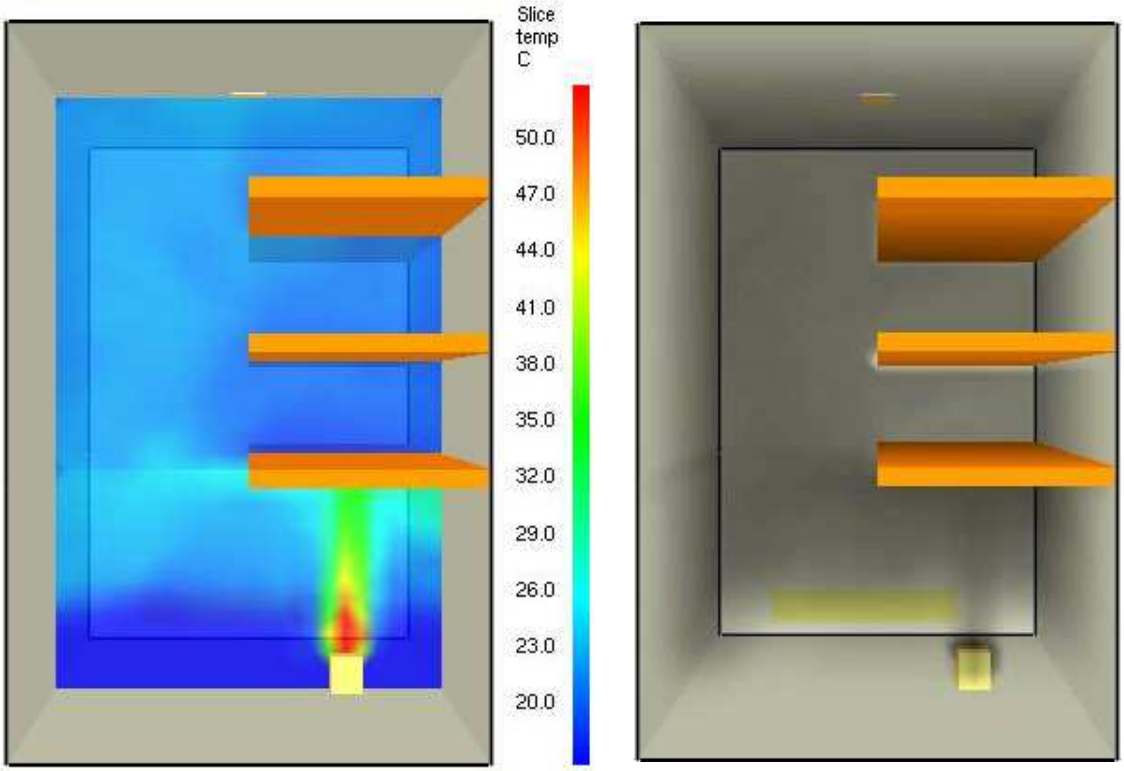

Air supply rate 0.006 m^3/s, smoke exhaust rate 22.9 m^3/h

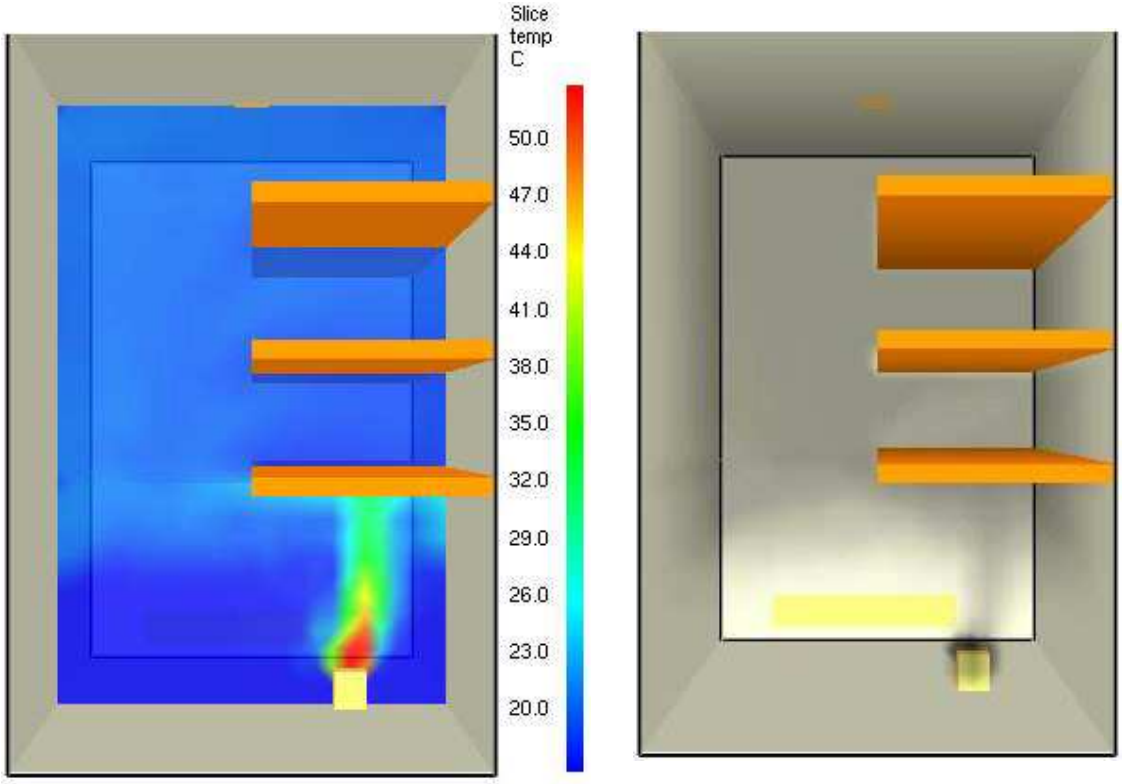

Air supply rate 0.03 m^3/s, smoke exhaust rate 108.5 m^3/h

Fig. 6.12 Temperature and smoke FDS simulation for the case AD

The smoke layer interface height obtained by video and FDS for the case AE are

shown in Fig. 1 and Fig. 2 in Appendix B.

The smoke layer interface height obtained by video and FDS simulation for the case AF are shown in Fig. 3 and Fig. 4 in Appendix B.

6.3 Balcony Plume Entrainment

Different geometrical arrangements of fire inside a building could lead to different entrainment, and hence different plume expressions. Basically, three types of plumes are commonly encountered in designing smoke control system.

Axisymmetric plumes: for a fire placed at the center of a big hall, ambient air is entrained from all sides along the height of the plume. The research on this section sees section 5 in this report.

Balcony spill plumes: for a fire in a shop adjacent to the atrium, scenarios with balcony spill plumes involve smoke rising above the fire; reaching the ceiling, balcony, or other significant horizontal projection; then traveling horizontally toward the edges of the balcony.

Door plumes: plumes issuing from openings, such as doors and windows, into a large-volume, open space.

A typical balcony spill plume due to a fire located at a recessed ground level room is shown in Fig. 6.7. Hot smoke generated by the fire rises up to the ceiling of the room, forms an elevated layer of thickness Db under the wide balcony, spills into the atrium and then rises due to buoyancy. More ambient air is entrained into it. The estimation of the air entrainment rate is very important for designing the smoke control system in an atrium. Entrainment into the smoke flows at the balcony edge and into the rising plume might be calculated by plume equation. For example BRE spill plume model and plume model of Thomas detailed descriptions of this method can be found in the literature.

Plume model of Thomas

Plume model of Thomas was taken as a ‘far plume’ rising from a line source of zero thickness some distance below the void edge. A relatively simple plume equation with virtual source correction on mass flow rate mp at height Zp can be given as

$$m_p = 0.58\rho_g \left[\frac{gQ_c W^2}{\rho_g C_p T_a}\right]^{1/3} \left(Z_p + \Delta\right)\left[1 + \frac{0.22\left(Z_p + 2\Delta\right)}{W}\right]^{2/3} \tag{6.1}$$

Where Δ is the empirical height of the virtual source below the balcony, Z_p is the height

above the balcony, and W is the width of the plume as it spills under the balcony. For small Z_p/W, the main term is consistent with Lee and Emmons model [28]. The results would be reduced to the conventional point source plume theory for Z_p>>W.

Spill plume model of Poreh et al [36]

By assuming that the entrainment into the curved section of the spilling plume is approximately equal to the entrainment into a vertical free plume rising through the same height, a very simple model was proposed by Poreh et al. for calculating the mass flux of free plumes in relatively wide atria. The mass entrainment rate mp of the spill plume at Z_p is given by:

$$m_p = m_b + CQ_c^{1/3}\left(Z_p + D_b\right) \tag{6.2}$$

Where, m_b is the mass flow of gases beneath the balcony, D_b is the depth of the smoke layer beneath the balcony, and C is a constant, which is defined as:

$$C = 0.3C_{m1}\rho_a W^{2/3} \tag{6.3}$$

Where, C_{m1} is the dimensionless entrainment coefficient, determined experimentally to be 0.44 for a free plume.

Spill plume model of Thomas et al. [37]

Applying dimensional analysis without taking the assumptions on similarity or constant entrainment coefficient into account, an entrainment coefficient of 0.11 was deduced, rather than assumed for the larger hood. The value is consistent with the more recent studies of line plumes. The mass entrainment rate mp at Zp can be estimated by:

$$m_p = 1.20m_b + 0.159Z_p(Q_c W^2)^{1/3}\left(0.0027Q_c\right) \tag{6.4}$$

Taking the entrainment into both free ends Δmp as:

$$\Delta m_p = 1.20m_b + 0.159Z_p(Q_c W^2)^{1/3}\left(0.0027Q_c\right) \tag{6.5}$$

The total entrainment rate becomes:

$$m_p = 1.2m_b + 0.16Z_p(Q_c W^2)^{1/3}0.0027Q_c + 0.09Z_p\left(Q_c/W\right)^{1/3} \tag{6.6}$$

NFPA spill plume equation

Based on the interpretation of the small-scale experiments by Morgan and Marshall, a good linear relationship between mp and Z_b was found by Law [38]. The mass production rate can be expressed as:

$$m_p = 0.36(QW^2)^{1/3}\left(Z_b + 0.25h_b\right) \tag{6.7}$$

Where, h_b is the height of the balcony, Z_b is the height above the balcony (Z_b=Z_p-h_b) and Q is the heat release of the fire.

Although all these models were based on the same set of experimental data, different mass flow equations were derived. The difference is due to the method for estimating the air entrainment into the plume while hot smoke is spilling underneath a balcony edge and rising into the large atrium void. Further studies of these models are needed.
Three cases, AD, AE and AF, that is a fire located at the center, beside the wall and the corner of a recessed ground level room, as shown in Fig. 6.3, were considered for studying the mass entrainment rate of the balcony spill plumes.

The experiment was designed to test the smoke layer height on the steady fire and smoke exhaust rate condition. The equilibrium smoke layer interface position can be estimated for a particular heat release rate and exhaust rate using the test data in experiment.

The basic principle of such an estimate is based on a statement of conservation of mass applied to the upper smoke layer. The mass entrainment rate is obtained by the following formula:

$$m = m_{out} \tag{6.8}$$

Where, m is the mass flow rate of the balcony spill plume.
Volumetric smoke exhaust from the upper layer is:

$$m_{out} = \rho_s Ve \tag{6.9}$$

Where
V_e--volumetric flow rate of exhaust gases (m^3/s);
ρ_s--density of smoke exhaust (kg/m^3), determined based on the ideal gas law as:

$$\rho_s = \frac{353}{T_s} \tag{6.10}$$

Where
T_s--temperature of exhaust smoke (℃).

The temperature of the exhaust smoke and volumetric flow rate of exhaust gases were tested in the experiment.

FDS simulation and experiment results of the case AD, AE, and AF with the heat release 300W are compared with those by different spill plume models shown in Fig. 6.13. It is obvious that a linear relationship between the numerical mp and Z_p can be observed. The coefficient of the mass flow rate of the balcony plume is between 0.342 and 0.468. A good agreement is found between the results of CFD simulation and experiment in this report and those predicted by the NFPA plume equations.

Larger discrepancies among the simulation, experiment results and those estimated by the Thomas equation were found.

The possible explanations are:

NFPA equation was derived from experimental data. The equation of Thomas was derived from two-dimensional plumes. The plume might not be two-dimensional and there might be end entrainment.

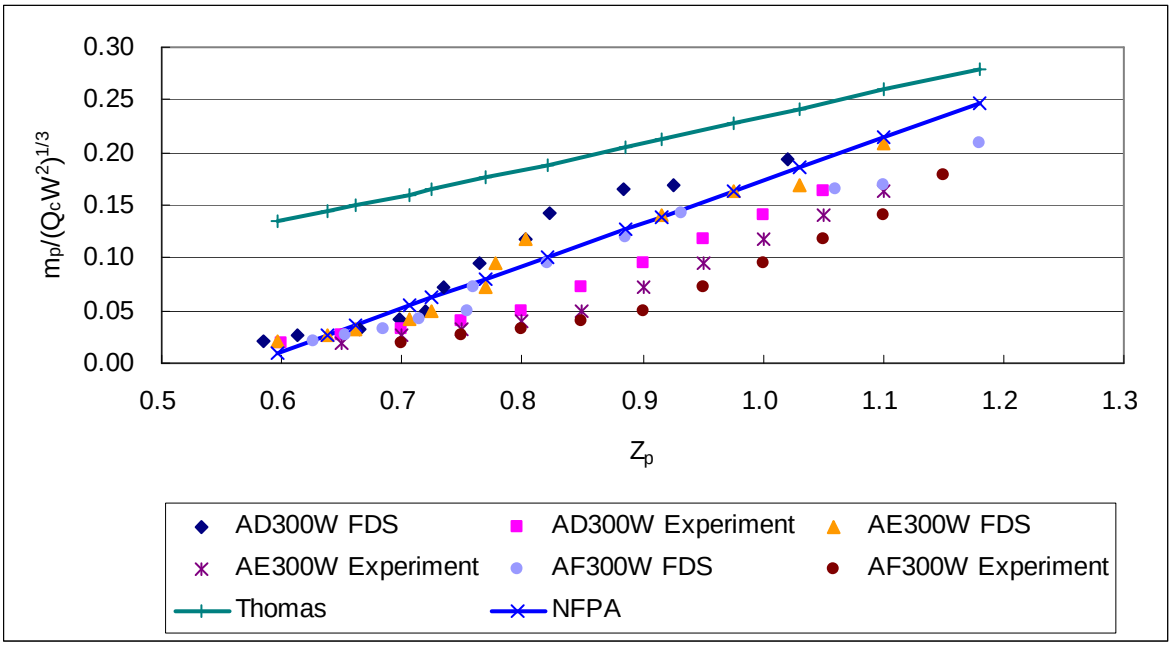

Fig. 6.13 Relationship between Z_p and $m_p/(Q_cW^2)^{1/3}$ in three cases for the FDS simulation and experiment (300W fire)

The smoke temperature and smoke layer height tested in the experiment and simulated by FDS for the 500w fire are shown in Table 6.12 and Table 6.13.

FDS simulation and experiment results of the case AD with heat release 500W are compared with those by different spill plume models shown in Fig. 6.14. It is obvious that a good agreement is found between the 500W fire results and those predicted by the NFPA plume equations.

Fig. 6.15 shows a comparison of CFD and experiment results for case AD, AE, and AF are compared with that by spill plume models in NFPA. It is obvious that the balcony plume entrainment coefficient is independent of the fire location. And compared with the NFPA model, the error range of the results from the experiment and FDS simulation data in this report is between -0.08 and 0.05. The balcony equation in NFPA would give good predictions on the mass flow rate.

Table 6.12 Inlet air and exhaust smoke temperature, smoke layer height, and Archimedes number for the case AD 500W

AD500W								
q_{in} [m^3/s]	v_{in}[m/s]	T_{in} [°C]	T_{out} [°C]	Smoke layer height Z_p[m]	dimensionless height Z_p/H	Z_b [m]	Z_b/h_b	Archimedes number
0.006	0.031	21.0	30.7	0.450	0.219	0.400	0.524	654.91
0.009	0.044	21.3	33.7	0.500	0.243	0.400	0.524	410.23
0.012	0.060	21.3	33.7	0.550	0.268	0.400	0.524	222.59
0.016	0.079	21.5	34.6	0.600	0.292	0.400	0.524	137.13
0.020	0.097	21.8	32.4	0.650	0.316	0.400	0.524	73.19
0.025	0.122	21.8	31.8	0.700	0.341	0.400	0.524	43.26
0.030	0.147	21.1	27.5	0.750	0.365	0.400	0.524	19.06
0.044	0.215	21.4	27.5	0.800	0.389	0.500	0.655	8.52
0.058	0.283	21.2	27.2	0.850	0.414	0.500	0.655	4.85
0.071	0.350	21.5	27.0	0.900	0.438	0.500	0.655	2.89
0.085	0.418	21.4	26.4	0.950	0.462	0.500	0.655	1.85
0.099	0.486	21.7	26.0	1.000	0.487	0.500	0.655	1.18

Table 6.13 Inlet air and exhaust smoke temperature, smoke layer height, and Archimedes number for the case AD 500W by FDS

AD500W								
q_{in} [m^3/s]	v_{in}[m/s]	T_{in} [°C]	T_{out} [°C]	Smoke layer height Z_p[m]	dimensionless height Z_p/H	Z_b [m]	Z_b/h_b	Archimedes number
0.012	0.060	20.0	25.8	0.579	0.282	0.414	0.543	104.12
0.016	0.079	20.0	25.6	0.591	0.288	0.450	0.590	58.62
0.020	0.097	20.0	25.0	0.610	0.297	0.461	0.604	34.52
0.025	0.122	20.0	24.8	0.685	0.333	0.461	0.604	20.76
0.030	0.147	20.0	24.7	0.697	0.339	0.468	0.613	13.99
0.044	0.215	20.0	24.6	0.739	0.360	0.482	0.632	6.43
0.058	0.283	20.0	24.0	0.781	0.380	0.500	0.655	3.23
0.071	0.350	20.0	23.9	0.800	0.389	0.501	0.657	2.05
0.085	0.418	20.0	23.2	0.819	0.399	0.504	0.661	1.18
0.099	0.486	20.0	22.5	0.854	0.416	0.509	0.667	0.68
0.012	0.060	20.0	22.3	0.891	0.434	0.510	0.668	0.59
0.016	0.079	20.0	21.9	0.963	0.469	0.512	0.671	0.38

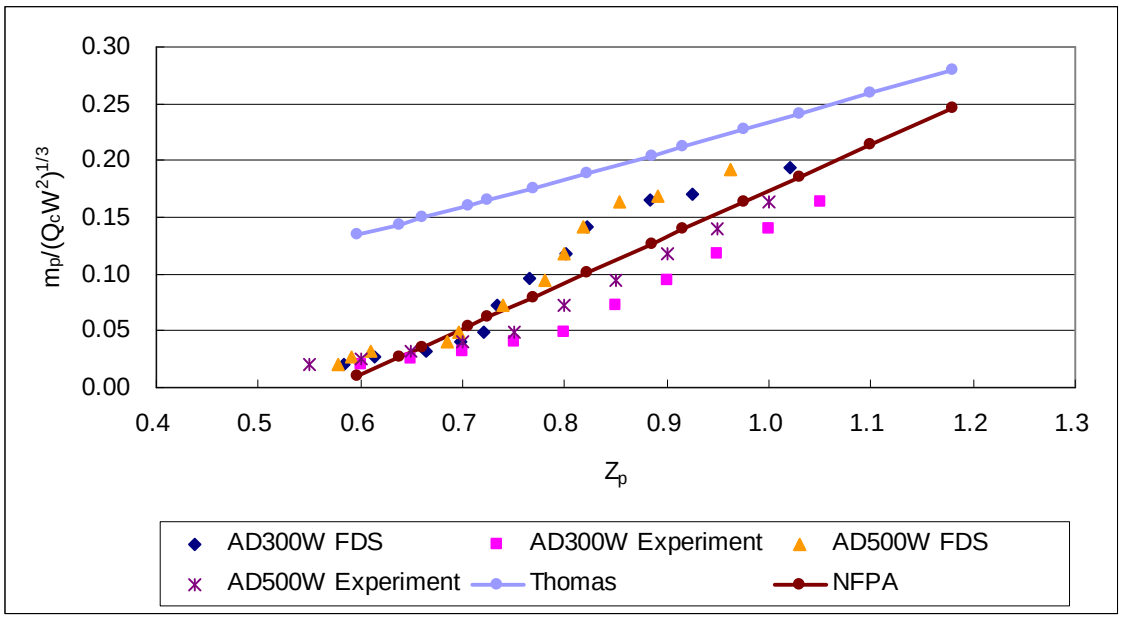

Fig. 6.14 Relationship between Z_p and $m_p/(Q_cW^2)^{1/3}$ for case AD 500W

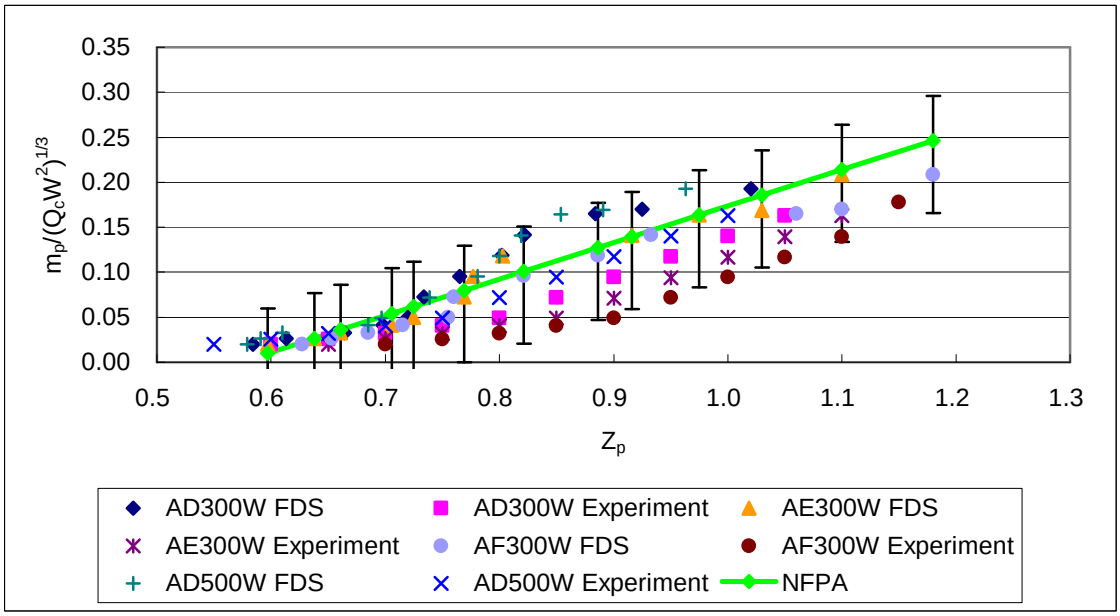

Fig. 6.15 Comparison of the predicted mass flux with those by NFPA balcony spill plume model

7 Experiment and FDS Simulation on Smoke Movement in Large Space Building with Sloping Floor

As many large space buildings such as cinema, sports arenas containing the sloping floor are designed to meet the function and aesthetic requirement. In this chapter, smoke movement in this kind of building is discussed.

The scheme of the compartment with sloping floor is shown in Fig. 7.1. The half of floor is designed as the sloping floor shown in Fig. 7.2. The sloping floor was made of the filter.

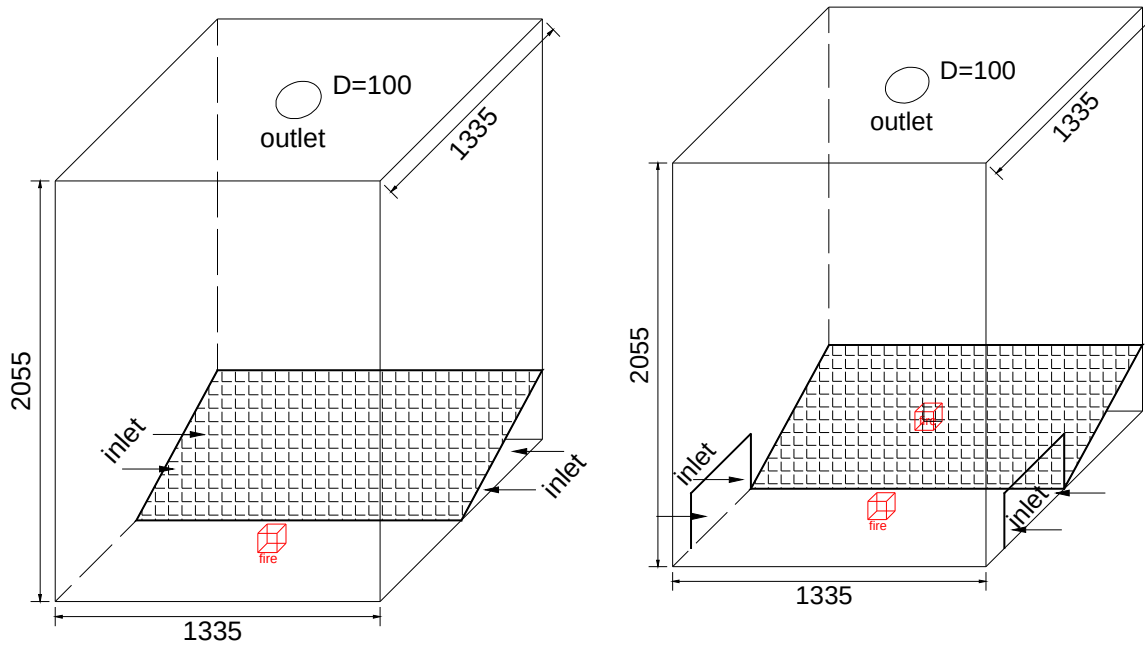

Fig. 7.1 Scheme of model with Sloping Floor

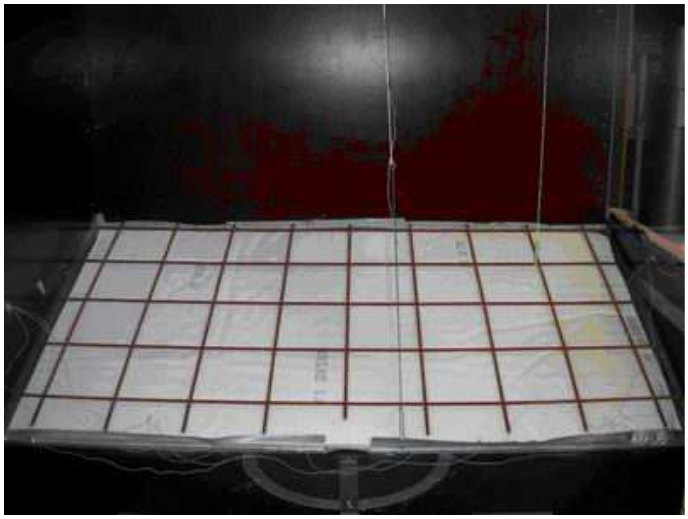

Fig. 7.2 Sloping floor

In the test compartment there were three thermocouple trees. A set of 6 thermocouples with 380mm intervals was vertically placed at the center of the compartment over the fire source. A second set of 7 thermocouples with 380mm intervals was also vertically placed at the corner of the compartment, and a third set of 3 thermocouples with 380mm, 155mm intervals was also vertically placed at the other corner of the compartment, as shown in Fig. 7.3.

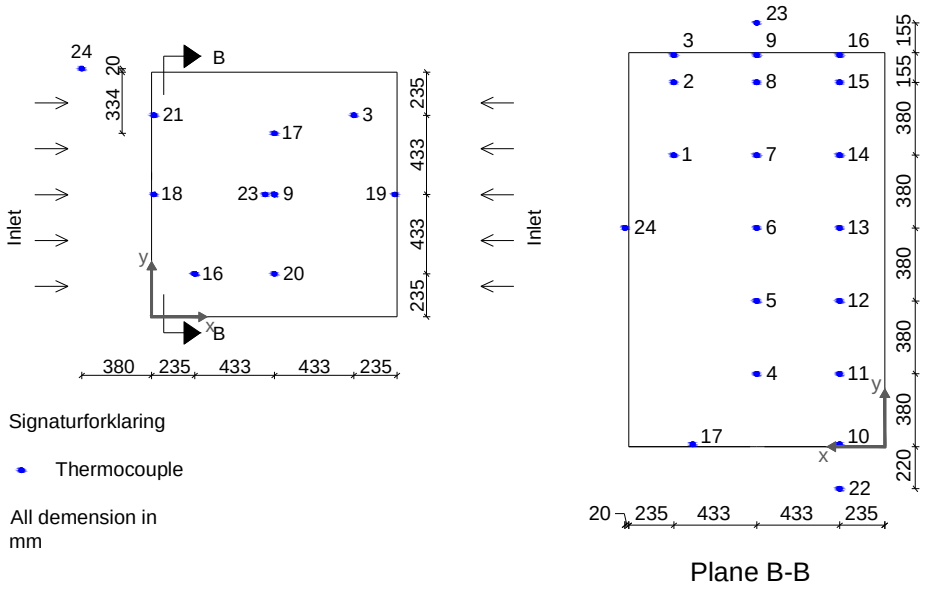

a) b)

Fig. 7.3 Thermocouple in the sloping floor space

Three degree sloping floor are designed as shown in Fig. 7.4.

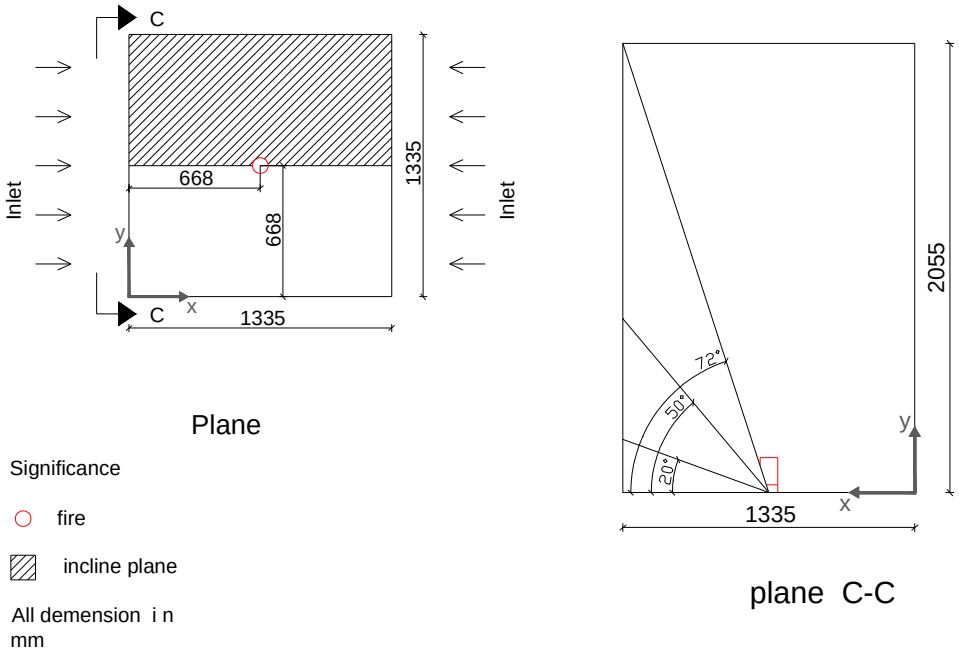

Fig. 7.4 Scheme of the sloping floor with different degree

7.1 Experiment Condition

The series of experiments were conducted. The experimental schemes for the different degrees of the sloping floor are shown in Table 7.1. For the 20 degree sloping floor five cases have been designed to study the fire location and other heat source on smoke movement. One of them was that there was a cable with heat source 100W on the sloping floor, and the inlet air was induced from the opening in the two side of the model as shown in Fig. 7.1b. The other two cases were fire heat power with 300W and 500W. And the inlet air from the opening in the two side of the model was induced into the compartment through the sloping floor as shown in Fig. 7.1a.

Table 7.1 Degree of sloping floor and experiment scheme

case	angle	location	heat	cables	Air supply
SA	20	floor	300	0	slope
SB	50	floor	300	0	slope
SC	72	floor	300	0	slope
SD	20	floor	300	100	slope
SE	20	slope	300	0	sides
SF	20	slope	300	100	sides

In the experiment beginning the fire source produced smoke and the smoke plume rose quickly up to the ceiling and then the plume spread horizontally and down, eventually formed steady smoke depth and then stopped at a certain height in several minutes. During the test, the inlet air temperature, smoke exhaust temperature and smoke layer height were measured.

7.2 Experimental Result of the Sloping Floor with Different Angle

On the condition of 300W fire in the center of the model, three sets of experiment were conducted for the different angle sloping floor, as shown in Table 7.1. The tested inlet air temperature, smoke temperature, smoke layer height, and Archimedes number for the sloping floor are shown in Table 7.1.

The smoker layer height vs. Archimedes number and inlet air volumetric flow rate are shown in Table 7.2, Table 7.3 and Table 7.4. The result from the center fire without sloping floor is also shown in the Figure. It is obvious that smoke layer height of the case SC is the lowest on the same inlet air supply rate. That is that the compartment volume is smaller as the degree sloping floor is bigger. But the discrepancy is not very distinct. The same dimensionless smoke layer height the Archimedes number is bigger for the case SC, as the inlet areas is bigger and then the inlet air velocity is smaller.

Table 7.2 The experiment result for the 20 degree sloping floor (300W center fire)

Case	q_{in} (m^3/s)	Inlet air velocity (m/s)	Smoke exhaust rate (m^3/h)	Layer heighZ(m)	T_{in}/℃	T_{out}/℃	Dimensionless height Z/H	Archimedes number
SA1	0.006	0.011	22.9	0.350	18.4	25.7	0.170	4115
SA2	0.009	0.016	32.6	0.400	18.5	25.4	0.195	1907
SA3	0.012	0.021	44.2	0.500	18.9	25.3	0.243	960
SA4	0.016	0.027	56.3	0.600	19	25.2	0.292	571
SA5	0.030	0.053	108.5	0.900	19.6	24.8	0.438	129
SA6	0.037	0.065	133.4	0.950	19.9	24.5	0.462	75
SA7	0.044	0.077	158.1	1.150	19.1	24.2	0.560	59
SA8	0.058	0.101	207.8	1.300	19.1	23.1	0.633	27
SA9	0.071	0.126	257.4	1.400	19.3	22.8	0.681	15

SA10	0.085	0.150	307.1	1.450	19.6	23.2	0.706	11
SA11	0.099	0.174	356.7	1.650	19.7	21.5	0.803	4

Table 7.3 The experiment result for the 50 degree sloping floor (300W center fire)

Case	q_{in} (m^3/s)	Inlet air velocity (m/s)	Smoke exhaust rate (m^3/h)	Layer height Z(m)	T_{in}/℃	T_{out}/℃	Dimensionless height Z/H	Archimedes number
SB1	0.006	0.008	22.9	0.450	19.0	28.3	0.219	9068
SB2	0.007	0.009	25.4	0.450	18.9	28.1	0.219	7431
SB3	0.009	0.012	32.6	0.500	19.0	27.1	0.243	3958
SB4	0.012	0.016	44.2	0.600	19.3	26.5	0.292	1909
SB5	0.016	0.021	56.3	0.700	19.3	26.0	0.341	1092
SB6	0.025	0.033	89.8	0.850	19.7	24.8	0.414	326
SB7	0.030	0.040	108.5	1.100	18.3	22.9	0.535	201
SB8	0.037	0.049	133.4	1.150	18.3	22.9	0.560	133
SB9	0.044	0.058	158.1	1.300	18.0	22.7	0.633	97
SB10	0.058	0.076	207.8	1.450	18.7	22.5	0.706	45
SB11	0.065	0.086	234.2	1.500	18.8	22.3	0.730	33
SB12	0.071	0.094	257.4	-	-	-	-	-
SB13	0.085	0.113	307.1	-	-	-	-	-
SB14	0.099	0.131	356.7	-	-	-	-	-

Table 7.4 The experiment result for the 72 degree sloping floor (300W center fire)

Case	q_{in} (m^3/s)	Inlet air velocity (m/s)	Smoke exhaust rate (m^3/h)	Layer height Z(m)	T_{in}/℃	T_{out}/℃	Dimensionless height Z/H	Archimedes number
SC1	0.006	0.004	22.9	0.400	18.4	27.1	0.195	40172
SC2	0.007	0.004	25.4	0.450	18.3	26.9	0.219	32137
SC3	0.009	0.005	32.6	0.500	18.5	26.5	0.243	20464
SC4	0.012	0.007	44.2	0.550	18.5	26.3	0.268	10826
SC5	0.016	0.009	56.3	0.600	19.0	26.3	0.292	6228
SC6	0.025	0.014	89.8	0.700	19.4	25.8	0.341	2145

SC7	0.030	0.017	108.5	0.850	17.5	24.1	0.414	1512
SC8	0.037	0.021	133.4	1.000	17.8	23.6	0.487	878
SC9	0.044	0.025	158.1	1.200	18.0	22.1	0.584	442
SC10	0.058	0.033	207.8	1.450	18.2	22.6	0.706	274
SC11	0.065	0.038	234.2	-	-	-	-	-
SC12	0.071	0.041	257.4	-	-	-	-	-
SC13	0.085	0.049	307.1	-	-	-	-	-
SC14	0.099	0.057	356.7	-	-	-	-	-

The dimensionless smoker layer height vs. Archimedes number and inlet air volumetric flow rate are shown in Fig. 7.3 and Fig. 7.4. The result from the center fire without sloping floor (case FA) is also shown in the Figure. It is obvious that smoke layer height of the case SC is the lowest on the same inlet air supply rate. That is that the compartment volume is smaller as the degree sloping floor is bigger. But the discrepancy is not very distinct. At the same dimensionless smoke layer height the Archimedes number is larger for the case SC, as the inlet areas is larger and then the inlet air velocity is smaller.

The relationship between Archimedes number and dimensionless smoke layer height for the 20, 50, and 72 degree sloping floor can be described as equation (7.1), (7.2) and (7.3) respectively.

$$\frac{z}{H} = 1.2879 Ar^{-0.237} \tag{7.1}$$

$$\frac{z}{H} = 1.6993 Ar^{-0.2299} \tag{7.2}$$

$$\frac{\mathrm{Z}}{\mathrm{H}} = 2.4378 \mathrm{Ar}^{-0.2378} \tag{7.3}$$

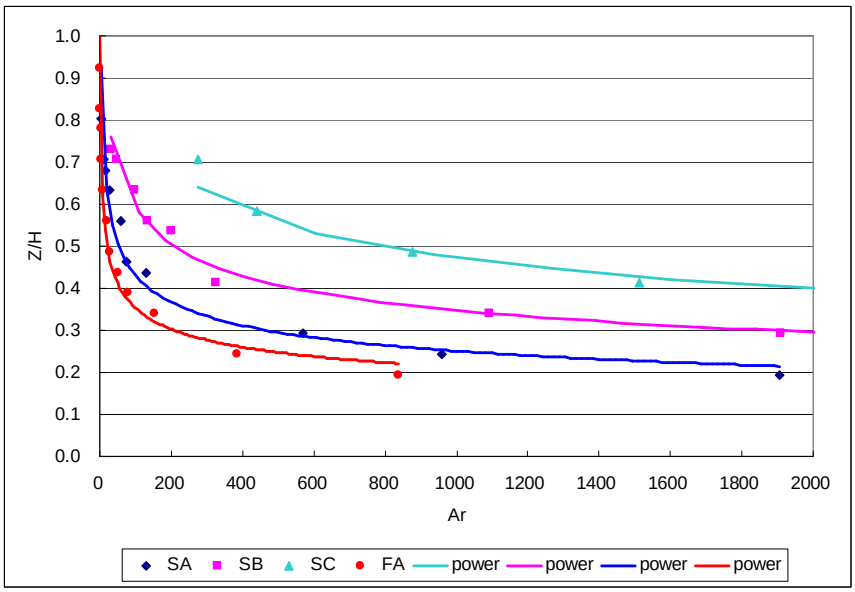

Fig. 7.3 Dimensionless smoke layer height Vs. Archimedes number

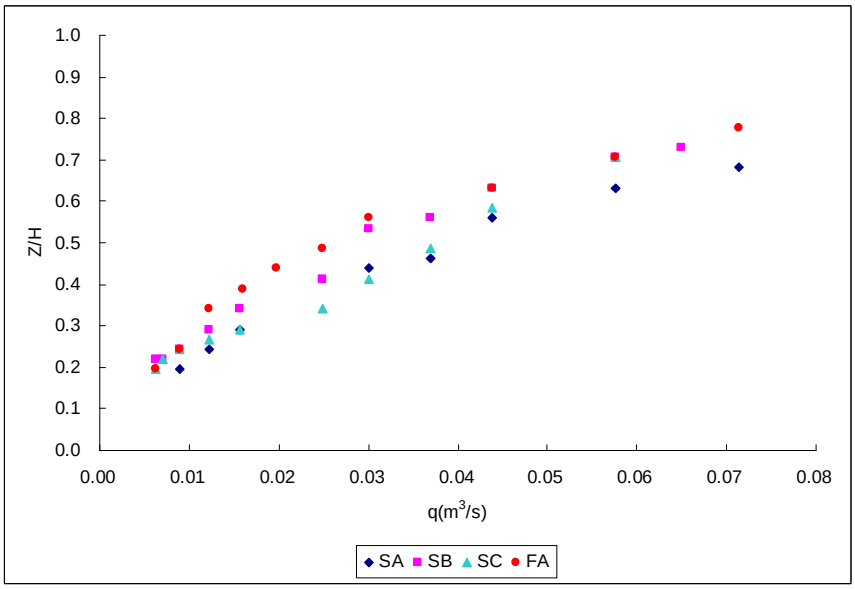

Fig. 7.4 Dimensionless smoker layer height vs. inlet air flow rate for the different degree sloping floor (300W)

The photos of the smoke layer interface height obtained by the video for the sloping floor are shown in Fig. 1 in Appendix C.

7.3 Experimental Result of the Sloping Floor with 20 Degree

1) Fire on the center of the floor

In order to analyze the effect of other heat source on smoke movement, the fire was located on the center of the model and 100W cable was put on the sloping as case SD. The tested inlet air temperature, smoke temperature, smoke layer height, and Archimedes number for the heat source on sloping floor and fire in the center of compartment are shown in Table 7.5.

Table 7.5 The experiment result for the 20 degree sloping floor (300W floor fire, 100W cable)

Case	q_{in} (m^3/s)	Inlet air velocity (m/s)	Smoke exhaust rate (m^3/h)	Layer height Z(m)	T_{in}/℃	T_{out}/℃	Dimensionless height Z/H	Archimedes number
SD1	0.006	0.011	22.9	0.001	20.9	29.2	0.000	4679
SD2	0.009	0.016	32.6	0.100	21.2	30.9	0.049	2681
SD3	0.012	0.021	44.2	0.200	21.3	30.5	0.097	1380
SD4	0.016	0.027	56.3	0.450	21.3	30.5	0.219	848
SD5	0.025	0.044	89.8	0.550	21.9	29.1	0.268	261
SD6	0.030	0.053	108.5	0.550	20.4	27.5	0.268	176
SD7	0.037	0.065	133.4	0.550	20.7	27.8	0.268	116
SD8	0.044	0.077	158.1	0.750	20.5	26.6	0.365	71
SD9	0.058	0.101	207.8	0.850	20.9	26.6	0.414	38
SD10	0.071	0.126	257.4	1.000	20.9	26.2	0.487	23
SD11	0.085	0.150	307.1	1.150	21.2	26.9	0.560	18
SD12	0.099	0.174	356.7	1.300	21.2	25.8	0.633	11

The dimensionless smoker layer height vs. Archimedes number and inlet air volumetric flow rate are shown in Fig. 7.5 and Fig. 7.6. The result from the center fire without cable (case SA) is also shown in the Figures.

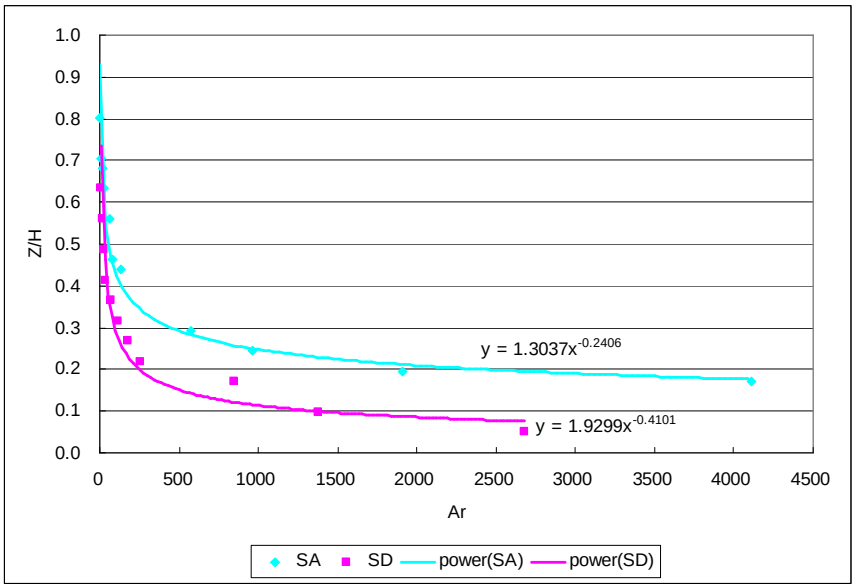

Fig. 7.5 Dimensionless smoke height vs. Archimedes number, cable on the sloping floor, fire in the center of compartment

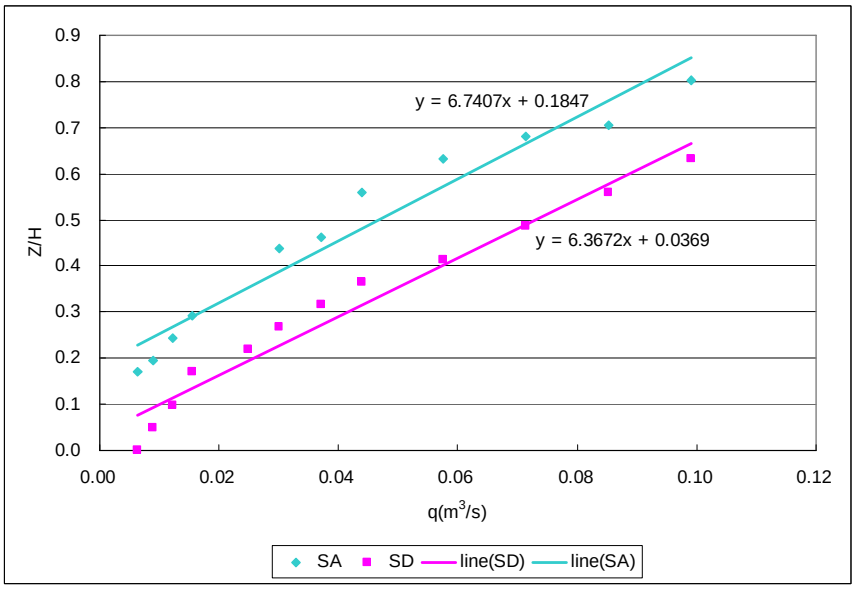

Fig. 7.6 Dimensionless smoke height vs. inlet air flow rate, cable on the sloping floor, fire in the center of compartment

It is obvious that the smoke layer height descends sharply with Archimedes number for the case SD. When there is a cable on the sloping floor, the heat release rate produced by the cable disturbs the smoke movement. Especially the inlet air comes through the sloping floor. The smoke layer height captured by video is shown in Fig. 2 in Appendix C.

The relationship between Archimedes number and dimensionless smoke layer height for the case SD can be described as equation (7.4).

$$\frac{z}{H} = 1.3037 Ar^{-0.2408} \tag{7.4}$$

2) Fire on the center of the sloping floor

In order to analyze the effect of the other heat source and fire location on smoke movement, the fire was located on the center of the sloping floor as the case SE and SF in the Table 7.1. In these two measurements the inlet air was supplied from the side vent as shown in Fig. 7.1b.

The tested inlet air temperature, smoke temperature, smoke layer height, and Archimedes number for the fire on the sloping floor are shown in Table 7.6 and Table 7.7.

Table 7.6 The experiment result for the 20 degree sloping floor (300W slope fire)

Case	q_{in} (m^3/s)	Inlet air velocity (m/s)	Smoke exhaust rate (m3/h)	Layer height Z(m)	T_{in}/℃	T_{out}/℃	Dimensionless height Z/H	Archimedes number
SE1	0.006	0.062	22.9	0.450	20.1	27.1	0.219	127
SE2	0.009	0.088	32.6	0.550	19.9	26.8	0.268	61
SE3	0.012	0.120	44.2	0.650	20.2	26.9	0.316	32
SE4	0.016	0.153	56.3	0.700	20.7	26.9	0.341	18
SE5	0.025	0.244	89.8	0.950	21.5	26.5	0.462	6
SE6	0.030	0.295	108.5	1.000	19.9	25.3	0.487	4
SE7	0.037	0.363	133.4	1.100	20.4	25.8	0.535	3
SE8	0.044	0.430	158.1	1.300	20.4	25.4	0.633	2
SE9	0.058	0.566	207.8	1.450	20.6	25.1	0.706	1
SE10	0.072	0.701	257.4	1.600	20.3	24.6	0.779	1
SE11	0.085	0.836	307.1	1.700	20.5	24.3	0.827	0
SE12	0.099	0.972	356.7	-	-	-	-	-

Table 7.7 The experiment result for the 20 degree sloping floor (300W slope fire, 100W cable)

Case	q_{in} (m^3/s)	Inlet air velocity (m/s)	Smoke exhaust rate (m3/h)	Layer height Z(m)	T_{in}/℃	T_{out}/℃	Dimensionless height Z/H	Archimedes number
SF1	0.006	0.062	22.9	-	-	-	-	-
SF2	0.009	0.088	32.6	-	-	-	-	-
SF3	0.012	0.120	44.2	0.550	21.3	29.7	0.268	40.4
SF4	0.016	0.153	56.3	0.650	21.4	28.8	0.316	21.9
SF5	0.025	0.244	89.8	0.800	21.8	28.1	0.389	7.3
SF6	0.030	0.295	108.5	0.900	20.4	26.6	0.438	4.9
SF7	0.037	0.363	133.4	1.100	20.6	26.9	0.535	3.3
SF8	0.044	0.430	158.1	1.150	20.5	26.2	0.560	2.1
SF9	0.058	0.566	207.8	1.400	20.5	25.6	0.681	1.1
SF10	0.072	0.701	257.4	1.650	20.6	24.8	0.803	0.6
SF11	0.085	0.836	307.1	1.700	20.6	24.4	0.827	0.4
SF12	0.099	0.972	356.7	-	-	-	-	-

The dimensionless smoker layer height vs. Archimedes number and inlet air volumetric flow rate are shown in Fig. 7.7 and Fig. 7.8. The result from the center fire without cable (case SA) is also shown in the Figures.

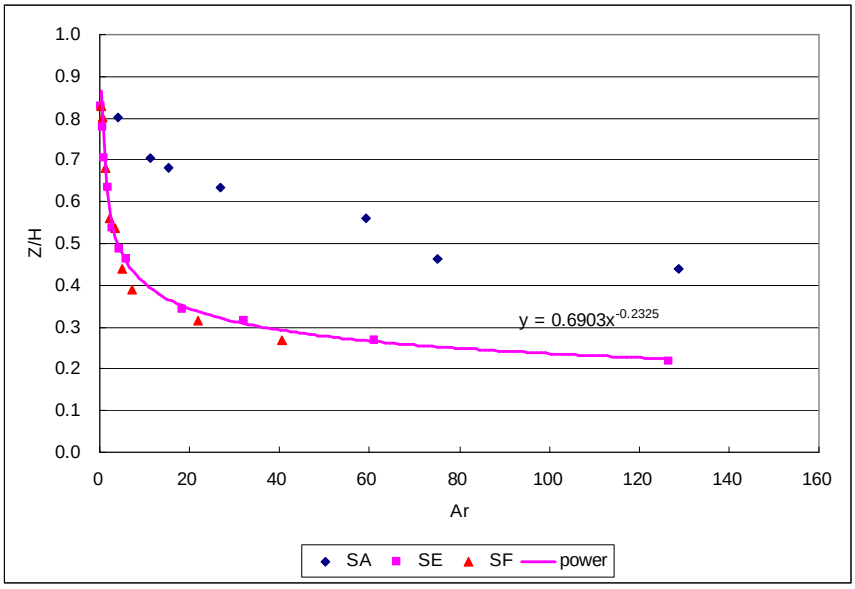

Fig. 7.7 Dimensionless smoke height vs. Archimedes number, cable on the sloping floor, fire in the center of the sloping floor

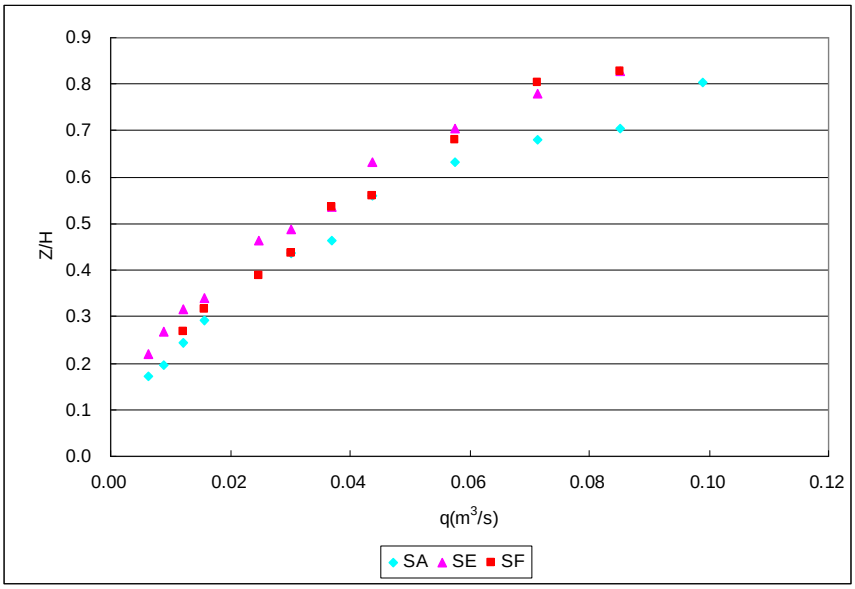

Fig. 7.8 Dimensionless smoke height vs. inlet air flow rate, cable on the sloping floor, fire in the center of the sloping floor

It shows that the effect of the cable on smoke is not very distinct while the fire on the center of sloping floor and the inlet air supply directly comes in the compartment from the side vent. On the condition of the same inlet air supply the dimensionless smoke layer height is almost same compare to the fire in the center of the compartment. But the Archimedes number is different as the inlet areas are smaller than that in the sloping floor supplement.

The relationship between Archimedes number and dimensionless smoke layer height for the case SE can be described as equation (7.5).

$$\frac{z}{H} = 0.6903 Ar^{-0.2925} \tag{7.5}$$

The photos of the smoke layer interface height obtained by video are shown in Fig. 3 in appendix C.

7.4 FDS Simulation

1. 20 degree sloping floor simulation and experimental result

Fig. 7.9 shows the temperature and smoke layer result simulated by FDS for the case A and case E in the condition of air supply rate 0.006m^3/s and smoke exhaust rate 22.9 m^3/h.

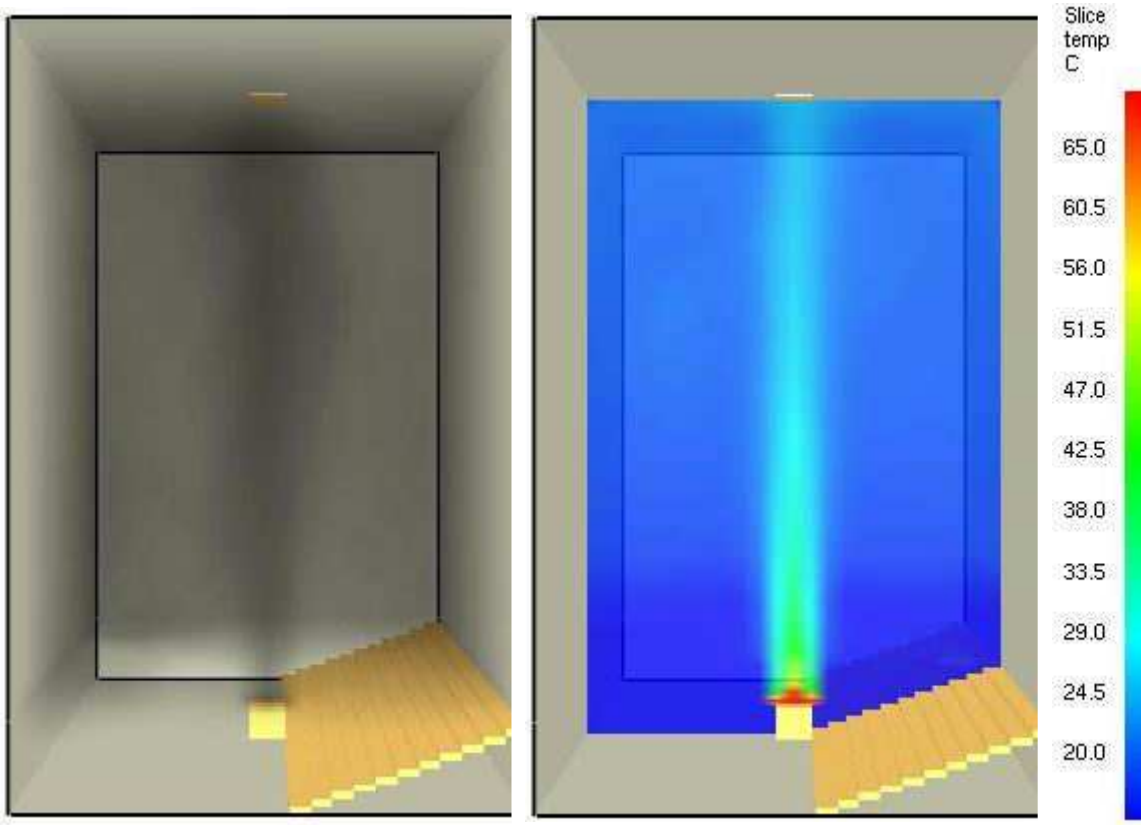

Case SA air supply rate 0.006 m^3/s and smoke exhaust rate 22.9 m^3/h

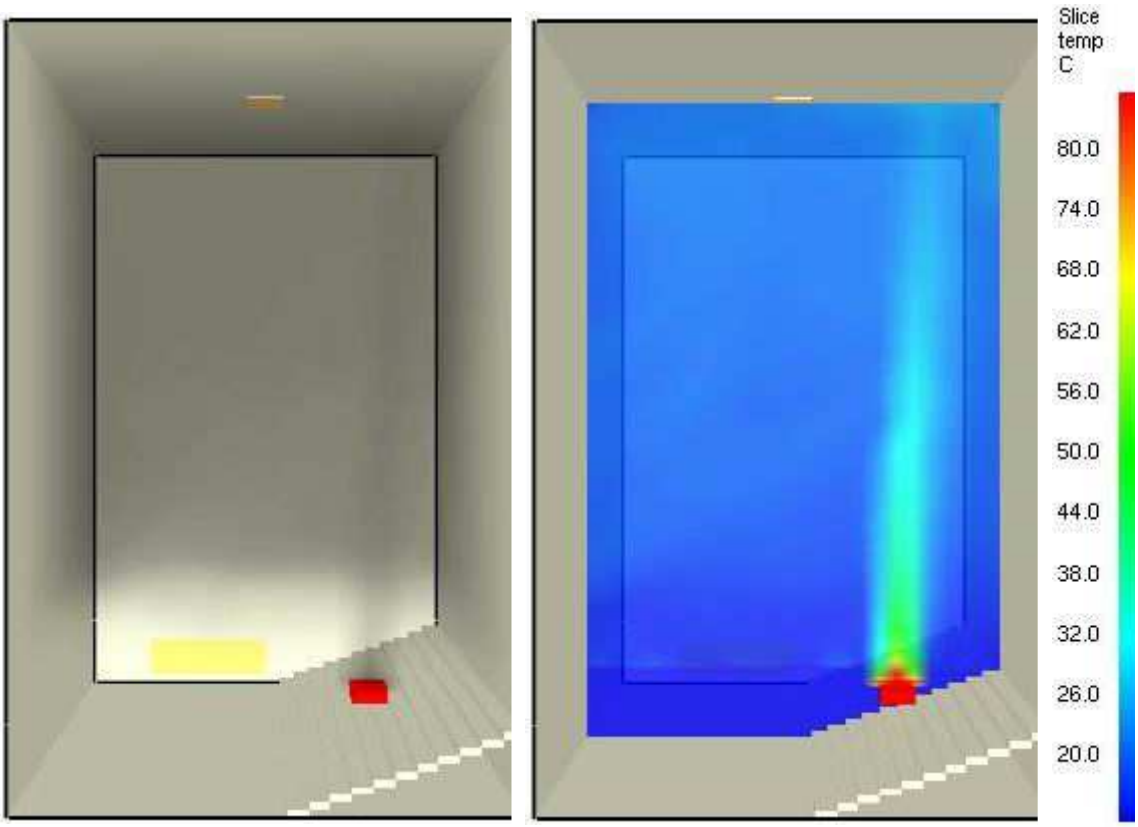

Case SE air supply rate 0.006 m^3/s and smoke exhaust rate 22.9 m^3/h

Fig. 7.9 FDS simulation for the case A and Case E

Fig. 7.10and Fig. 7.11 show a comparison of smoke temperature profile at the corner of the model between experimental and numerical temperature simulated by FDS for the case SA and SE respectively. The CFD simulation seems to show a smoke layer temperature gradient, while the FDS simulation and experimental data indicate that the temperature in the hot layer is uniform.

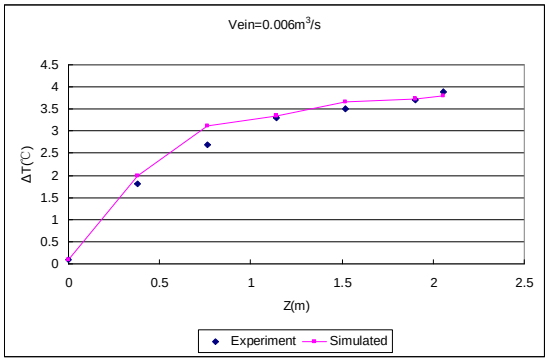

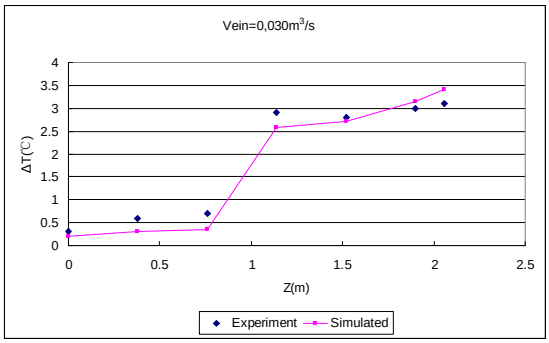

Air supply rate 0.006 m^3/s Air supply rate 0.03 m^3/s

Smoke exhaust rate 22.9 m^3/h Smoke exhaust rate 108.5 m^3/h

Fig. 7.10Comparison of experimental and Simulation, Fire located in the center of compartment, inlet air supply from the 20 degree sloping floor (case SA)

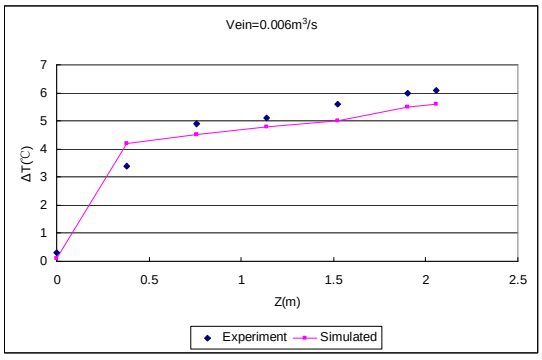

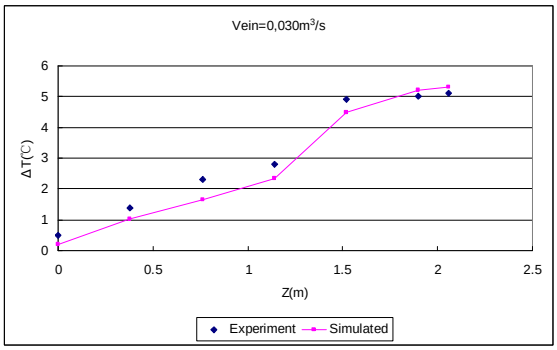

Air supply rate 0.006 m^3/s Air supply rate 0.03 m^3/s

Smoke exhaust rate 22.9 m^3/h Smoke exhaust rate 108.5 m^3/h

Fig. 7.11 Comparison of experimental and Simulation, Fire located in the center of the 20 degree sloping floor, inlet air supply from side vent (case SE)

2. Side Vent Simulation

FDS was used to analyze the effect of the air supply mode on the smoke. Fig. 7.12 shows the result that inlet air comes in the compartment through the side vent directly.

There are two schemes to simulate as showed in Table 7.8. One is that there is no heat source on the sloping floor. The other is that there is 100W heat source on the sloping floor. Fire is located in the center of the model.

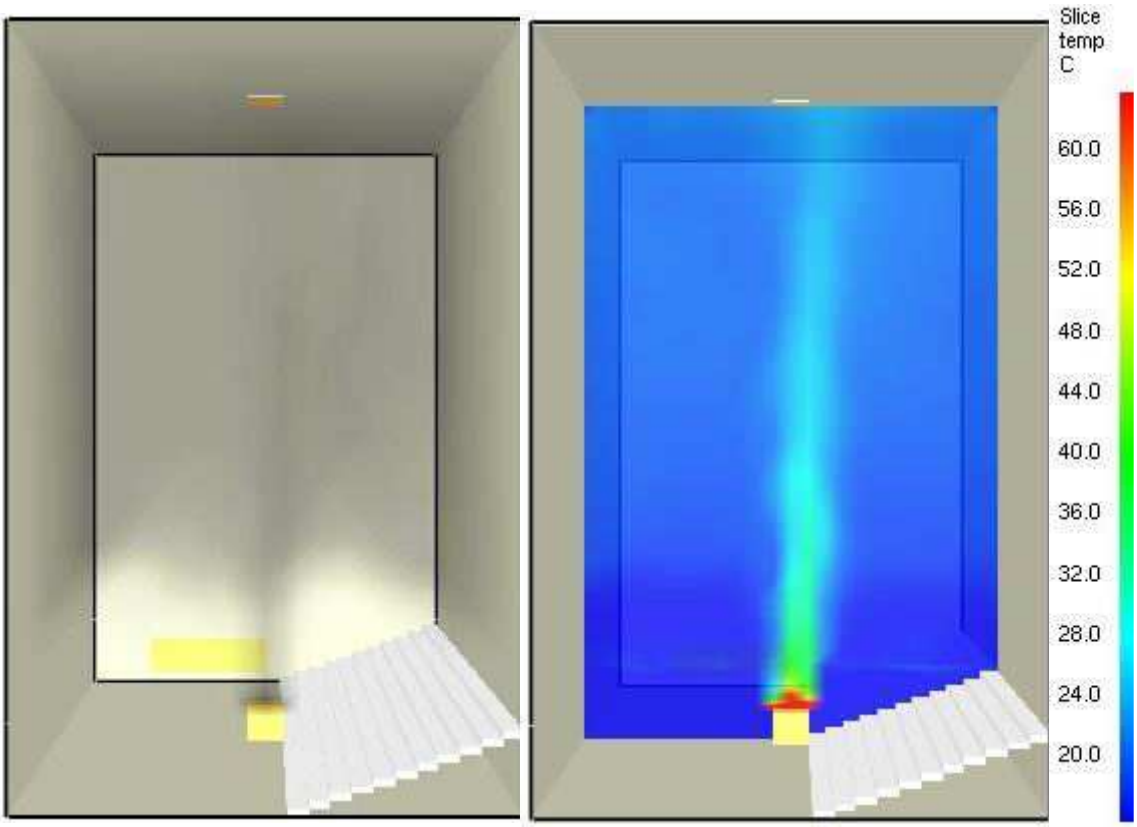

FDS simulation for the case SG, Air supply rate 0.006m^3/s, Smoke exhaust rate 22.9m^3/h

Fig. 7.12 shows the model that inlet air comes in the compartment through the side vent directly

Table 7.8 FDS simulation case

case	angle	location	Heat(W)	Cables(W)	Air supply
SG	20	floor	300	0	side
SH	20	floor	300	100	side

The simulated inlet air temperature, smoke temperature, smoke layer height, and Archimedes number for the case SG and SH are shown in Table 7.9 and Table 7.10.

Table 7.9 The FDS result for the 20 degree sloping floor (Case SG)

Case	q_{in} (m^3/s)	Inlet air velocity (m/s)	Smoke exhaust rate (m^3/h)	Layer height Z(m)	T_{in}/℃	T_{out}/℃	Dimensionless height Z/H	Archimedes number
SG1	0.006	0.059	22.9	0.390	20.0	25.3	0.190	105.83
SG2	0.009	0.088	32.6	0.480	20.0	25.0	0.234	44.37
SG3	0.012	0.118	44.2	0.513	20.0	24.8	0.250	23.96
SG4	0.016	0.157	56.3	0.540	20.0	23.9	0.263	10.95
SG5	0.030	0.294	89.8	0.568	20.0	23.9	0.276	3.11
SG6	0.037	0.363	108.5	0.632	20.0	23.6	0.308	1.89
SG7	0.044	0.432	133.4	0.682	20.0	23.3	0.332	1.23
SG8	0.058	0.569	158.1	0.732	20.0	22.6	0.356	0.56
SG9	0.071	0.697	207.8	0.795	20.0	22.5	0.387	0.36
SG10	0.085	0.834	257.4	0.834	20.0	22.0	0.406	0.20
SG11	0.099	0.971	307.1	0.939	20.0	21.6	0.457	0.12

Table 7.10 The experiment result for the 20 degree sloping floor (Case SH)

Case	q_{in} (m^3/s)	Inlet air velocity (m/s)	Smoke exhaust rate (m^3/h)	Layer height Z(m)	T_{in}/℃	T_{out}/℃	Dimensionless height Z/H	Archimedes number
SH1	0.006	0.059	22.9	0.202	20.0	25.3	0.098	129.79
SH2	0.009	0.088	32.6	0.252	20.0	25.0	0.123	55.02
SH3	0.012	0.118	44.2	0.306	20.0	24.8	0.149	28.95
SH4	0.016	0.157	56.3	0.417	20.0	23.9	0.203	15.72
SH5	0.030	0.294	89.8	0.467	20.0	23.9	0.227	3.91
SH6	0.037	0.363	108.5	0.559	20.0	23.6	0.272	2.21
SH7	0.044	0.432	133.4	0.600	20.0	23.3	0.292	1.49
SH8	0.058	0.569	158.1	0.629	20.0	22.6	0.306	0.75
SH9	0.071	0.697	207.8	0.669	20.0	22.5	0.326	0.46
SH10	0.085	0.834	257.4	0.704	20.0	22.0	0.343	0.29
SH11	0.099	0.971	307.1	0.817	20.0	21.6	0.398	0.18

The photos of the smoke layer interface height obtained by FDS are shown in Fig. 4 to Fig. 7 in Appendix C.

The smoker layer height vs. Archimedes number and inlet air volumetric flow rate are shown in Fig. 7.13 and Fig. 7.14. The result from the center fire case SA that is the

inlet air supply from sloping floor is also shown in the Figure. The smoke layer height is lower while there is heat source on the floor but its effect is not very distinct. It is obvious that smoke layer height of the case SA is the highest on the same inlet air supply rate. This is that the inlet air velocity is lower as the inlet areas in case SA is larger than that in case SD.

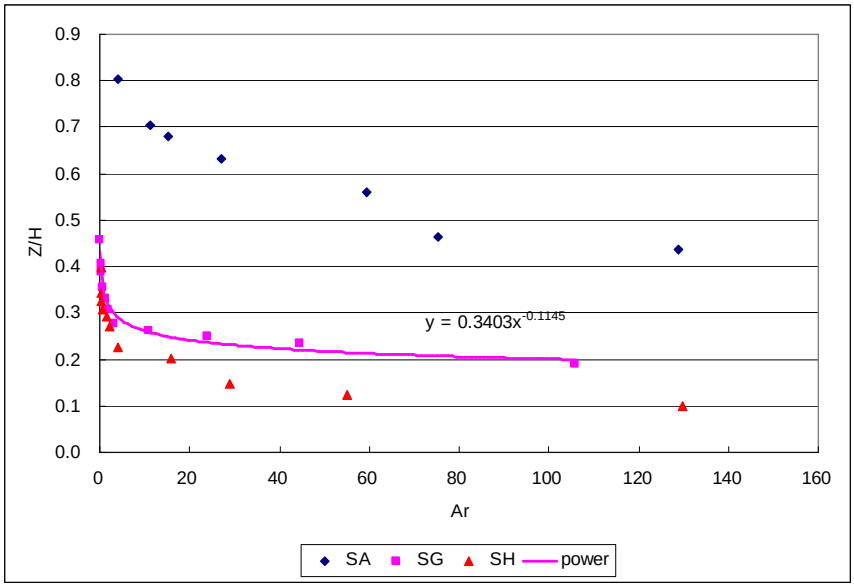

Fig. 7.13 Dimensionless smoke height vs. Archimedes number simulated by FDS, fire in the center of the floor

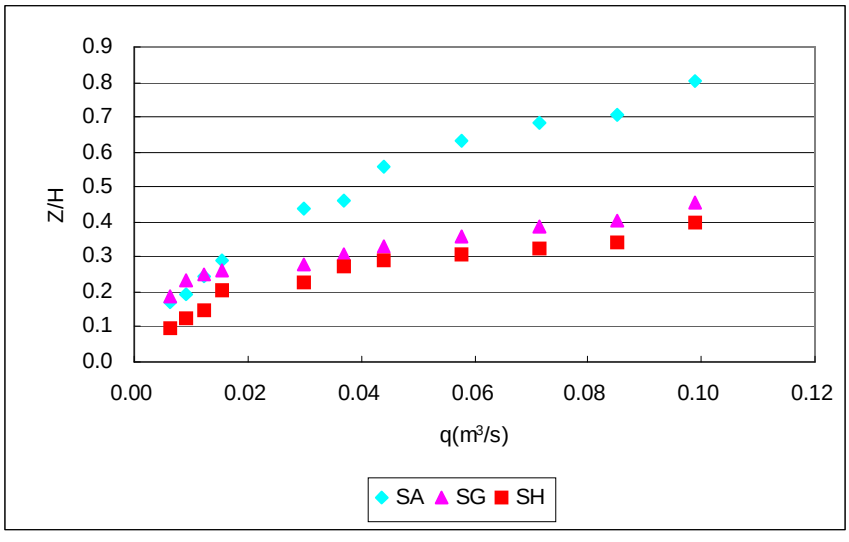

Fig. 7.14 Dimensionless smoke height vs. inlet air flow rate simulated by FDS, fire in the center of the floor

The relationship between Archimedes number and dimensionless smoke layer height

for the case SE can be described as equation (7.6).

$$\frac{z}{H} = 0.3403Ar^{-0.1145} \tag{7.6}$$

8 Conclusion

For the axisymmetric plume, CFD and experiment results agree well with the results estimated by the NFPA-92B equation and Zukoski equation. The mass entrainment rate might be overestimated by McCaffrey's equation. The plume entrainment coefficient of the wall plume and corner plume are 64% and 48% of the axisymmetric plume respectively.

The coefficient of the mass flow rate of the balcony plume is between 0.342 and 0.468, and the balcony plume entrainment coefficient is independent of the fire location. Compared with the NFPA model, the error range of the results from the experiment and FDS simulation data in this report is between -0.08 and 0.05. The balcony equation in NFPA would give good predictions on the mass flow rate.

On the same air supply and smoke exhaust condition, the smoke layer height is lower while the angle of the sloping floor is larger; the smoke layer height is lower while there is a heat source on the sloping floor. And the type of ventilation also affects the smoke layer height.

As the limit of the experiment condition, the further research is needed for the wall and corner plume.

This report was written as a work report of my stay at the department of civil engineering of AAU from January 2007 to June 2007. As the time limitation the further analysis of the result is needed.

Nomenclature

Z--the height of the room, m;

t--time, s;

H--ceiling height above the fire, m;

Q--steady-state heat release rate, kW;

A-- cross-sectional area of the atrium, m^2.

V_e--volumetric rate of smoke production, m^3/s;

Q_c--convective portion o the heat release rate, kW; (Q_c=0.7Q)

m--mass flow rate in plume at height Z, kg/s;

ρ--density of smoke, kg/m^3;

T_p--adiabatic exhaust temperature, ℃;

T_a--ambient temperature, ℃;

m--mass flow of exhaust air, kg/s;

C_p--specific heat of plume gases, kJ/(kg·℃);

α--growth coefficient;

g--acceleration of gravity, m/s^2;

T_f --temperature of heated smoke, K;

T_0--temperature of ambient air, K;

ΔT_g--gas temperature rise at ceiling, K;

t_a--actuation time, s;

τ--time constant, $m^{3/2}s^{3/2}$;

ρ_s--density of smoke exhaust ,kg/m^3;

T_s--temperature of exhaust smoke, ℃;

C_{m1}--the dimensionless entrainment coefficient;

h_b--the height of the balcony, m;

Z_b--the height above the balcony, m. ($Z_b=Z_p-h_b$)

References

[1] J.R. Jones. A Summary of Analytical Method and Case Study Monitoring of Atria. ASHRAE Transaction. 1993. 1070-1080.

[2] IBryn. Atrium Buildings Environmental Design and Energy Use. ASHRAE Transaction. 1994. 1082-1091

[3] Chow, W. K. 1989. Smoke movement and design of smoke control in atrium buildings. International Journal of housing Science and its Application 13(4): 307-322.

[4] Chow, W. K. 1990. Smoke movement and design of smoke control in atrium building- Part2: Diagrams. International Journal of housing Science and its Application 14(2): 147-159.

[5] Ying Ping.1996. Design method for smoke management in atria. Heating, Ventilating & Air Conditioning 26(5): 55-59.

[6] Morgan H P, Ghosh B K, Garrad G, Pamlitschka R, De Smedt J-C and Schoonbaert L R. Design methodologies for smoke and heat exhaust ventilation. BRE Report 368, 1999.

[7] Chow, W. K. and W. K. Wong. 1993a. on the simulation of atrium fire environment in Hong Kong using zone models. Journal of Fire Sciences 11(1): 3-51.

[8] Chow, W. K. and W. K. Wong. 1993b. Application of the zone model FIRST on the development of smoke layer and evaluation of smoke extraction design for atria in Hong Kong. Journal of Fire Sciences 11(4): 329-349.

[9] Chow, W. K. 1989. Smoke movement and design of smoke control in atrium buildings. International Journal of housing Science and its Application 13(4): 307-322.

[10] Chow, W. K. and C. Y. Chau. 1994. General views on fire aspect of atrium buildings in Hong Kong. International Journal of housing Science and its Application 18(1): 43-52.

[11] Klote J H and Milke J A. Design of smoke management systems. American Society of Heating, Refrigerating and Air-conditioning Engineers, Atlanta, GA, 1992.

[12] Klote, J. K. 1997. Prediction of smoke movement in atria: Part Ⅰ-physical concepts. ASHRAE Transactions 103(1): 534-544.

[13] Klote, J. K. 1997. Prediction of smoke movement in atria: Part Ⅱ-application to smoke management. ASHRAE Transactions 103(2): 545-513.

[14] NFPA. 1995. NFPA 92B, Guide for smoke management system in malls, atria and large area. Quincy, Mass.: National Fire Protection Association.

[15] Brooks, W. N. 1997. Comparison of “regular” and “irregular” methods of calculating smoke layer interface heights in 1996 BOCA National Building Code.

ASHRAE Transactions 103(2):554-569.

[16] Xiong Hong. 1994. Modes of smoke exhaust system and performances in atrium buildings. Heating, Ventilating & Air Conditioning 24(5):25-27.

[17] Ying Ping.1996. Design method for smoke management in atria. Heating, Ventilating & Air Conditioning 26(5): 55-59.

[18] Lougheed, G. K. 1997. Investigation of atrium smoke exhaust effectiveness. ASHRAE Transactions 103(2): 519-533

[19] Chow, W. K. 1994. A short note on the simulation of atrium smoke filling process using fire zone models. Journal of Fire Sciences 12(6): 516-528.

[20] Chow, W. K. 1993. Simulation of the atrium fire environment in Hong Kong. ASHRAE Transactions 99(2): 163-168.

[21] Heskestad G. Engineering relations for fire plumes. Fire Safety Journal, 7,No 1, pp 25-32, 1984.

[22] Zukoski E E. Properties of fire plumes, in Combustion Fundamentals of Fire, Cox G, Editor. Academic Press, London, 1995.

[23] Michael Poreh, Gordon Garrad. A study of wall and corner plumes. Fire Safety Journal 34 (2000) 81}98

[24] Klote J H and Milke J A. Design of smoke management systems. American Society of Heating, Refrigerating and Air-conditioning Engineers, Atlanta, GA, 1992.

[25] H.Y. Wang*, M. Coutin, J.M. Most Large-eddy-simulation of buoyancy-driven fire propagation behind a pyrolysis zone alonga vertical wall. Fire Safety Journal 37 (2002) 259–285

[26] K.B. McGrattan and G.P. Forney, 2004a, Fire Dynamics Simulator—User's Manual, National Institute of Standards and Technology, NIST Special Publication 1019, Gaithersburg, MD, 2004.

[27] P. V. Nielsen. Lecture Notes on Scale Model Experiments. Indoor Environmental Engineering , September,1999

[28] Poreh, M., Morgan, H.P., Marshall, N.R. and Harrison, R. Entrainment by Two-dimensional Spill Plumes, Fire Safety Journal, 1998, 30:1-19.

[29] Zukoski, E.E., Kubota, T. and Cetegen, B. Entrainment in Fire Plumes, Fire Safety Journal, 3: 107–121. (1980/81)

[30] McCaffrey, B.J. (1983). Momentum Implication for Buoyant Diffusion Flames, Combustion and Flame, 52: 149-167.

[31] Cegeten, B., Zukoski, E.E. and Kubota, T. (1984). Entrainment in the near and Far Field of Plumes, Combustion Science and Technology, 39: 305-331.

[32] Hinkley, P.L. (1986). Rates of ‘Production’ of Hot Gases in Roof Venting Experiments, Fire Safety Journal, 10: 57–65.

[33] McCaffrey, B.J. Purely Buoyant Diffusion Flames Some Experimental Results, NBSIR 79-1910, National Bureau of Standards, October (1979).

[34] McCaffrey, B.J. and Cox, G. Entrainment and Heat Flux of Buoyant Diffusion Flames, NBSIR 82-2473, National Bureau of Standards, February (1982).

[35] Lee, L. and Emmons, H.W. (1961). A Study of Natural Convection above Line Fires, J. Fluid Mechanics, 11: 353–368.

[36] Poreh, M., Morgan, H.P., Marshall, N.R. and Harrison, R. (1998). Entrainment by two dimensional Spill Plumes, Fire Safety Journal, 30:1–19.

[37] Thomas, P.H. (1987). On the Upward Movement of Smoke and Related Shopping Mall Problems, Fire Safety Journal, 12:191–203.

[38] Law, M. (1995). Measurements of Balcony Smoke Flow, Fire Safety Journal, 24: 189–195.

Appendix A

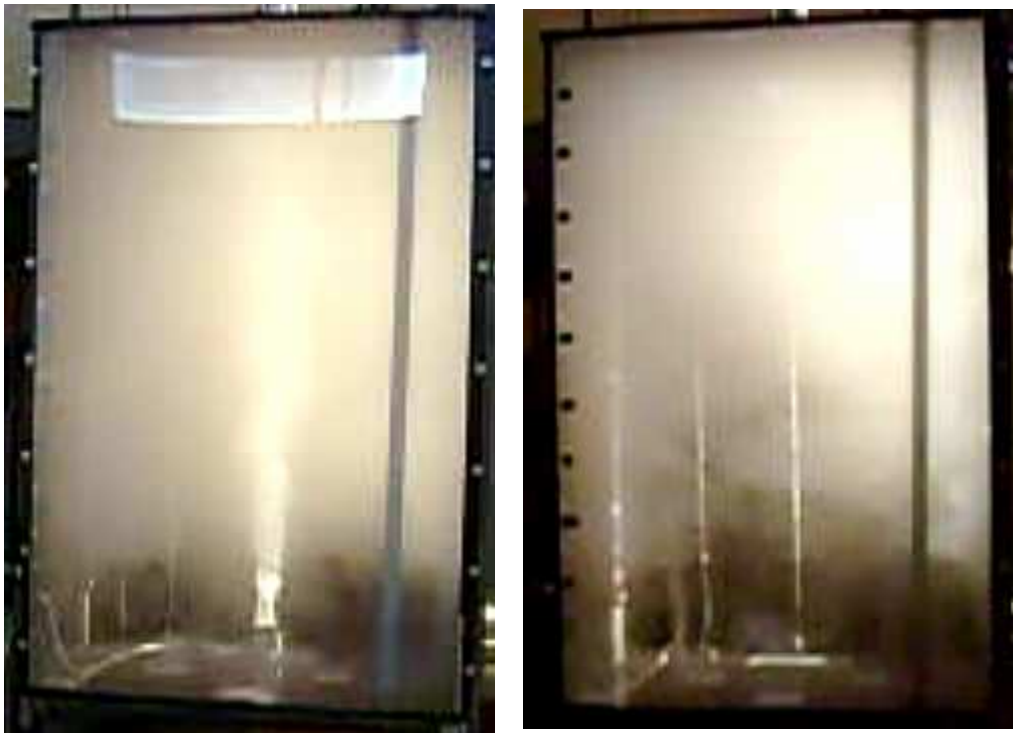

Center fire (Fire A ,300W) Corner fire (Fire C, 300W)

Fig. 1 smoke filling in experiment (300W)

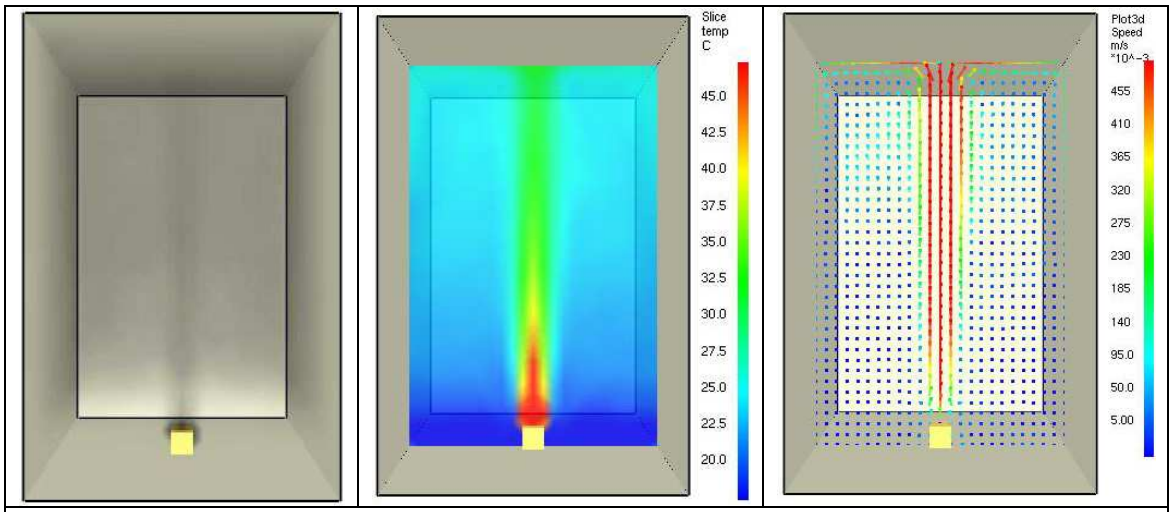

Fire A

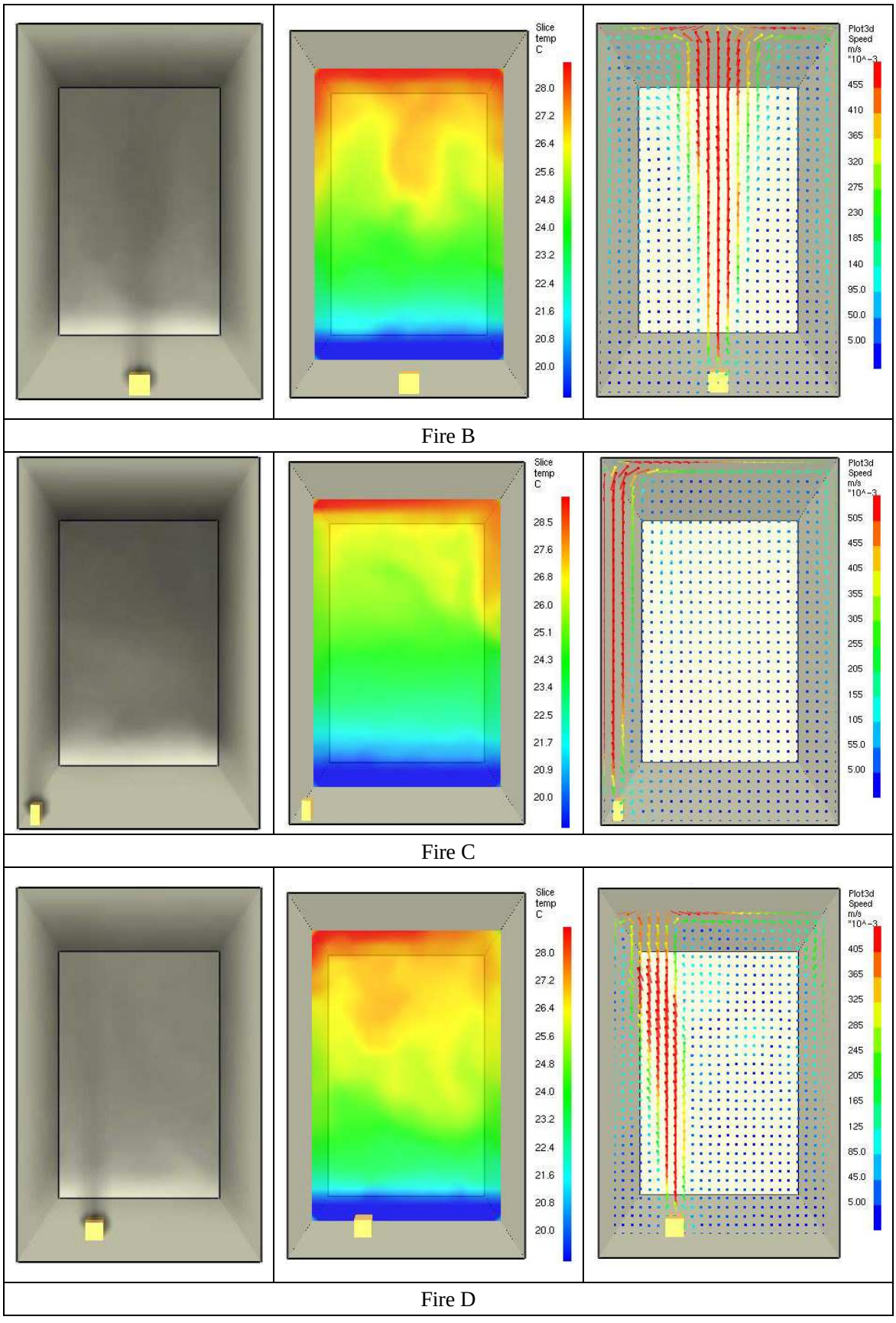

Fig. 2 Smoke filling by FDS (300W)

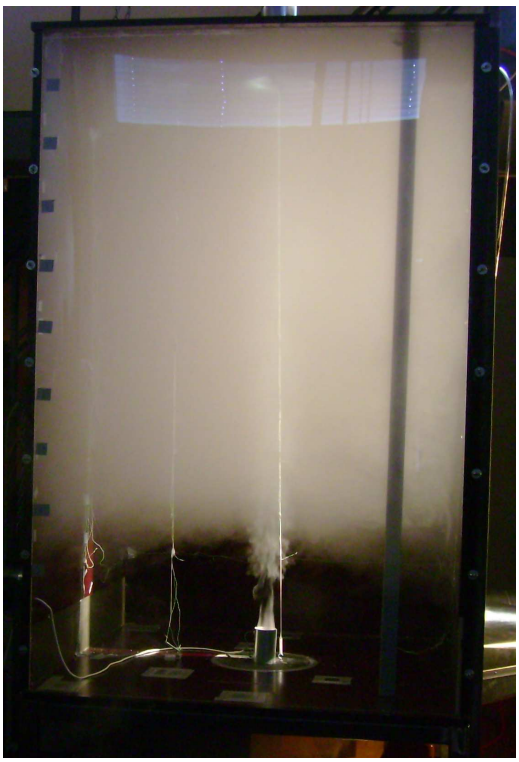

Air supply rate 0.006 m^3/s
Smoke exhaust rate 22.9 m^3/h

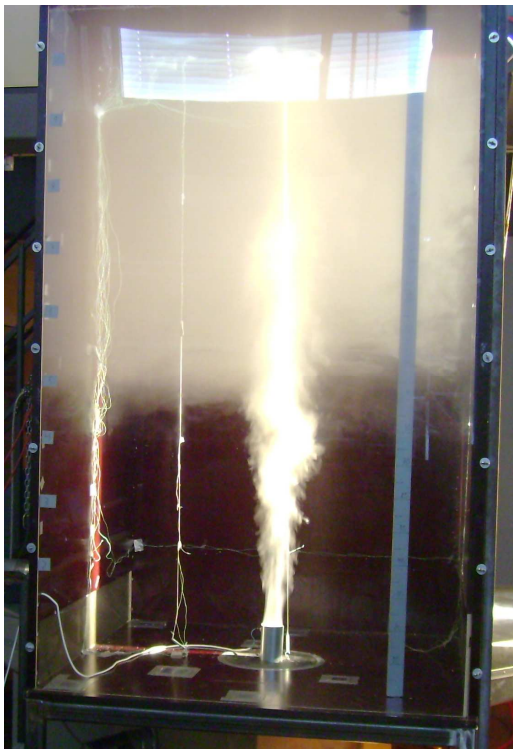

Air supply rate 0.03 m^3/s
Smoke exhaust rate 108.2 m^3/h

Fig. 3 Smoke layer height caught by video, center fire

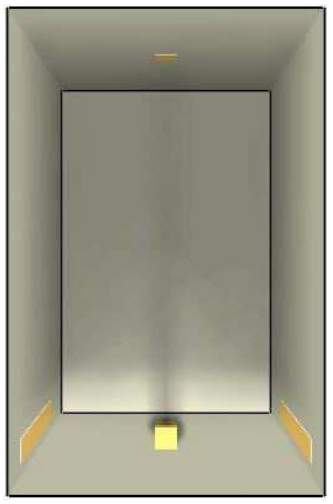

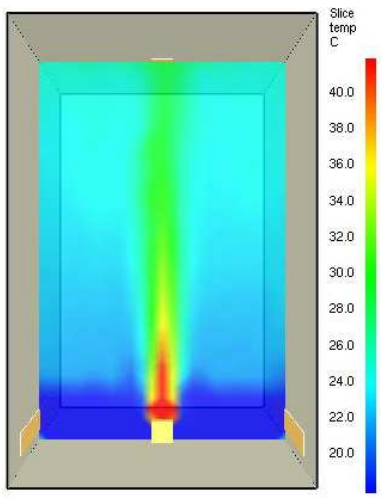

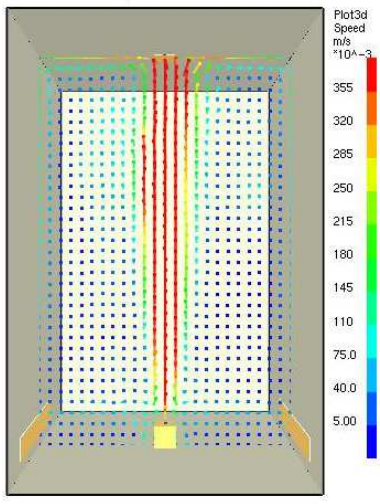

Air supply rate 0.006 m^3/s, smoke exhaust rate 22.9 m^3/h

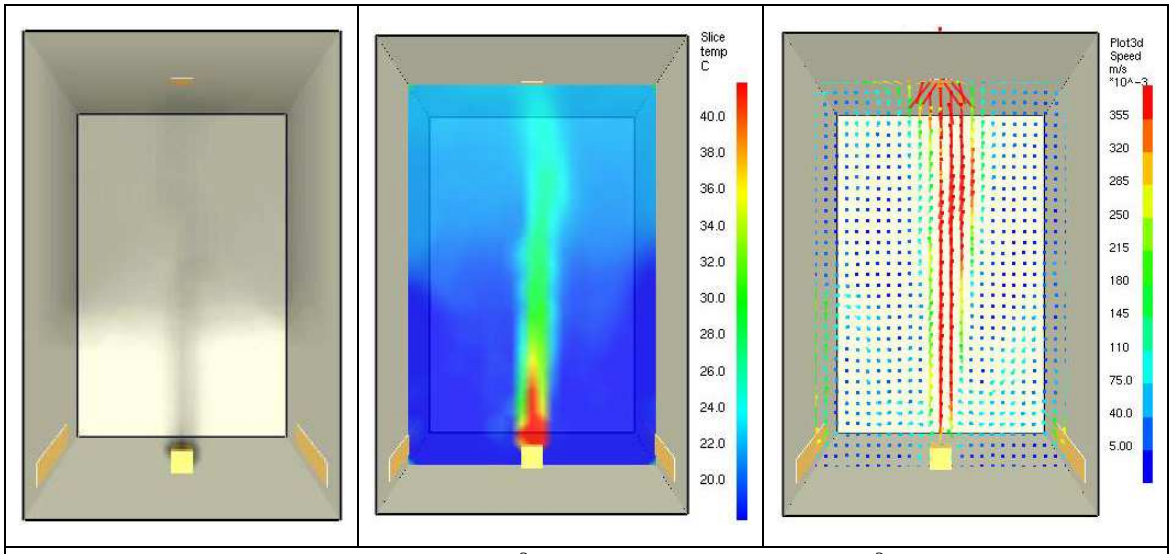

Air supply rate 0.03 m^3/s, smoke exhaust rate 108.2 m^3/h

Fig. 4 Smoke layer height simulated by FDS, center fire

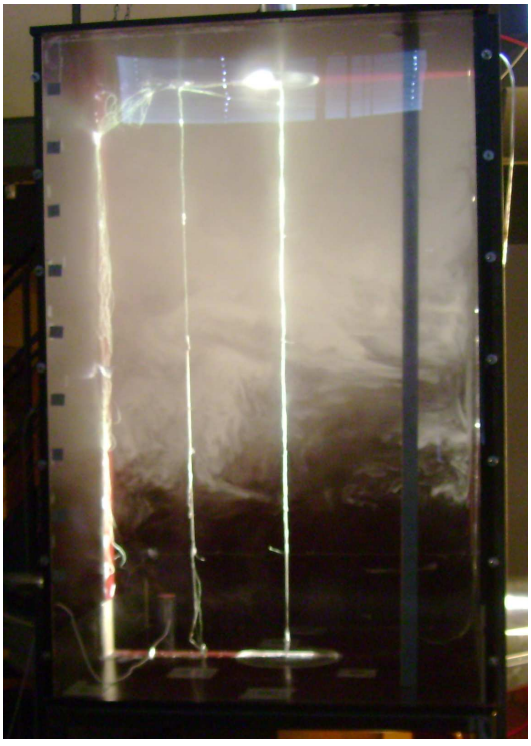

Air supply rate 0.006 m^3/s
Smoke exhaust rate 22.9 m^3/h

Air supply rate 0.03 m^3/s
Smoke exhaust rate 108.2 m^3/h

Fig. 5 Smoke layer height caught by video, corner fire

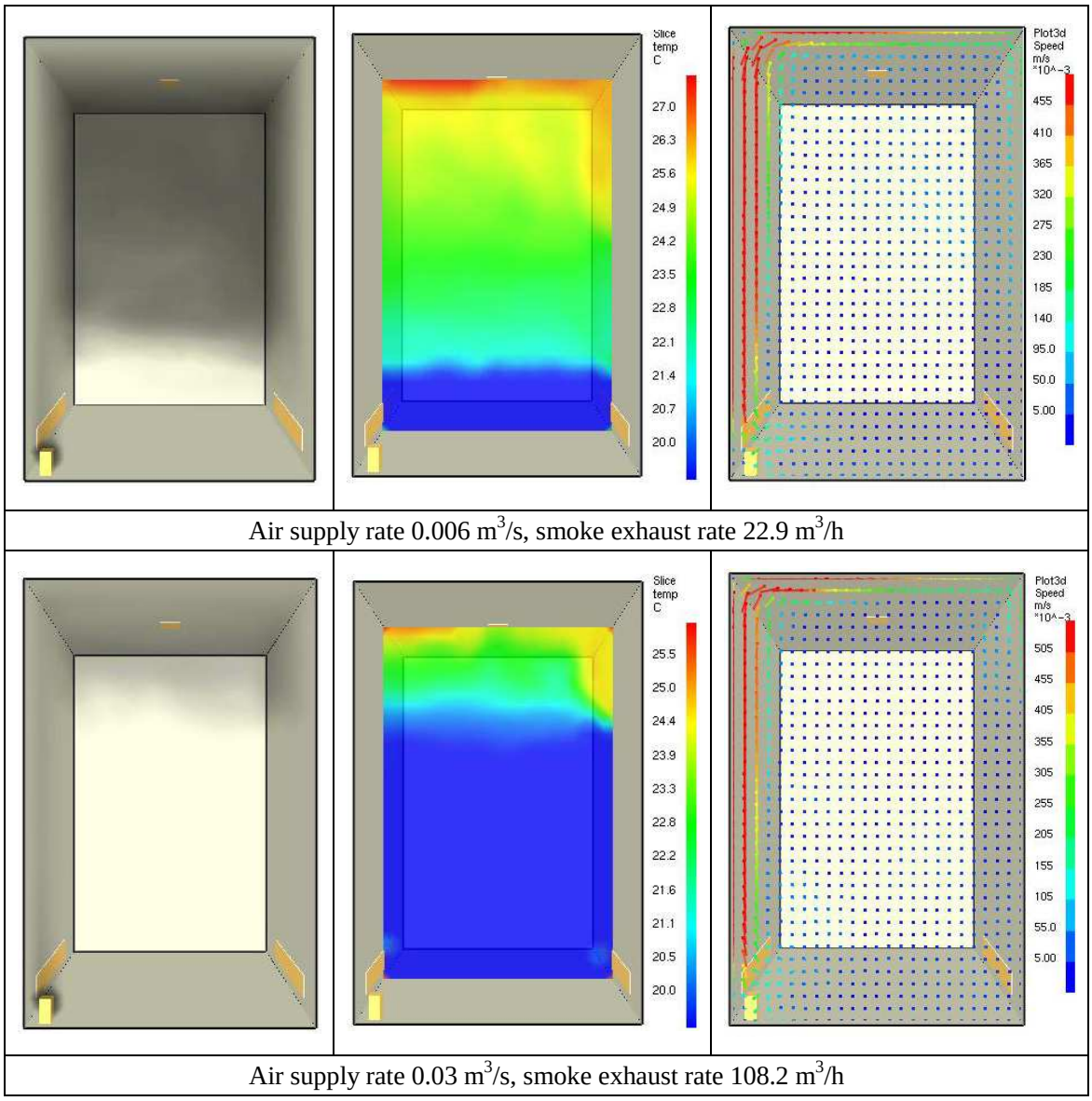

Air supply rate 0.006 m^3/s, smoke exhaust rate 22.9 m^3/h

Air supply rate 0.03 m^3/s, smoke exhaust rate 108.2 m^3/h

Fig. 6 Smoke layer height simulated by FDS, corner fire

Appendix B

Air supply rate 0.006 m^3/s | Air supply rate 0.03 m^3/s

Smoke exhaust rate 22.9 m^3/h | Smoke exhaust rate 108.2 m^3/h

Fig. 1 Smoke layer height caught by video, case AE

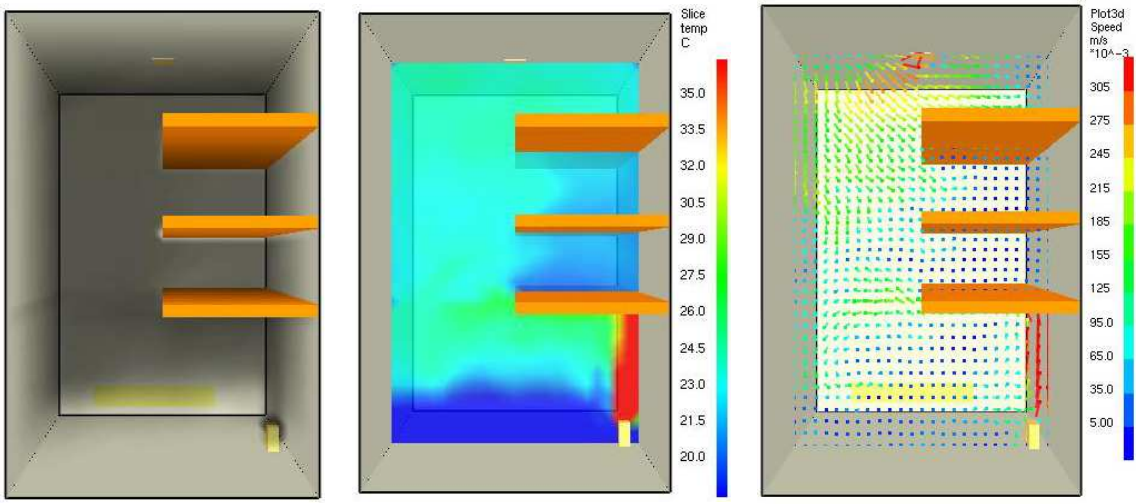

Air supply rate 0.006 m^3/s, smoke exhaust rate 22.9 m^3/h

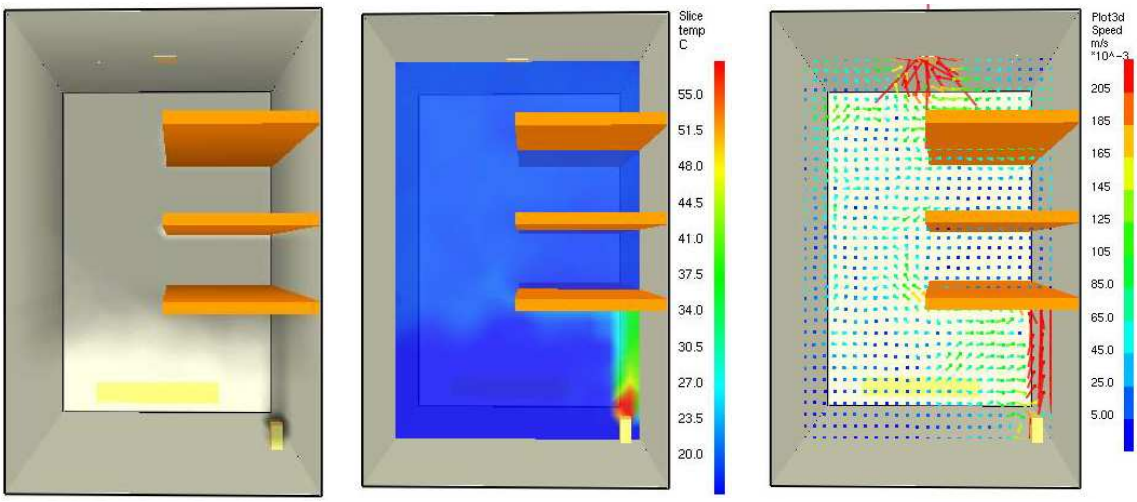

Air supply rate 0.03 m^3/s, smoke exhaust rate 108.2 m^3/h

Fig. 2 Smoke layer height caught by FDS, case AE

Air supply rate 0.006 m^3/s
Smoke exhaust rate 22.9 m^3/h

Air supply rate 0.03 m^3/s
Smoke exhaust rate 108.2 m^3/h

Fig. 3 Smoke layer height caught by video, case AF

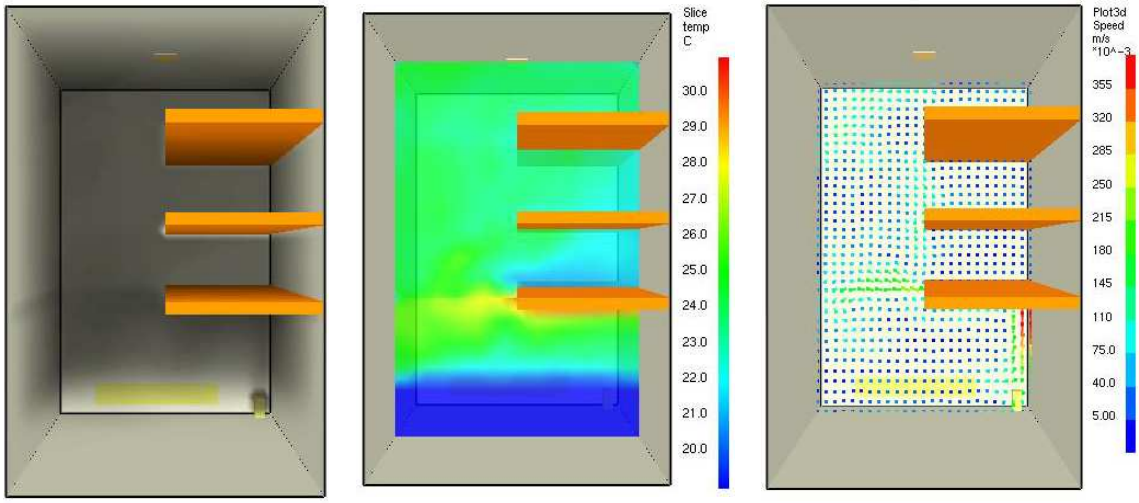

Air supply rate 0.006 m^3/s, smoke exhaust rate 22.9 m^3/h

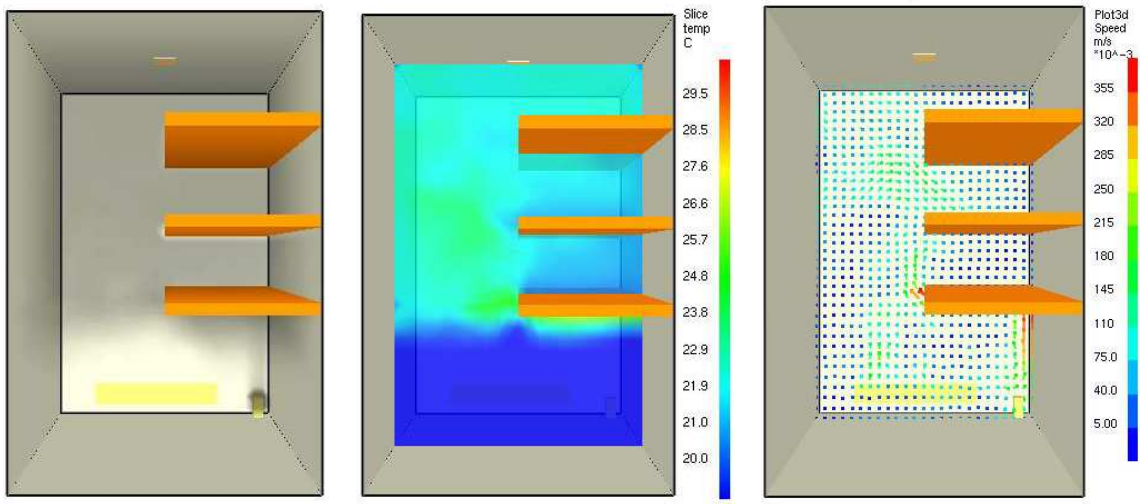

Air supply rate 0.03 m^3/s, smoke exhaust rate 108.2 m^3/h

Fig. 4 Smoke layer height caught by FDS, case AF

Appendix C

Air supply rate 0.03 m^3/s, smoke exhaust rate 108.5m^3/h, 20 degree sloping floor

Air supply rate 0.03 m^3/s, smoke exhaust rate 108.5m^3/h, 70 degree sloping floor

Fig. 1 smoke layer height caught by video (300W fire in the center)

Air supply rate 0.03 m^3/s, smoke exhaust rate 108.5m^3/h, 20 degree sloping floor

Fig. 2 smoke layer height caught by video (300W fire in the center, 100W cable on the sloping floor)

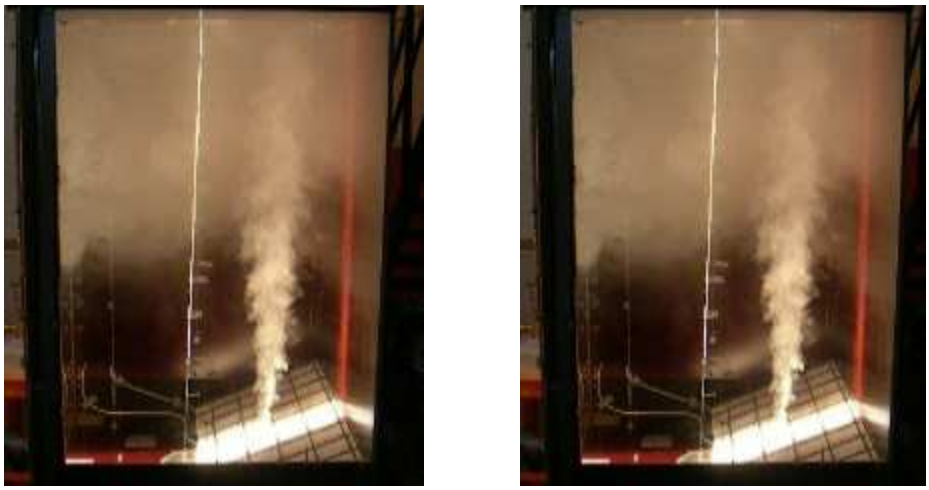

Air supply rate 0.03 m^3/s
Smoke exhaust rate 108.5 m^3/h

Air supply rate 0.03 m^3/s
Smoke exhaust rate 108.5 m^3/h
100W on the sloping floor

Fig. 3 Fire on the center of 20 degree sloping floor, 300W

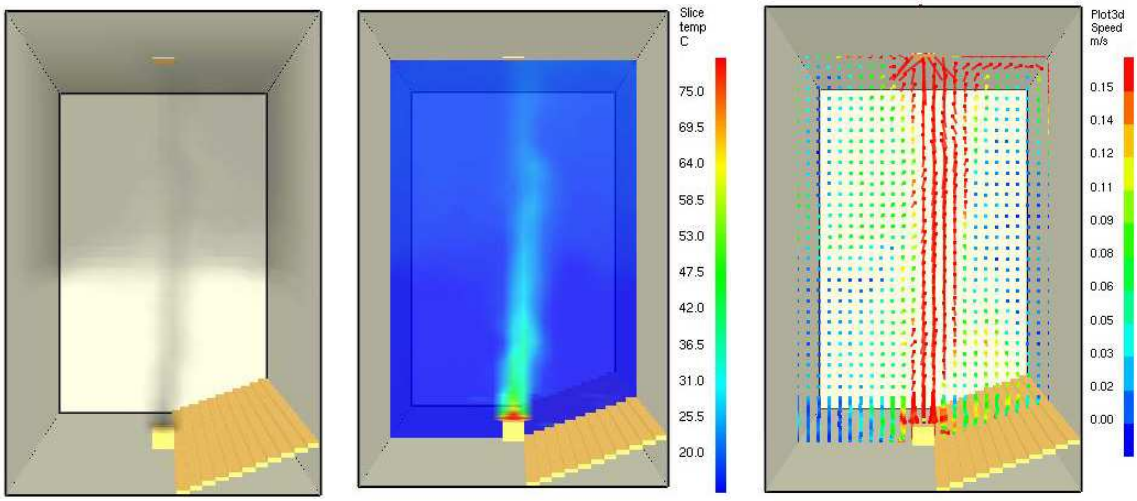

Air supply rate 0.03 m^3/s, smoke exhaust rate 108.2 m^3/h

Fig. 4 smoke layer height caught by FDS, case SA

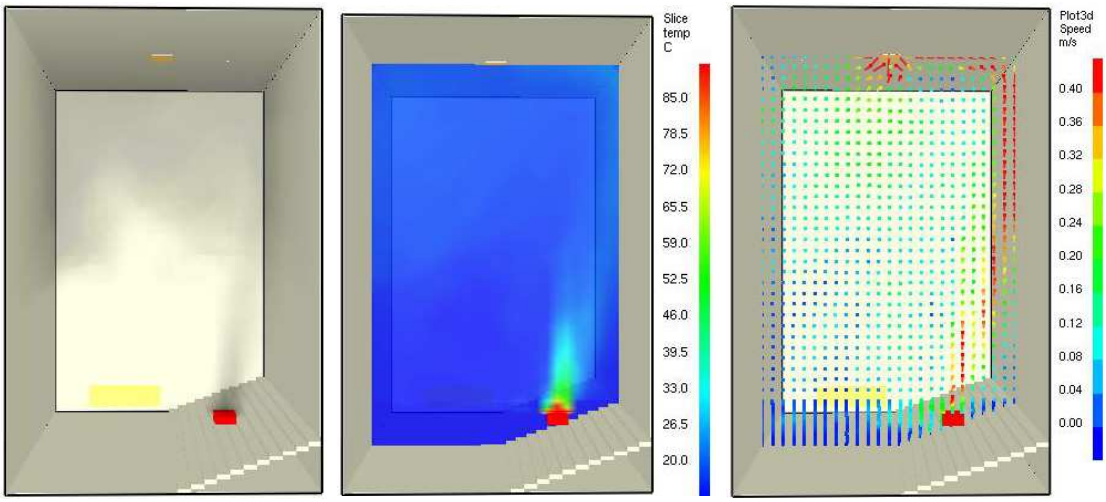

Air supply rate 0.03 m^3/s, smoke exhaust rate 108.2 m^3/h

Fig. 5 smoke layer height caught by FDS, case SE

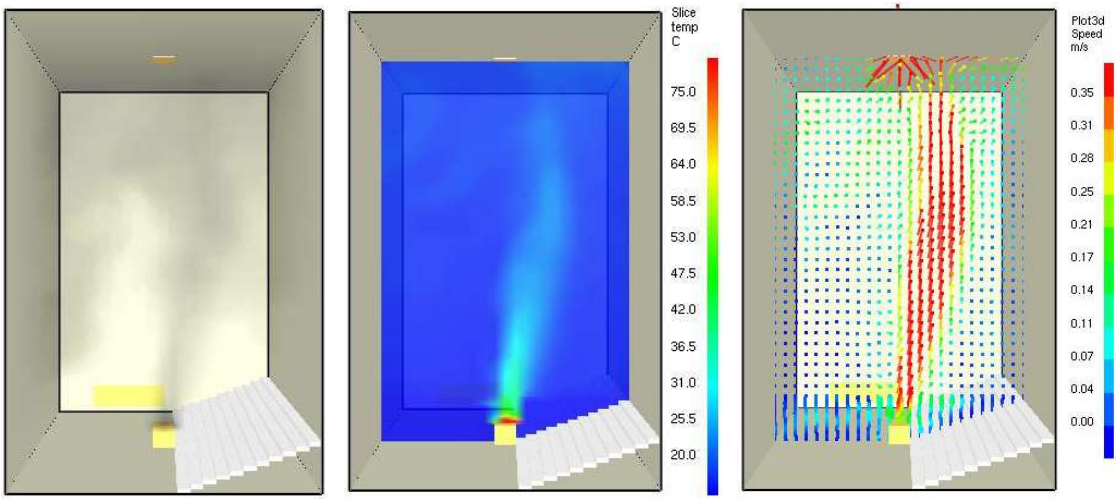

Air supply rate 0.03 m^3/s, smoke exhaust rate 108.2 m^3/h

Fig. 6 smoke layer height caught by FDS, case SG

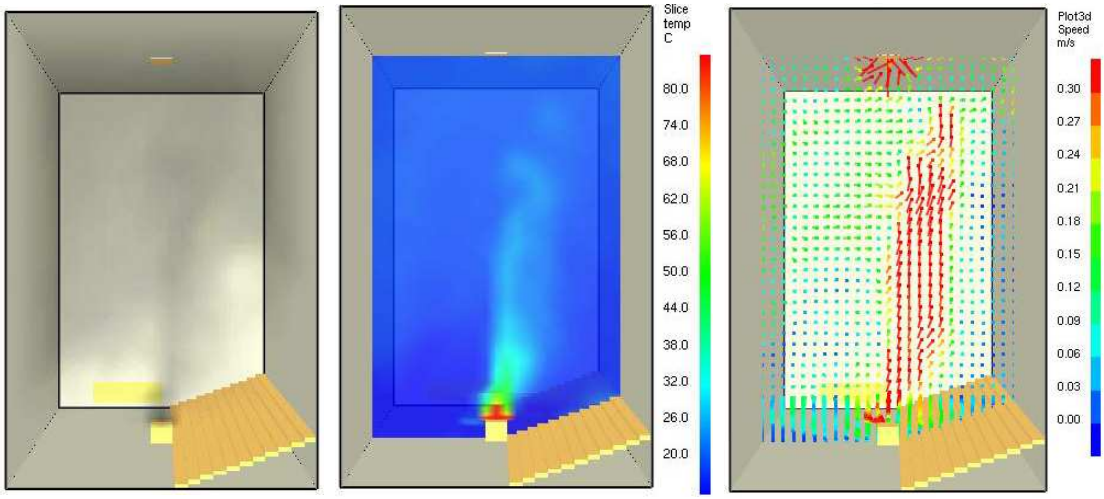

Air supply rate 0.03 m^3/s, smoke exhaust rate 108.2 m^3/h

Fig. 7 smoke layer height caught by FDS, case SH